

# UNCLASSIFIED

AD NUMBER
AD807686
NEW LIMITATION CHANGE
TO Approved for public release, distribution unlimited
FROM Distribution authorized to U.S. Gov't. agencies and their contractors; Critical Technology; AUG 1966. Other requests shall be referred to Air Force Aero Propulsion Lab., Wright-Patterson AFB, OH 45433.
AUTHORITY
AFAPL ltr dtd 12 Apr 1972

THIS PAGE IS UNCLASSIFIED

## REPRODUCTION QUALITY NOTICE

This document is the best quality available. The copy furnished to DTIC contained pages that may have the following quality problems:

- Pages smaller or larger than normal.
- Pages with background color or light colored printing.
- Pages with small type or poor printing; and or
- Pages with continuous tone material or color photographs.

Due to various output media available these conditions may or may not cause poor legibility in the microfiche or hardcopy output you receive.

☐

If this block is checked, the copy furnished to DTIC contained pages with color printing, that when reproduced in Black and White, may change detail of the original copy.

AFAPL-TR-66-72

807686

## THE ELECTROHYDRODYNAMIC GENERATION OF CHARGED DROPLET BEAMS

S. H. WINELAND

W. C. BURSON

R. E. HUNTER

TECHNICAL REPORT AFAPL-TR-66-72

AUGUST 1966

This document is subject to special export controls and each transmittal to foreign governments or foreign nationals may be made only with prior approval of the Air Force Aero Propulsion Laboratory, Wright-Patterson Air Force Base, Ohio.

AIR FORCE AERO PROPULSION LABORATORY  
RESEARCH AND TECHNOLOGY DIVISION  
AIR FORCE SYSTEMS COMMAND  
WRIGHT-PATTERSON AIR FORCE BASE, OHIO

## NOTICES

When Government drawings, specifications, or other data are used for any purpose other than in connection with a definitely related Government procurement operation, the United States Government thereby incurs no responsibility nor any obligation whatsoever; and the fact that the Government may have formulated, furnished, or in any way supplied the said drawings, specifications, or other data, is not to be regarded by implication or otherwise as in any manner licensing the holder or any other person or corporation, or conveying any rights or permission to manufacture, use, or sell any patented invention that may in any way be related thereto.

Copies of this report should not be returned to the Research and Technology Division unless return is required by security considerations, contractual obligations, or notice on a specific document.

AFAPL-TR-68-72

## THE ELECTROHYDRODYNAMIC GENERATION OF CHARGED DROPLET BEAMS

S. H. WINELAND

W. C. BURSON

R. E. HUNTER

This document is subject to special export controls and each transmittal to foreign governments or foreign nationals may be made only with prior approval of the Air Force Aero Propulsion Laboratory, Wright-Patterson Air Force Base, Ohio.

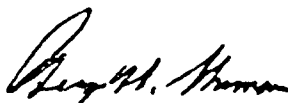
FOREWORD

This report was prepared by Mr. Stanley Wineland, Dr. R. E. Hunter, and Mr. W. C. Burson, Jr., of the Air Force Aero Propulsion Laboratory, Research and Technology Division, Wright-Patterson Air Force Base, Ohio. The work was conducted in-house under Project 3141, "Electric and Advanced Propulsion," Task 314104, "Advanced Concepts." This work was accomplished between June 1963 and June 1966. Mr. S. Wineland and later Mr. W. C. Burson served as project engineer.

The report was submitted by the authors in June 1966.

The authors wish to express their appreciation to Mr. E. Francescone, technician, of the Air Force Aero Propulsion Laboratory, for his assistance in the laboratory work.

Publication of this report does not constitute Air Force approval of the report's findings or conclusions. It is published only for the exchange and stimulation of ideas.



GEORGE W. SHERMAN  
Chief, Aerospace Power Division  
Air Force Aero Propulsion Laboratory

ABSTRACT

Thrustors capable of high exhaust velocity (specific impulse) and efficiency are desirable for space propulsion. The acceleration of charged droplets (colloids) by an electric field can provide a thrustor that meets these requirements. This effort was concentrated on producing positive and negative colloids by the electrohydrodynamic spraying of ionically doped glycerol solutions from metal capillary needles.

To date, the results of this program indicate that both positive and negative colloids can be produced with charge-to-mass ratios of sufficient magnitude to be utilized by an electrostatic space thrustor. Charge-to-mass ratios have been obtained in the ranges of approximately 100-30,000 coulombs/kilogram for positive colloids and 100-4000 coulombs/kilogram for negative colloids. Current levels of 10 microamps per needle are easily obtained.

TABLE OF CONTENTS

SECTION	PAGE
I INTRODUCTION	1
II DIAGNOSTIC EQUIPMENT	3
1. The Quadrupole Mass Spectrometer	3
2. The Time-of-Flight Spectrometer	9
3. The Faraday Detector	21
III CAPILLARY AND FLUID PREPARATION	22
IV SOME EXPERIMENTAL RESULTS	23
V SOME THEORETICAL CONSIDERATIONS	45
VI APPLICATION OF COLLOIDS TO PROPULSION	54
REFERENCES	67



## ILLUSTRATIONS

FIGURE		PAGE
1.	Electrohydrodynamic Spraying Apparatus	2
2.	Quadrupole Spectrometer Schematic	4
3.	Stability Diagram of Mathieu's Function	6
4.	Stability Diagram of Mathieu's Function	6
5.	Frequency Vs. Charge-to-Mass Ratio	7
6.	Quadrupole Driver Circuit	8
7.	Time-of-Flight Spectrometer Schematic Diagram	9
8.	Oscilloscope Display of Idealized T.O.F. Decay	11
9.	Massenfilter/T.O.F. Comparison	12
10.	T.O.F. Collector Housing and Quadrupole Adapter	16
11.	Variable Bias Circuit for T.O.F. Collector	17
12.	Adjustable Source Mount	18
13.	Schematic Illustration of Combined Quadrupole and T.O.F. Spectrometer Facility	19
14.	Combined Quadrupole and T.O.F. Spectrometer Facility	20
15.	Faraday Detector Schematic	21
16.	Mode I Spraying Sequence	24
17.	Examples of Mode I Spraying	24
18.	Current Contributions by Individual Droplets During a Pulse	25
19.	Examples of Mode II Spraying	26
20.	Mode III Spraying	27
21.	Mode I to Mode III Transition	27
22.	Modified Mode III Spraying	27
23.	Superimposed T.O.F. Decays, Mode I and Mode III Beam	29
24.	Momentary Current Fluctuation in Mode III	29
25.	Three Superimposed T.O.F. Traces with Steady-State Currents, Taken Before and After Decays	29

## ILLUSTRATIONS (Continued)

FIGURE		PAGE
26.	Discharge at Capillary Tip	30
27.	Specific Charge Vs. Capillary Potential	33
28.	Beam Current Vs. Capillary Potential	33
29.	$q/m$ Vs. Capillary Potential for Different Reservoir Pressures	34
30.	$q/m$ Vs. Capillary Potential for Various Concentrations of NaI in Glycerol	35
31.	Transition Behavior of NaI/Glycerol Solutions at Positive and Negative Capillary Potentials	35
32.	Capillary Tip Deterioration	38
33.	Capillaries After Extended Operation	39
34.	Erosion Pattern on T.O.F. Collector After Extended Operation	40
35.	$q/m$ Variation with Horizontal Angle	41
36.	$q/m$ Angular Variation at Two Voltages	41
37.	Angular Variation of $q/m$	42
38.	Ion Jet	43
39.	Jet with Heavy Particles and Ions	43
40.	Negative Ion Quadrupole Trace	44
41.	Rayleigh and Field Emission Limits for Glycerol	47
42.	Electron Levels of Sodium and Iodine Ions	51
43.	Schematic Diagrams of Ion and Colloid Thrusters	54
44.	Schematic of Electrodeless Colloid Thruster	55
45.	Schematic of Electrodeless Thruster with Extractor as Common Ground	55
46a.	Accelerating Potential Vs SMR Specific Charge	56
46b.	Divergence Efficiency Variation with Spray Half-Angle	56
47.	Ratio of Propulsion System Mass to Total Impulse Vs. $I_{sp}$ for Solar Cells	59

ILLUSTRATIONS (Continued)

FIGURE		PAGE
48.	Ratio of Propulsion System Mass to Total Impulse Vs. $I_{sp}$ for Nuclear Power Supply	60
49.	Optimum SMR Specific Charge Vs. Mission Time for Various Accelerating Voltages, Nuclear Power Supply	62
50.	Optimum SMR Specific Charge Vs. Mission Time for Various Accelerating Voltages, Solar Cells	63
51.	Efficiency X Power-to-Thrust Ratio Vs. $I_{sp}$ and SMR Specific Charge for Various Accelerating Voltages	64
52.	Efficiency Vs. Specific Impulse for Various Power-to-Thrust Ratios	65
53.	Thrust Vs. Specific Charge for Various Accelerating Voltages and a Current of 1 Microamp	66

## LIST OF SYMBOLS

$c$	charge-to-mass ratio
$c$	capacitance
$c_{R_0}$	ion emission-limited specific charge
$C'_R$	limiting specific charge
$E$	electric field
$F$	thrust
$f$	frequency
$G$	gain
$g_0$	gravitational acceleration
$I$	current
$I_0$	initial current
$I_{sp}$	specific impulse
$J$	electron level in solution
$\phi$	ionization potential
$K$	dielectric constant
$L$	T.O.F. length
$m$	mass
$\dot{M}$	mass flow
$M_E$	engine mass
$M_p$	propellant mass
$M_{po}$	power supply mass
$M_{ps}$	propulsion system mass
$P$	power (kw)
$q$	charge
$q/m$	charge-to-mass ratio
$r$	droplet radius

## LIST OF SYMBOLS (Continued)

$R_o$	$\frac{c}{\Delta c} \frac{U_1}{U_o}$
T	mission time
T.O.F.	time of flight
t	time
$U_1$	particle accelerating voltage
$U_o$	accelerating voltage used during calibration
V	voltage
$V_{AC}$	alternating current voltage
$V_{DC}$	direct current voltage
v	particle velocity
W	solvation or hydration energy
$\epsilon_o$	permittivity
$\phi$	work function
$\gamma$	surface tension
$\alpha$	specific power or divergence half-angle
$\rho$	density
< >	average

## SECTION I

### INTRODUCTION

When a conducting liquid is exposed to an electric field of such intensity that the electrical forces on the charge carriers exceed the surface tension forces, then the liquid surface ruptures and small charged droplets are formed. This process, called electrohydrodynamic atomization, is usually carried out by establishing an intense electric field at the tip of a fine metallic capillary tube containing a suitable liquid. The action of the electric field on the charge carriers in the liquid is such that charges of one sign are forced to the liquid metal interface (where they are neutralized) while those of opposite sign move away from the capillary. In the presence of strong electric fields, these latter charge carriers are capable of overcoming surface tension forces and separating themselves from the bulk liquid. As they leave, the charge carriers carry along a certain amount of liquid; these charged liquid droplets are often referred to as "colloids." Depending on their charge and mass, the droplets can acquire an appreciable velocity as they pass out of the region of high electric field intensity.

In practice, the capillary is located in a vacuum environment so that viscous drag forces, corona discharges, and other extraneous effects are minimized. In order that a beam of droplets may be produced and studied, the capillary tip is usually placed perpendicular to a metallic plate containing a hole, the center of which lies on the axis of the capillary. In many instances, the capillary is inserted through the hole so that the tip protrudes a few millimeters beyond the front of the plate. By raising the potential of the capillary relative to the plate, a very high electric field can be produced at the capillary tip. The electric field, and hence the spraying process, can be controlled by adjusting the capillary potential. A typical arrangement of capillary, extractor plate, and liquid supply is shown in Figure 1.

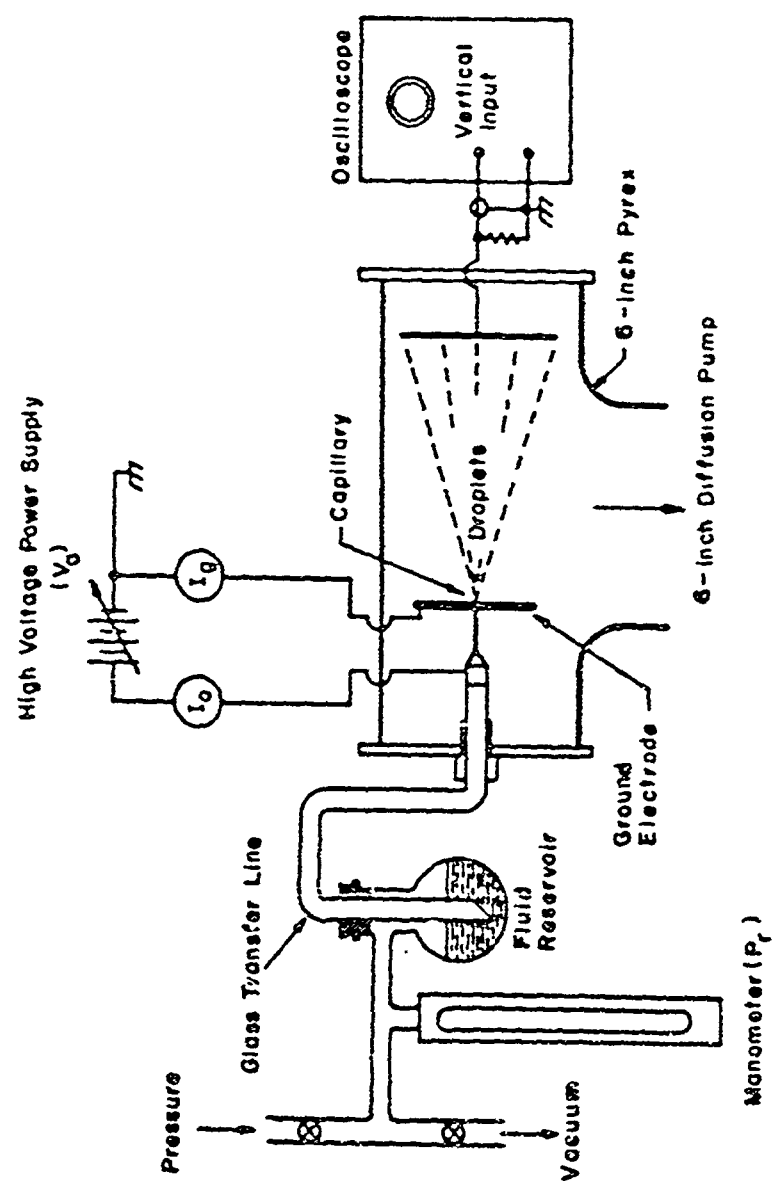


**Figure 1. Electrohydrodynamic Spraying Apparatus**

## SECTION II

### DIAGNOSTIC EQUIPMENT

Since the study of beams of charged droplets involves the use of specialized equipment and techniques which are not widely known, a brief review of these is presented before proceeding to a discussion of the spraying process itself. A parameter of major interest in droplet beam studies is the specific charge (charge-to-mass ratio) distribution of the droplets. Of the various types of mass spectrometers available, few possess the range and versatility necessary for examining charged droplet beams. By varying the capillary potential, a typical droplet source may be capable of generating beams with average specific charges ranging from a fraction of a coul/kg to several thousand coul/kg. In addition, these beams may contain both molecular and atomic ions. Thus, a mass spectrometer suitable for charged droplet studies should be able to scan rather quickly the entire spectrum of specific charge values between  $10^{-1}$  and  $10^7$  coul/kg.

#### 1. THE QUADRUPOLE MASS SPECTROMETER

One instrument capable of meeting the above requirements is the quadrupole mass spectrometer, or so-called "massenfilter," developed by Paul, et al. in 1954 (Reference 1). The massenfilter consists of four rails arranged symmetrically about an axis parallel to the rails themselves, as shown in Figure 2. The diagonally opposed pairs of rails are connected by a jumper wire, and each set is excited by the output of a special power supply. This power supply consists of a push-pull variable frequency oscillator whose output floats at a specified DC potential. The electrical potential in the interior of the quadrupole is a function of position and time:

$$V(x, y, t) = \frac{U(t)}{r_0^2} (x^2 - y^2) = \frac{V_{DC} + V_{AC} \cos \omega t}{r_0^2} (x^2 - y^2) \quad (1)$$

$r_0$  is the distance from the quadrupole axis of symmetry to the surface of a rail,

$x$  and  $y$  the position coordinates of a point inside the quadrupole,

$V_{AC}$  the voltage amplitude of the oscillator output,

$\omega$  the oscillator frequency, and

$V_{DC}$  the DC potential of the rails.

Application of Lagrange's equation to Equation 1 yields for a particle of mass,  $m$ , and charge,  $q$ , the following equations of motion

$$\left. \begin{aligned} m \frac{d^2 z}{dt^2} &= 0 \\ \frac{d^2 x}{dt^2} - \frac{2q(V_{DC} + V_{AC} \cos \omega t)x}{mr_0^2} &= 0 \\ \frac{d^2 y}{dt^2} + \frac{2q(V_{DC} + V_{AC} \cos \omega t)y}{mr_0^2} &= 0 \end{aligned} \right\} \quad (2)$$



which can be converted to Mathieu's differential equation

$$d^2 Z / d\zeta^2 + (a - 2b \cos 2\zeta) Z = 0 \quad (3)$$

by making the substitutions

$$\left. \begin{aligned} a &= 8qV_{DC} / r_0^2 m\omega^2 \\ b &= 4qV_{AC} / r_0^2 m\omega^2 \\ \zeta &= \omega t / 2 \end{aligned} \right\} \quad (4)$$

The general solution to Mathieu's equation is the Mathieu Function

$$Z = A e^{\mu\zeta} \sum_{n=-\infty}^{\infty} C_n e^{in\zeta} + B e^{-\mu\zeta} \sum_{n=-\infty}^{\infty} C_n e^{-in\zeta} \quad (5)$$

where  $\mu$  is a function of  $a$  and  $b$ .

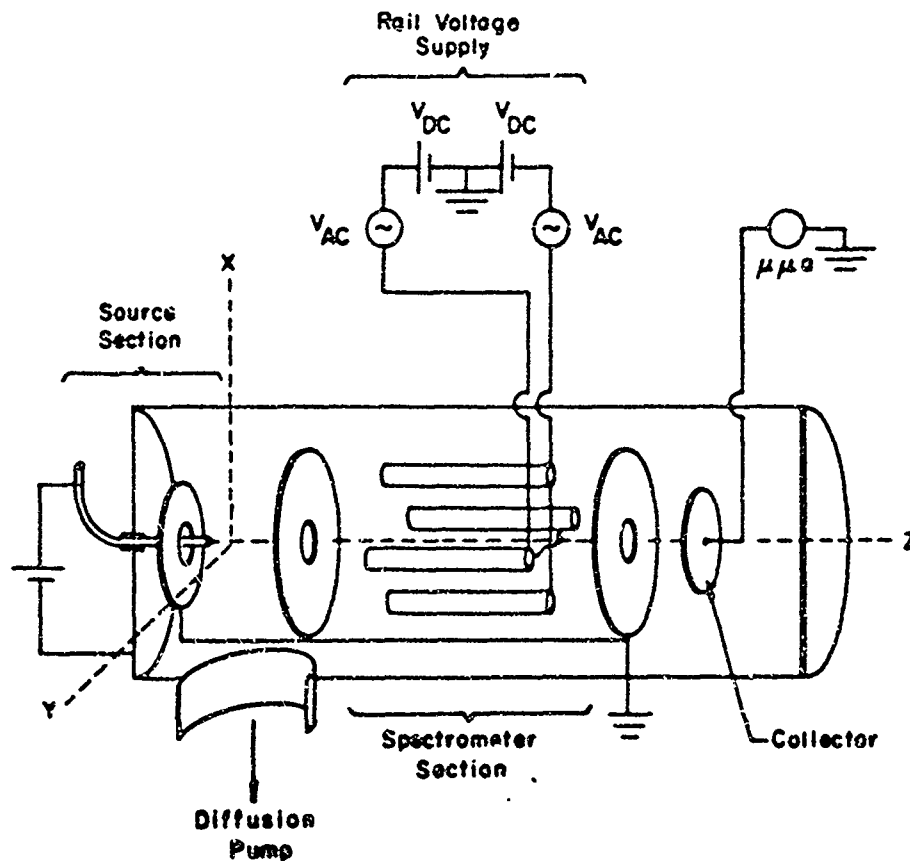


Figure 2. Quadrupole Spectrometer Schematic

The behavior of this function is shown in Figure 3. The shaded regions represent stable solutions; elsewhere the amplitude of the function increases exponentially and the solution is unstable. The regions of stability correspond to cases where  $\mu$  is purely imaginary. Physically, this means that the motion of a particle in the quadrupole field is confined and periodic. If  $\mu$  is real or complex, the particle will move with an exponentially increasing amplitude and strike the rails.

For operation of the quadrupole as a spectrometer, we concern ourselves with the stable region 1, which is shown in more detail in Figure 4. In this view, the portion of the region of stability below the b-axis has been "folded" up into the first quadrant. That this is a permissible manipulation may be seen by considering the lines determined by the ratio

$$u = V_{DC}/V_{AC} = a/2q \quad (6)$$

For a given  $u > 0$ , there will be a corresponding  $u$  of identical magnitude but opposite sign, since  $V_{DC}$  can be positive or negative, depending on which set of rails is considered. Thus, the region of stable orbital parameters (shaded) is bounded by  $a_0$ ,  $b_1$ , and the  $q$ -axis. In a quadrupole with fixed  $u$ ,  $r_0$ , and  $\omega$ , a particle with specific charge,  $q/m$ , will have a stable orbit only if its corresponding values of  $a$  and  $b$  lie in the ranges  $\Delta a$  and  $\Delta b$ , i.e., the projections of the segment of  $u$  in the region of stability into the  $a$ - and  $b$ -axes. Consequently, the bandwidth of the spectrometer is narrowed by increasing  $u$ , i.e., by increasing the ratio of the DC to AC voltages (Equation 6). It is apparent from Figure 4 that there is a maximum value of  $u$  which determines the minimum bandwidth. The values of  $a$  and  $q$  corresponding to  $u_{max}$  are

$$\left. \begin{aligned} a_0 &= 0.2369 \\ q_0 &= 0.706 \end{aligned} \right\} \quad (7)$$

Substituting these values into Equation 6 yields

$$u_{max} = a_0/2q_0 = 0.1679 \quad (8)$$

From Equations 4 and 7, we can determine the relationship between  $q/m$  and  $\omega$ ,  $V_{AC}$ , and  $r_0$  for given quadrupole operated as a spectrometer:

$$V_{AC} = a_0 \cdot r_0^2 m \omega^2 / 4q = 6.96 r_0^2 f^2 (q/m)^{-1} \quad (9)$$

where  $f$  is the frequency of the AC voltage in cycles per second.

A plot of  $f$  versus  $q/m$  for  $r_0 = 1.116$  cm and  $V_{AC} = 10$  volts, the operating parameters of the AFAPL spectrometer, is presented in Figure 5. It can be seen that a frequency range between 1 kc and 5 mc covers the specific charge spectrum between  $0.5$  and  $10^7$  coul/kg. The quadrupole driver circuit is shown in Figure 6. The frequency range is covered in 8 bands, and each band with the exception of the lowest is covered by varying the oscillator tank capacitance. In the lowest band (1-6 kc), the oscillator is operated as a push-pull amplifier and driven by a Hewlett-Packard Model 200 AB audio oscillator. However, use of special inductors could make the driver self-oscillating over the entire frequency range. The rails in this instrument are 1.92 cm in diameter and 1.14 meter long. Entrance apertures of 0.61 inch and 0.03 inch have been used; the latter allows better examination of low current beams.

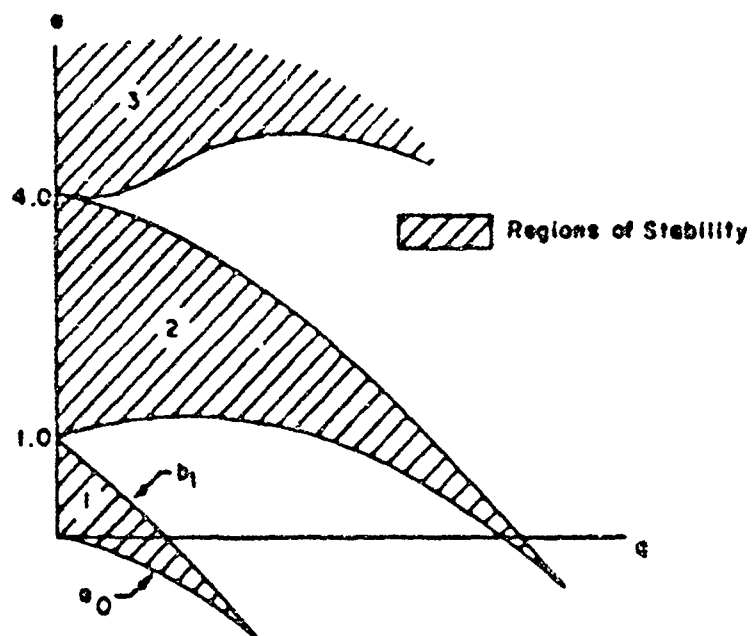


Figure 3. Stability Diagram of Mathieu's Function

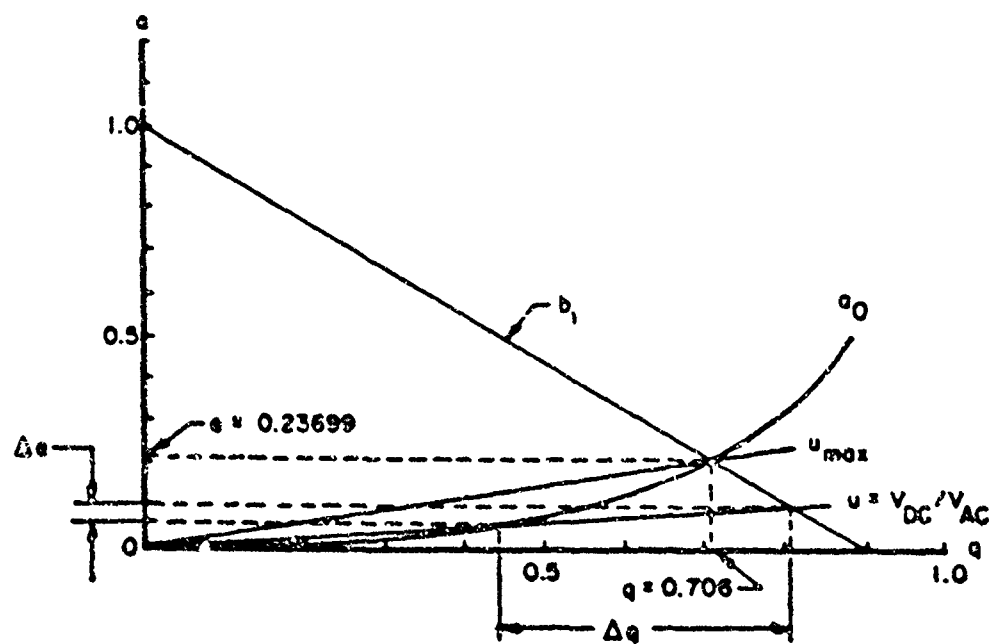


Figure 4. Stability Diagram of Mathieu's Function

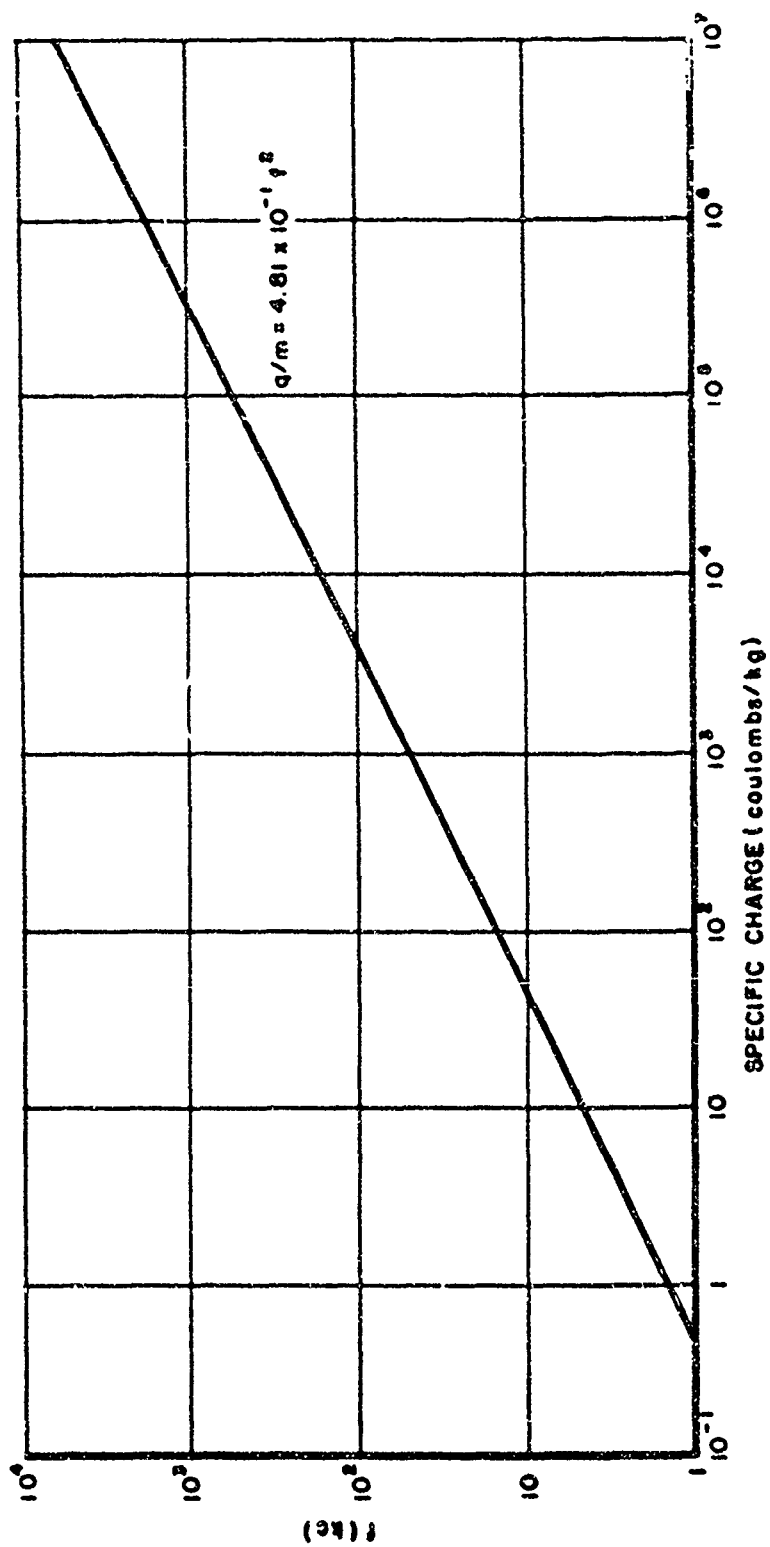


Figure 6. Frequency Vs. Charge-to-Mass Ratio



A very useful feature of the quadrupole spectrometer is its easily variable resolution. As Equation 6 shows, lowering the magnitude of  $V_{DC}$  lowers the resolution, i.e., increases the bandwidth of specific charge passed by the spectrometer. When searching for discrete jets from a droplet source,  $V_{DC}$  is switched off and  $f$  is adjusted to a value about twice as high as that at which a specific charge peak is expected. The source is then aimed until the collector current shows a maximum. The DC voltage is switched on and the specific charge spectrum is scanned. For low intensity beams,  $V_{DC}$  may have to be dropped to values on the order of 140 volts, depending on the sensitivity of the collector metering circuit. There is a tendency for peaks to shift as the resolution is lowered. When operating at high resolution, care must be taken to maintain  $V_{AC}$  constant as the frequency is varied to avoid exceeding  $v_{max}$ . If frequency is held constant and  $V_{AC}$  is varied to accomplish the specific charge scan, the circuit of the quadrupole driver must be modified so that the ratio  $V_{DC}/V_{AC}$  remains constant.

### 3. THE TIME-OF-FLIGHT SPECTROMETER

Despite its versatility and range, the quadrupole spectrometer is limited in that it can sample only a small portion of a beam at one time, and thus is incapable of providing an accurate representation of the total beam characteristics. In 1963, H. Shelton and E. Cohen (Reference 2) developed a time-of-flight spectrometer which, although lacking the precision and resolution of the quadrupole, permitted the specific charge distribution in the entire beam to be measured instantaneously. The device, pictured schematically in Figure 7, consists of a shielded collector located at a distance  $L$  from the charged droplet source. Operation of

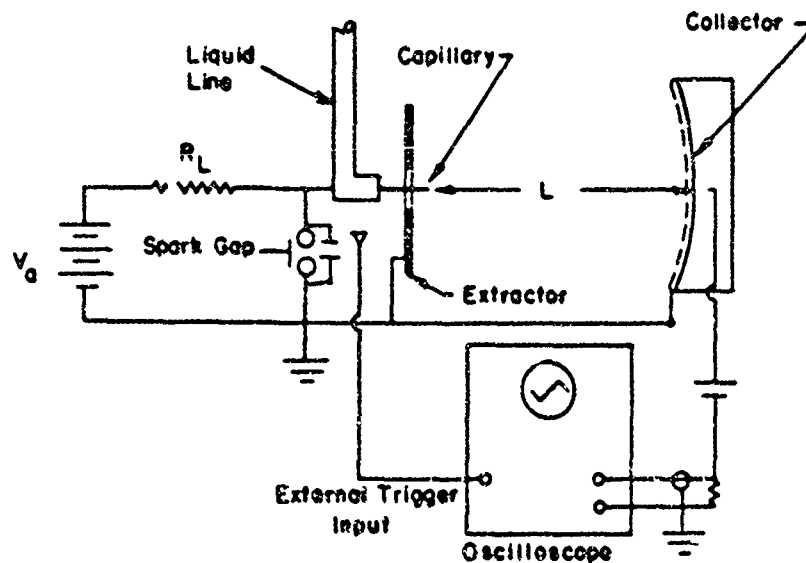


Figure 7. Time-of-Flight Spectrometer Schematic Diagram

the device is based on the following principles. The configuration of electric field at the capillary tip is such that the droplets acquire their terminal velocity within a few millimeters of the tip. The velocity,  $v$ , of a particle of charge,  $q$ , and mass,  $m$ , which has passed through a potential,  $V$ , is:

$$v = \sqrt{2(q/m)V} \quad (10)$$

Thus, since all the droplets fall through the same potential, there will be a velocity distribution in the beam corresponding to the droplet specific charge distribution. Those droplets having a high specific charge will have a higher velocity than those having a lower specific charge. The current observed at the collector is the sum of each of the currents contributed by the individual specific charge species. To determine the specific charge distribution in the beam, the steady state current  $i_0$  is observed on the oscilloscope and noted (usually photographically). The scope is then placed in the single-sweep, external-trigger, negative-slope mode and the spark gap is activated. When the gap closes, the capillary potential decays to ground in the order of a microsecond, and the droplet source stops operating for a few milliseconds. The oscilloscope, triggered by the spark gap signal, records the current decay at the collector. An idealized decay is pictured in Figure 8. Since no droplets are produced when the capillary is at ground potential, that species of droplets in the beam having the highest velocity and hence the highest specific charge, will be the first to stop contributing to the collector current. When the last droplet of this species arrives at the collector, the current will drop to a lower level; this level of current is contributed by species of lower specific charge. The decay shown in Figure 8 represents a beam consisting of three distinct species. The time at which the current decays to a new level represents the time required for the last particle of that species to travel from the needle tip to the collector. This time is measured by the scope and is simply the distance traveled,  $L$ , divided by the velocity of the droplet. From Equation 10 this is seen to be

$$t = \frac{L}{v} = \frac{L}{\sqrt{2Vq/m}} \quad (11)$$

which can be rearranged

$$q/m = \frac{L^2}{2Vt^2} \quad (12)$$

Thus, each point on the  $I$ -versus- $t$  decay corresponds to a specific value of  $q/m$ . If there is no current decay at time  $t$ , there were no particles present in the beam having a specific charge corresponding to  $t$ . In practice, specific charge distributions are usually continuous between an upper and lower limit, so that the decay is a continuous function such as that of Figure 9, rather than the step function of Figure 8.

The screen in front of the collector serves a twofold purpose. First, it increases the resolution of the device by keeping the collector from "seeing" a charged droplet until the droplet has passed the screen, i.e., traveled the complete distance  $L$ . Secondly, by making the collector positive relative to the screen, it prevents secondary electrons from leaving the collector and giving an erroneous value of  $i_0$ . A second screen, biased positive, may be placed in front of the first screen to prevent secondary electrons created at the first screen from traveling to the collector.

The maximum specific charge that can be measured with the time-of-flight mass spectrometer is determined by the time it takes the collector circuit to recover from the spark gap

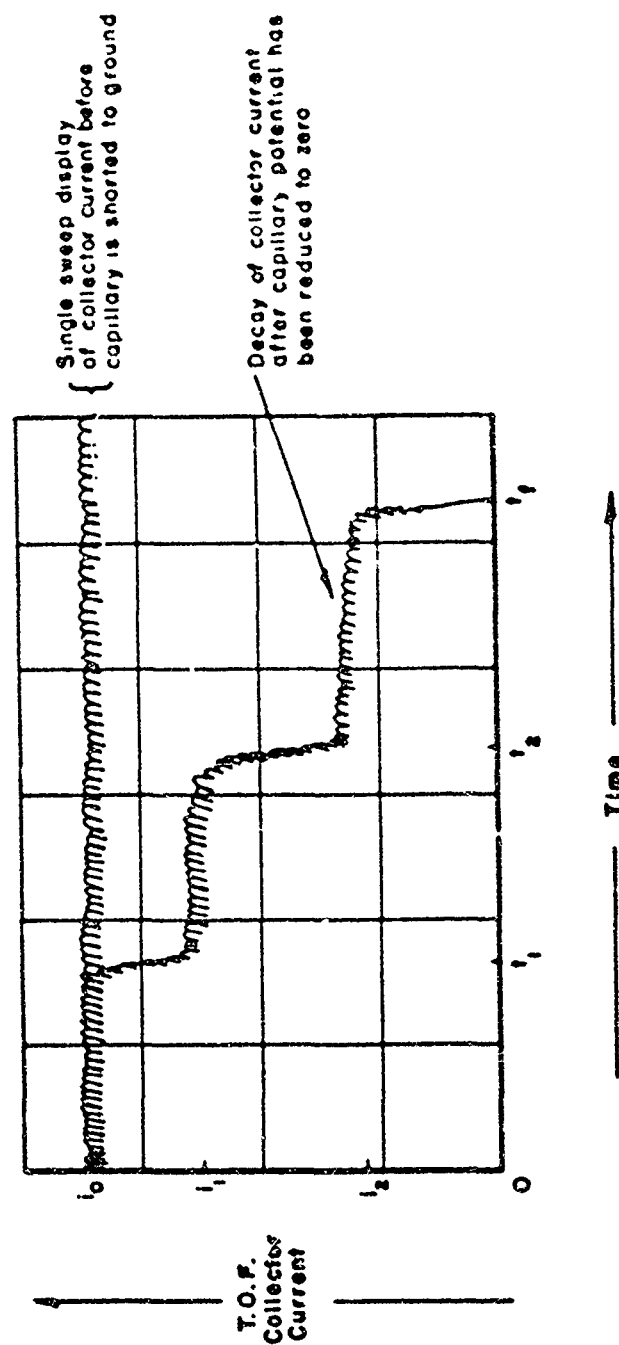


Figure 8. Oscilloscope Display of Idealized T.O.F. Decay



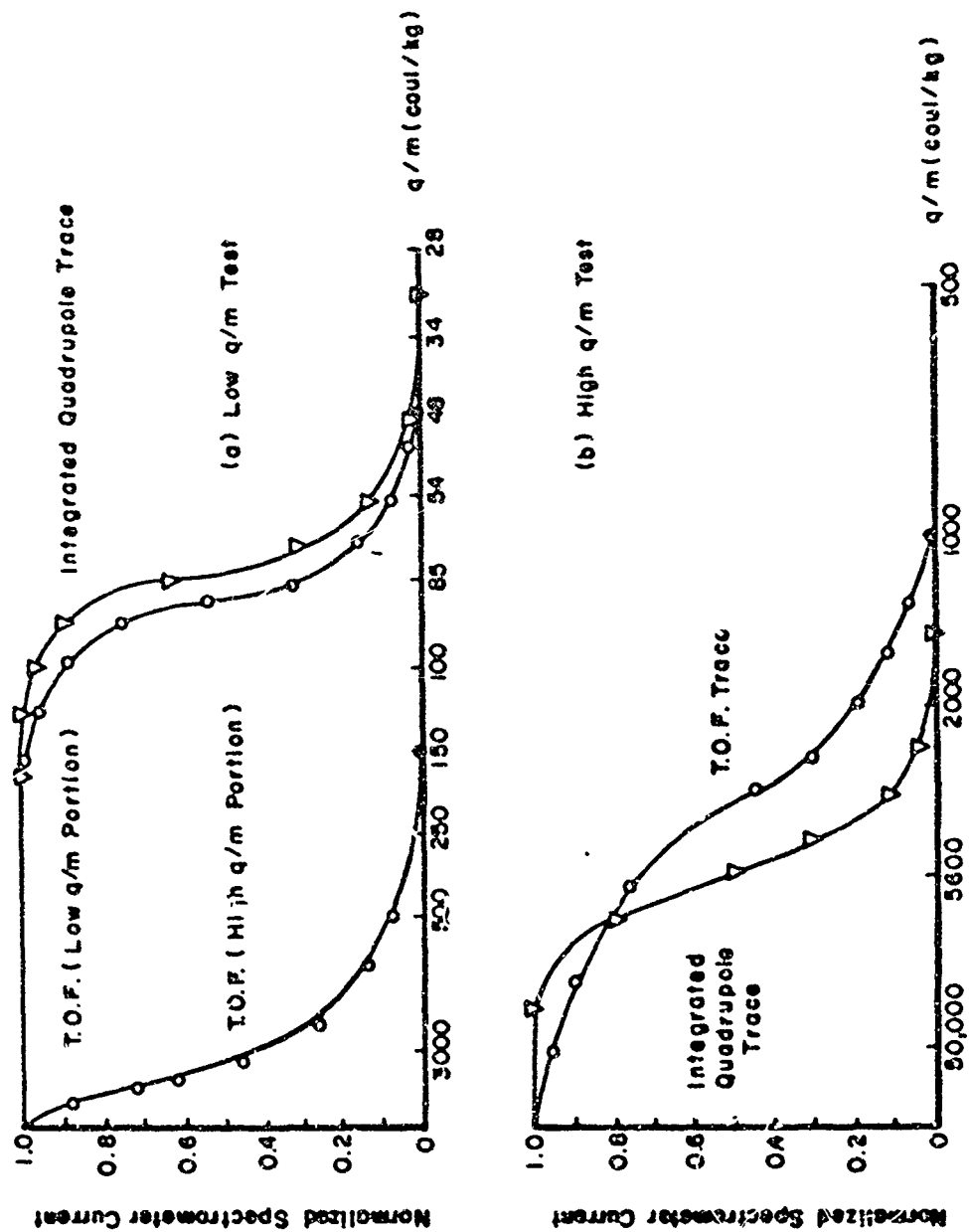


Figure 9. Massenfilter/T.O.F. Comparison

radiation. By careful shielding and judicious design of leads, this time can usually be reduced to the order of microseconds. Although it is not possible to measure atomic ion species with drift distances on the order of 10-30 cm, their presence can be detected by noting the position of the start of the decay relative to  $i_0$ . If there are no fluctuations in  $i_0$  and if the decay cannot be extrapolated back to  $i_0$ , then that portion of the current between the start of the decay and  $i_0$  was probably contributed by ions having very high specific charges that reached the collector during the spectrometer's "dead-time." At a sacrifice of trace resolution, the CRT beam intensity can be increased to observe this instantaneous drop when ions are present. This mode is particularly useful when the collector current is fluctuating, since it shows the actual value of  $i_0$  at the beginning of the decay.

Considering the many unknowns in the operation of the time-of-flight spectrometer, e.g., the effect of the decaying capillary potential on the steady state specific charge distribution, the spectrometer "dead-time," etc., one might well inquire as to the accuracy and reliability of data obtained with this instrument. It was primarily to answer this question that this laboratory constructed the combined quadrupole and time-of-flight spectrometer facility described below. The results of a series of investigations with the combined spectrometers demonstrated good quantitative agreement between the quadrupole and the time-of-flight device (Reference 3). Figure 9a shows a low average specific charge quadrupole trace that was transformed into a T.O.F. decay and superimposed on an actual T.O.F. decay made during the recording of the quadrupole data. A similar process has been carried out in Figure 9b for a beam with a much higher average specific charge.

The above analysis was made by simply comparing the  $I$ -versus- $q/m$  data obtained with the quadrupole with the  $I$ -versus- $t$  data of the T.O.F. spectrometer. More precise studies with the two instruments raise the question of the meaning of "peaks" as they are obtained with each device. This problem is particularly apparent in the interpretation of T.O.F. or quadrupole data for propulsion purposes, as shown in Section VI. In this case, it is necessary to obtain the two mass-weighted averages of specific charge,  $\langle c^{1/2} \rangle$  and  $\langle c \rangle$ , which are found by integrating the normalized mass distribution expressed as a function of specific charge,  $f(c)$ :

$$\langle c^{1/2} \rangle = \int_0^\infty c^{1/2} f(c) dc \quad (13)$$

$$\langle c \rangle = \int_0^\infty c f(c) dc \quad (14)$$

A problem arises in that neither the quadrupole nor the time-of-flight spectrometer gives  $f(c)$  directly. For the quadrupole, the number of cycles executed by a particle in the field is related to the quadrupole resolution. Using the empirical relationship determined by Paul in Reference 1, Hunter (Reference 4) obtained an expression for the bandwidth  $\Delta c$  of a quadrupole at specific charge  $c$  in terms of the measured resolution,  $R_q$ , and rail voltage. From this expression, it is found that the bandwidth of the spectrometer increases linearly with specific charge as a specific charge scan is made. To obtain the mass distribution function  $f(c)$ , one must divide the quadrupole current,  $i_q$ , by the bandwidth (to obtain the spectrometer current per unit specific charge); this is in turn divided by the specific charge,  $c$ , at each

point (yielding the mass flow per unit specific charge) and finally, for normalization, by the total mass flow,  $\dot{M}$ , of the sampled particles. Thus

$$f(c) = \frac{i_q}{\dot{M} c (\Delta c)} \quad (15)$$

where

$$\dot{M} = \int_0^{\infty} \frac{i_q}{c (\Delta c)} dc$$

In order to obtain  $\langle c^{1/2} \rangle$  and  $\langle c \rangle$  from T.O.F. traces, Equations 13 and 14 are modified to obtain specific charge and  $f(c)$  in terms of time  $t$ . A current distribution function corresponding to the T.O.F. trace is defined:

$$f(t) = -\frac{1}{i_0} \frac{di}{dt} \quad (16)$$

where  $i_0$  is the current at time  $t = 0$  and  $i$  is the T.O.F. collector current at time  $t$ . If  $t_f$  represents the time at which the current becomes zero on the T.O.F. trace, then

$$i = \int_0^{t_f} f(t) dt,$$

and, integrating by parts,

$$\langle t^2 \rangle = \int_0^{t_f} t^2 f(t) dt = \int_0^{t_f} \frac{t}{i_0} dt = \sum_{n=0}^f \frac{t \Delta t}{i_0} \Big|_{t_n} \quad (17)$$

$$\langle t \rangle = \int_0^{t_f} t f(t) dt = 2 \int_0^{t_f} \frac{1}{i_0} dt = \sum_{n=0}^f 2n \frac{(\Delta t)^2}{i_0} \Big|_{t_n} \quad (18)$$

From Equations 17, 18, and 12, one obtains

$$\langle c \rangle = \frac{L^2}{2V \langle t^2 \rangle} \quad (19)$$

$$\langle c^{1/2} \rangle^2 = \frac{L^2}{2V \langle t^2 \rangle} \eta = \langle c \rangle \eta \quad (20)$$

where

$$\eta = \frac{\langle c^{1/2} \rangle^2}{\langle c \rangle} = \frac{\langle t \rangle^2}{\langle t^2 \rangle}$$

is the distribution efficiency of the beam.

In the case of a linear decay from  $t = 0$  to  $t_f$ , the decay trace has the following values:

$$\begin{aligned}\langle t \rangle &= \frac{1}{2} t_f \\ \langle t^2 \rangle &= \frac{1}{3} t_f^2 \\ \eta &= 0.75 \\ \langle c^{1/2} \rangle^2 &= (9/4) c_{\min} \\ \langle c \rangle &= 3c_{\min}\end{aligned}$$

where  $c_{\min}$  is the specific charge corresponding to  $t_f$ .

An actual point-by-point comparison of  $\langle c \rangle$  and  $\langle c^{1/2} \rangle^2$  as obtained by the quadrupole and time-of-flight spectrometer is hardly worthwhile since the quadrupole samples only a small portion of the beam while the T.O.F. presents data representing the net beam characteristics. For this reason, the quadrupole is usually limited to studies of such parameters as the ionic species existing in a beam while the T.O.F. is used to study the gross operating characteristics of the beam. A detailed study of the electrohydrodynamic spraying process requires both instruments.

The successful operation of a time-of-flight spectrometer demands careful attention to shielding of both the collector and leads. A collector assembly which proved quite satisfactory from both a shielding and maintenance standpoint is shown in Figure 10. The quadrupole adaptor and hole in the collector can be eliminated if only a T.O.F. spectrometer is to be constructed. Biasing of the collector and frequency compensation have been successfully accomplished using the scheme of Figure 11. The compensating circuit is checked by applying a square wave signal to the collector and ascertaining that there is no distortion or attenuation of the signal at the oscilloscope as  $R_v$  is varied. The 10k precision resistor provides an input at the scope of 1 millivolt per 0.1  $\mu$ A of current at the collector. This value seems to provide an optimum compromise between noise level and sensitivity.

The value of load resistance required between the power supply and the spark gap depends on the power supply. If the latter is well regulated and can handle surge current, resistances on the order of a few hundred thousand ohms can be used. If the supply is small and not well regulated, however, it is best to use a high resistance. The scope is triggered at the start of the T.O.F. decay by placing a small length of wire near the spark gap and connecting it to the trigger input of the oscilloscope.

To use the quadrupole spectrometer to best advantage, some means must be provided for aiming the beam of droplets into the quadrupole entrance aperture. An adjustable source mount, evolved over a period of several years, is shown in Figure 12. Alignment is checked by removing the quadrupole collector and using a telescope to sight on the capillary tip. The complete combination quadrupole/time-of-flight spectrometer is shown in Figures 13 and 14. The y-axis of the x-y recorder is connected to the electrometer which measures quadrupole collector current. The x-axis is driven by the voltage between the wiper arm and ground of a potentiometer connected to the variable capacitors of the quadrupole oscillator. This arrangement allows a continuous  $I$ -versus- $f$  plot to be made.

The fluid reservoir and transfer line are simple but rugged and reliable. A half-filled 100 ml filtration flask provides a more than adequate supply of fluid for most purposes. The transfer line is made from glass tubing, 8 mm in diameter with a 2 mm bore. The connection between the transfer line and the capillary mount is made with Teflon tubing of sufficient length to allow for rotation of the source through an angle of 90° from the quadrupole axis.

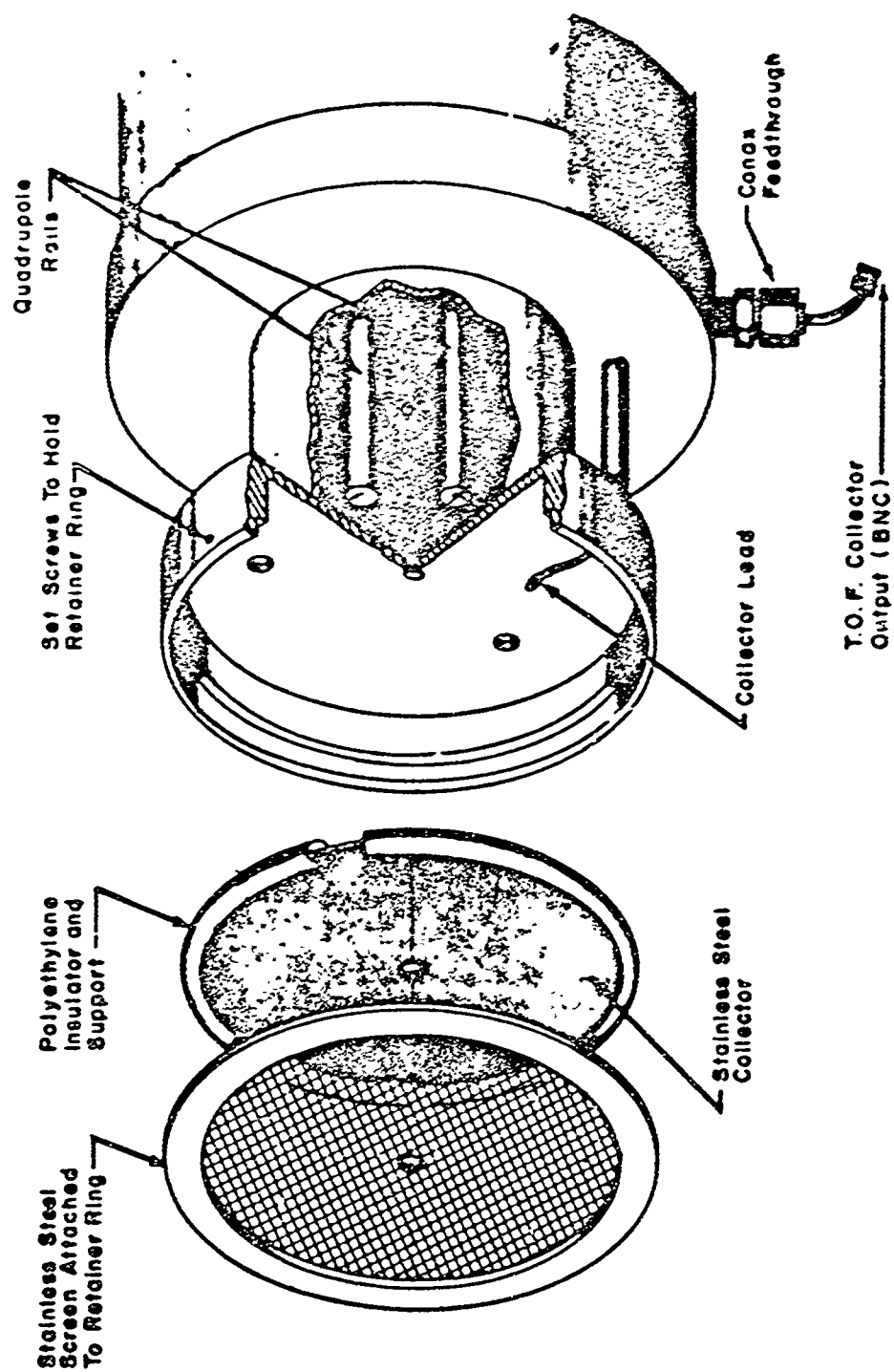


Figure 10. T.O.F. Collector Housing and Quadrupole Adapter

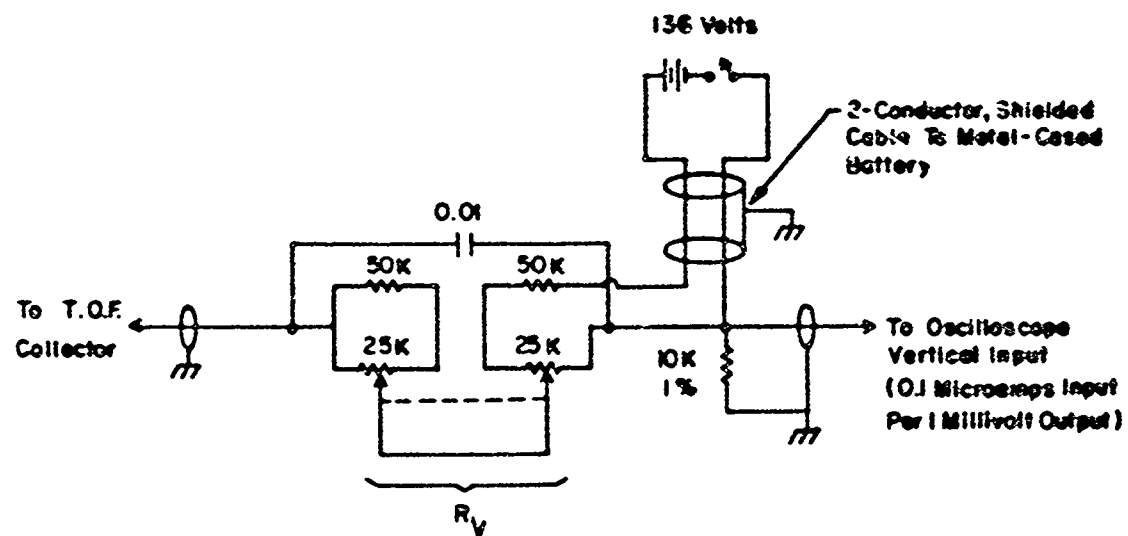


Figure 11. Variable Bias Circuit for T.O.F. Collector

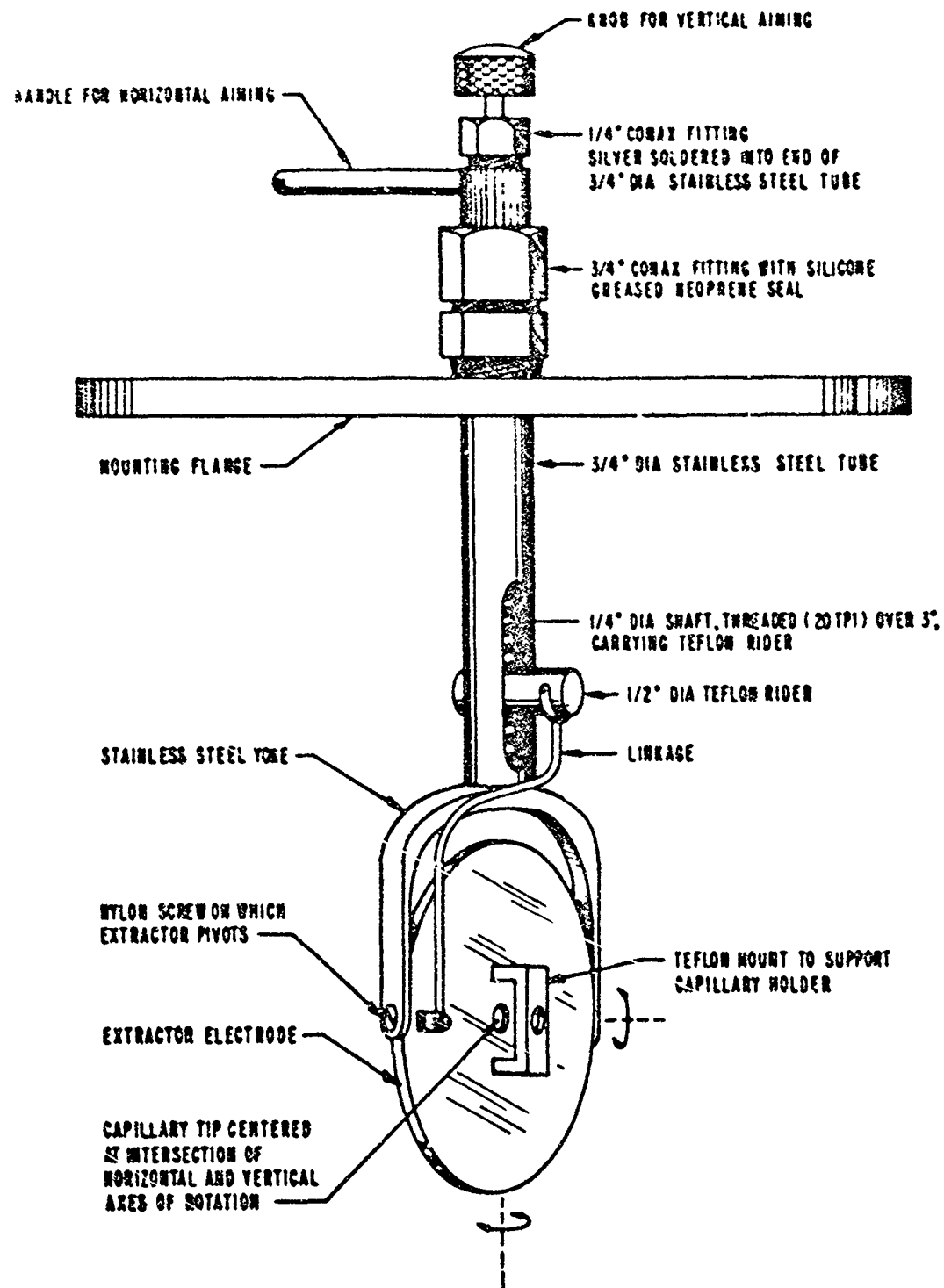


Figure 12. Adjustable Source Mount

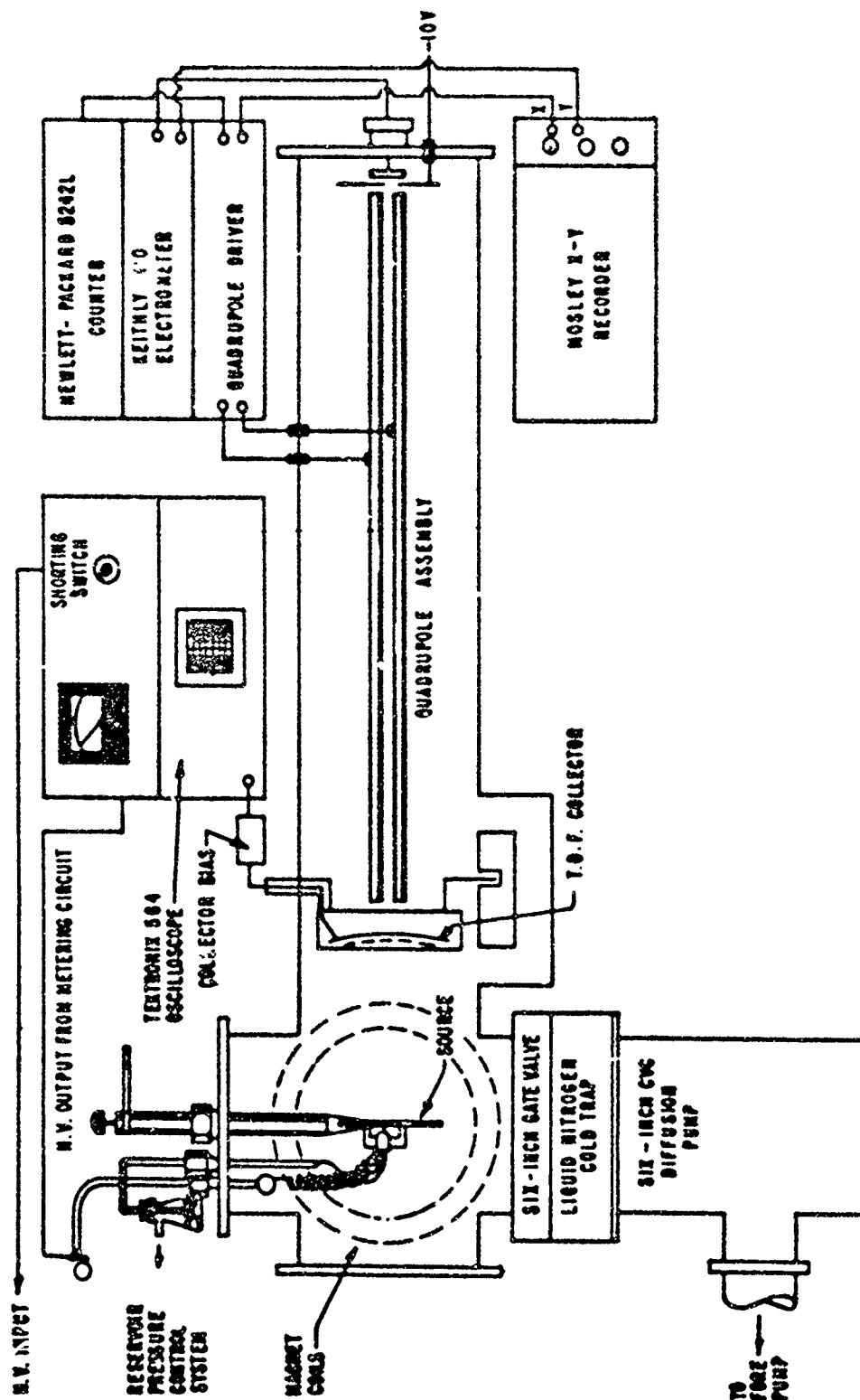


Figure 13. Schematic Illustration of Combined Quadrupole and T.O.F. Spectrometer Facility



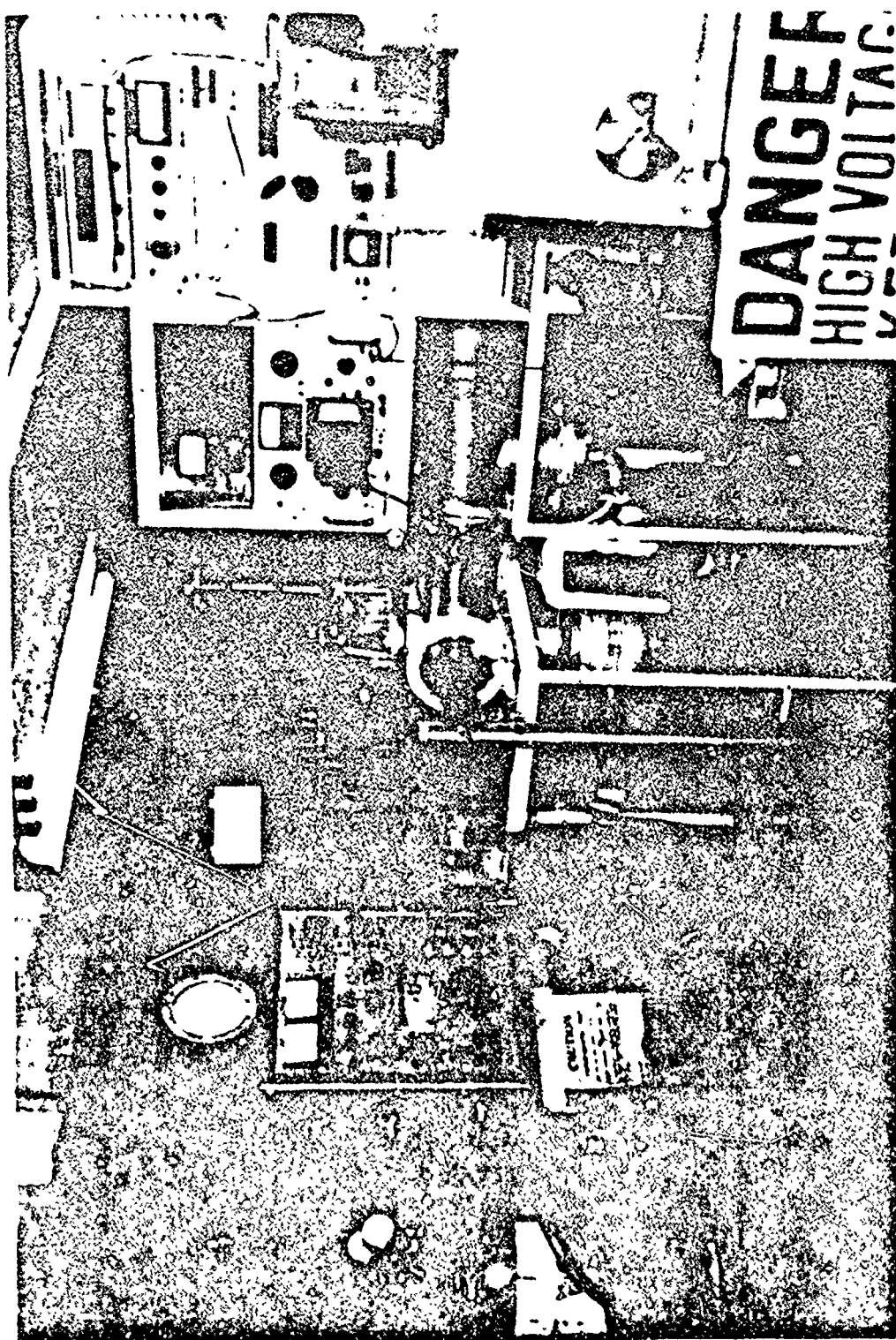


Figure 14. Combined Quadrupole and T.O.F. Spectrometer Facility

After the source chamber, reservoir, and transfer line are sufficiently evacuated, the flask containing the fluid is raised so that the tip of the short arm of the transfer line lies about 1 cm below the fluid level. The reservoir pressure is then raised to about 5 or 10 cm, causing the fluid to flow through the transfer line into the capillary. The mass flow rate of the fluid during operation is controlled by varying the reservoir pressure.

### 3. THE FARADAY DETECTOR

The third device which has been used in charged-droplet studies is the Faraday Detector (Reference 5). This device consists of a cylinder about 5 mm long and 1 mm in diameter mounted inside a shield and connected through a cathode follower to an oscilloscope (Figure 15). As charged droplets pass through the cylinder, approximately rectangular pulses are produced, from which the charge and mass of the droplet can be determined. If the gain and capacitance of the cathode follower and scope preamp are  $G$  and  $C$ , respectively, then the pulse height,  $V_0$ , is related to the charge  $q$  on the droplet by

$$q = CV_0 / G \quad (21)$$

If the accelerating potential of the droplet is  $V_a$ , the length of the cylindrical detector is  $d$ , and the pulse length is  $t$ , then the specific charge  $q/m$  of the droplet is

$$q/m = d^2 / 2 V_a t^2 \quad (22)$$

If the density  $\rho$  of the droplet is known, Equations 21 and 22 can be solved to determine the droplet radius, i.e.,

$$r = \left( \frac{3 V_a t^2 C V_0}{2 \pi \rho d^2 G} \right)^{1/3} \quad (23)$$

This detector is affected by background noise, and so its use is rather limited. The minimum charge that can be detected by this device is something on the order  $10^{-16}$  coulombs. In addition, we have found that the detector becomes clogged with fluid rather quickly when placed in a droplet beam of low specific charge.

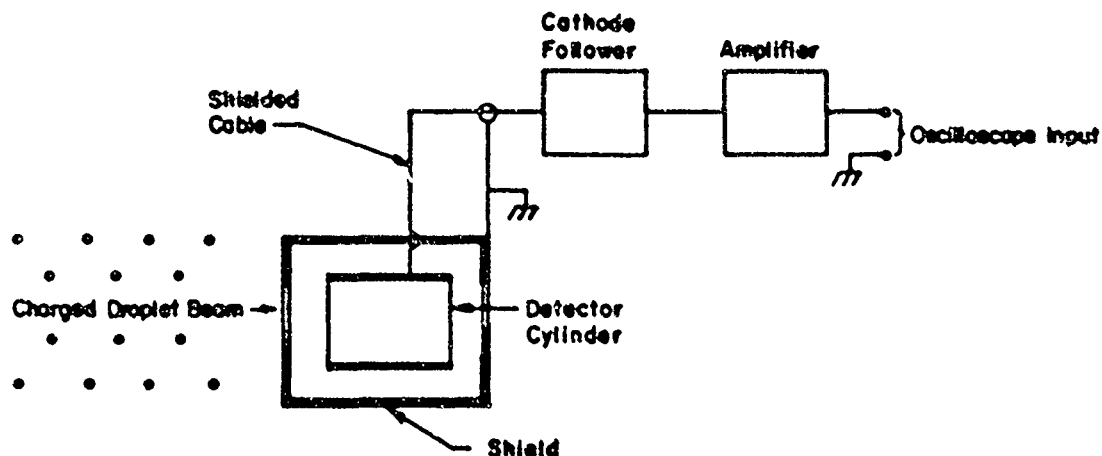


Figure 15. Faraday Detector Schematic

### SECTION III

#### CAPILLARY AND FLUID PREPARATION

Two of the major variables in the electrohydrodynamic spraying process are the capillary and the fluid sprayed. Of these, the capillary represents the primary source of difficulty, in both preparation and reproducibility. Although some work has been performed using glass and quartz tubes, (References 2, 5), by far the best results have been obtained with metallic capillaries (References 4, 6); platinum and stainless steel have been used most frequently. A prime requirement for these capillaries is that they be relatively smooth and axially symmetric. Capillary size is governed primarily by the vacuum system capabilities. A typical six-inch diffusion pump station with  $LN_2$  trap will handle most doped glycerol solutions in capillaries having bore diameters up to about 1/4 mm. Most of the work at AFAPL has employed capillaries with a bore of about 0.1 mm.

The capillaries are cut to length (~4 cm) from commercially available stock, and the tips are formed and polished by hand in an instrument lathe. The most satisfactory procedure for preparing the tips has been to machine the tip to roughly the configuration desired and then finish the surface with an orangewood stick impregnated with jeweler's rouge. During the polishing process, a wire must be run through the capillary occasionally to keep it from becoming plugged with rouge fragments. With softer metals such as platinum, it is sometimes necessary to finish the polishing with a light oil and rouge mixture on the stick.

After polishing, the capillary must be flushed thoroughly with acetone or similar solvent to remove rouge particles. The standard procedure in this laboratory has been to flush the capillary, boil it in distilled water, and rinse it in methyl alcohol. Following the cleaning procedure, the capillary is mounted in the source assembly and installed in the vacuum system. The capillary is usually maintained at 10kv for some time prior to spraying.

Different tip shapes have been tried by various researchers (References 3, 5, 7, 8). In general, a sharp tip will produce beams of higher specific charge than blunt tips. The sharp tips are more subject to deterioration during operation, however, and produce beams that are harder to control.

The location of the capillary tip relative to the extractor plane does not appear to be particularly critical. If the extractor plane is biased negative relative to the chamber walls to prevent secondary electrons from reaching the capillary tip, it is best to place the tip flush with the front surface of the plate.

The fluid, after mixing, is usually filtered through a 0.8 millipore filter and then outgassed by heating in vacuo at about 80°C for one or two hours. Following this, some or all of the properties are measured, including resistivity, density, viscosity, and PH. The sample to be sprayed is again outgassed at 80°C in vacuo. Immediately before transferring the flask and fluid to the experimental system, while the fluid is still rather warm, the pressure in the flask is raised to one atmosphere by introducing an inert gas such as argon. The flask is then quickly transferred to the system and re-evacuated. With a small bore capillary and a good  $LN_2$  trapped diffusion pump on the system, the entire procedure can be carried out while the source chamber is evacuated.

## SECTION IV

## SOME EXPERIMENTAL RESULTS

The spraying process is initiated in the following manner: After the preliminary steps have been completed, the fluid is allowed to flow through the transfer line to the capillary. The arrival of the fluid at the capillary tip is observed by means of a small telescope. If the fluid has been properly outgassed, a small drop will form at the tip and gradually increase in size. Any evidence of bubbles or other unusual activity at this point is an indication of entrapped gas. (Experience has shown that this condition invariably results in poor source operation, e.g., sparking, broad specific charge distributions, etc.) If a clear stable drop appears, however, the capillary potential is increased until the droplet is removed and spraying begins. The capillary is usually allowed to operate at this potential for about 30 minutes to allow the source to "break in." This break-in period permits that initial portion of the fluid, which may have picked up dirt or other contaminants from the transfer line, Teflon tube, and capillary, to pass out of the system before operation begins.

After the break-in procedure, the capillary potential can be varied over a wide range, providing a number of interesting spray modes. Following Cohen (Reference 2), we can classify these modes into three general categories, as follows:

2. Mode I. This is the mode that occurs at the onset of spraying and at slightly higher potentials. With a suitable telescope or microscope, one can observe a drop of fluid going through the formation and ejection cycle pictured in Figure 16. Typical current pulses corresponding to this mode are presented in Figure 17. These data were obtained by allowing the charged droplets to strike a collector arranged as in Figure 7. However, many different pulse patterns have been observed. For a given reservoir pressure, increasing the capillary potential generally results in decreasing the pulse length and pulse period. At a given capillary potential, however, varying the reservoir pressure affects the pulse amplitude and length, very little but increasing the reservoir pressure induces the pulse period considerably.

This spraying mode has been investigated in detail by Carson (Reference 9), who showed that each pulse is composed of a multitude of small charged droplets. By allowing the droplets to pass through a variation of the Faraday Detector, described previously, he was able to show that the charge on the droplets was greatest at the peak of the current pulse (Figure 18).

The spraying appears to take place continuously from the tip of the filament. As the length and radius of the filament change, one would expect to find the charge and mass of the emitted droplets undergoing a corresponding change, due primarily to variation in the charge density and hydrodynamic stability of the filament. Using a time-of-flight mass spectrometer, Carson verified this and found that, in general, the specific charge spectrum itself varied from pulse to pulse, and that the sprayed droplets had higher specific charges at the beginning and end of the pulses than at the peaks. This information, coupled with his observation that the droplet charge is a maximum at the peak of the pulse, indicates that more massive droplets are generated during this portion of the pulse. Carson also observed a maximum spread of specific charge values at the peak of the pulse.

The pulses which characterize Mode I are extremely regular. This can be demonstrated by triggering the oscilloscope sweep on the initial positive-going part of the pulse and observing the pulse length and period. Only slight fluctuation is observed in pulse period and amplitude over a period of several minutes.

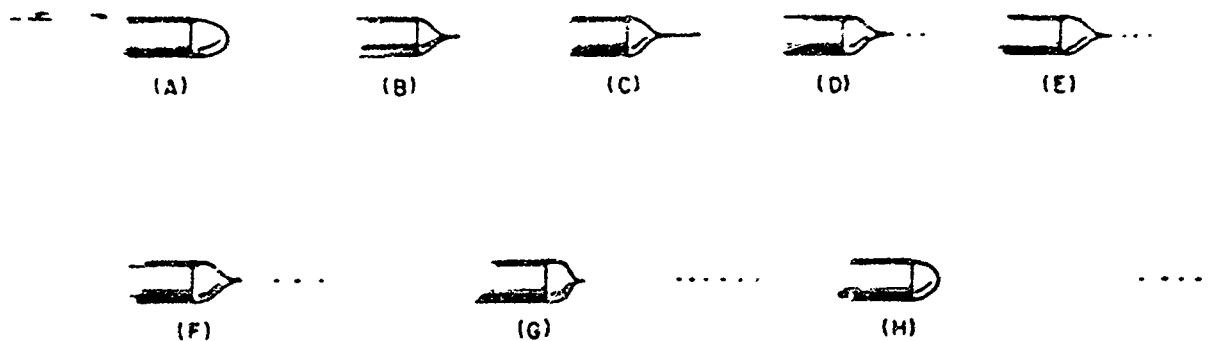


Figure 16. Mode I Spraying Sequences

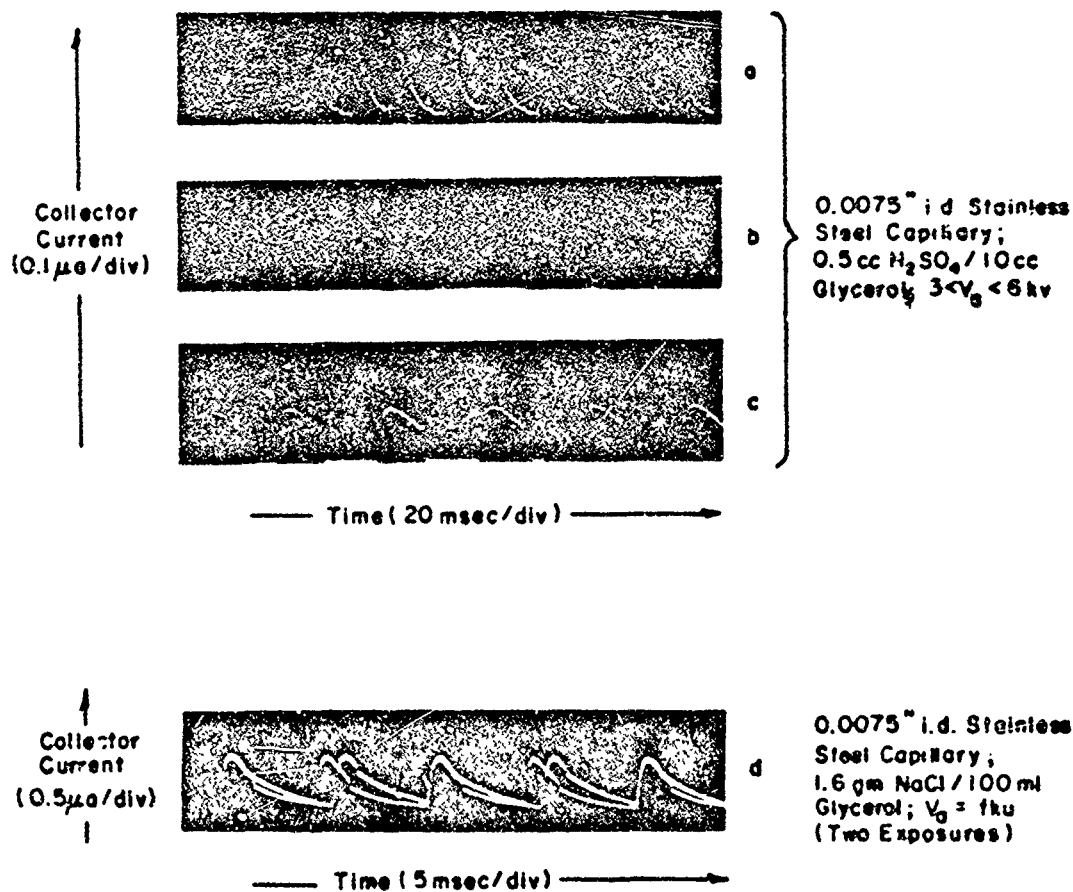


Figure 17. Examples of Mode I Spraying

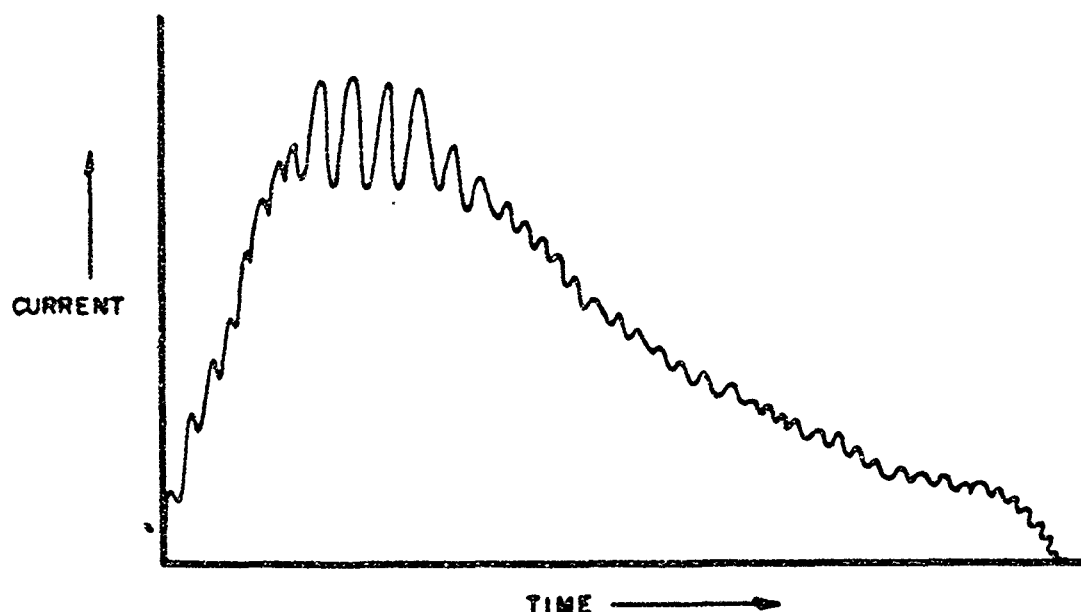


Figure 18. Current Contributions by Individual Droplets During a Pulse  
(From Reference 9)

b. Mode II. As the capillary potential is increased, the regularity of the pulsing often deteriorates, resulting in a collector current that consists of random noise at DC level (Figure 19). It is generally postulated that this mode is the result of a number of filaments operating in Mode I but independently of one another. Very little quantitative data is available concerning this mode.

c. Mode III. The most attention to date has been given to Mode III, or the so-called "DC mode," which is characterized by a steady emission of charged droplets at a constant current and specific charge distribution, (Figure 20). This mode is sometimes obtained directly from Mode I by increasing the capillary potential (Figure 21). On other occasions, it is possible to drive a Mode II beam into the DC mode by adjusting both the capillary potential and mass-flow rate. In some instances, usually with a damaged capillary or poor fluid, it is impossible to make a source operate in Mode III. Some solution/capillary combinations have proved capable of operating in this mode over a wide range of potentials without degenerating into Mode I or II.

Often a beam is referred to as DC even though there is some "noise" or pulsing present. Usually this labeling is limited to beams in which the pulse height is less than 10% of the DC current level. Figure 22a shows such a beam current. The presence of additional pulses on the DC level does not appear to adversely affect source operation. Figure 23 shows three superimposed T.O.F. traces of a pulsed + DC beam. A slight adjustment of either capillary potential or mass flow rate is sometimes sufficient to eliminate the pulsing.

The DC current observed at a collector placed in a beam operating in Mode III is the net result of the myriads of charged droplets produced by a number of filaments located on the periphery of the capillary tip. The individual filaments probably are spraying in a modified

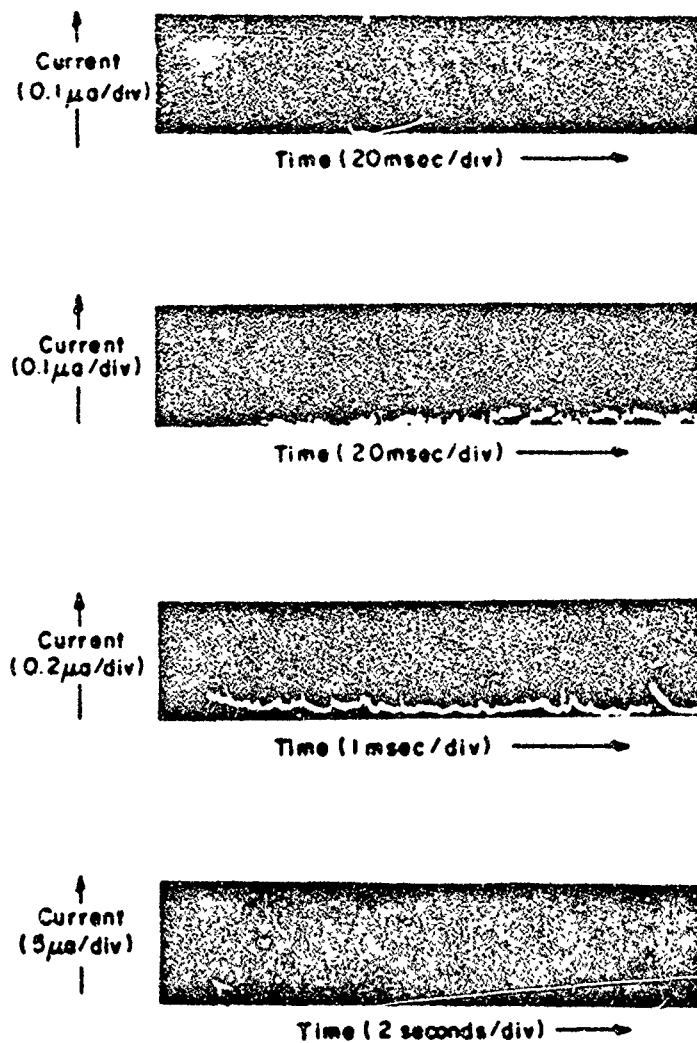


Figure 19. Examples of Mode II Spraying

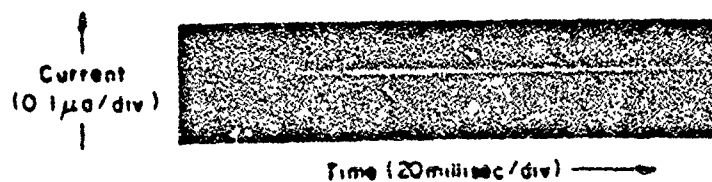


Figure 20. Mode III Spraying

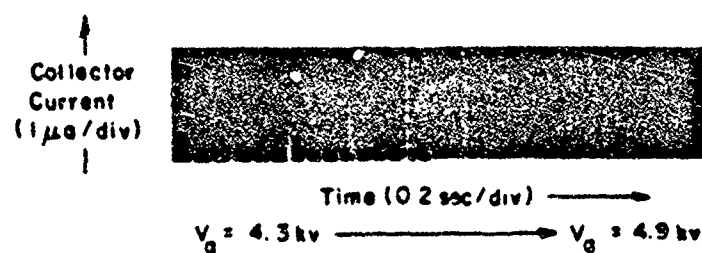


Figure 21. Mode I to Mode III Transition

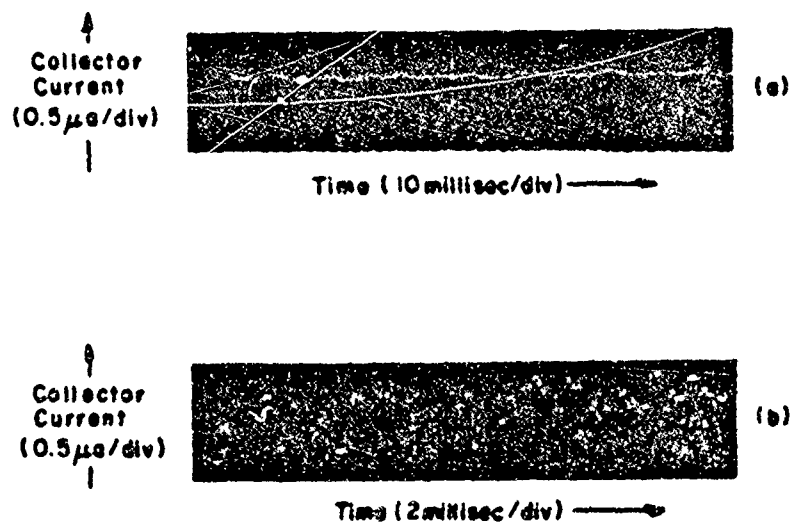


Figure 22. Modified Mode III Spraying



Mode I. Thus, Mode III is most likely a special case of Mode II in which the pulse frequency and the period of the various filaments are high enough to overcome the effects of phase difference. An indication of the number of filaments contributing to such operation can be obtained by observing the momentary fluctuations (Reference 10) in current which sometimes occur in an otherwise stable beam (Figure 14). The shape of this pulse indicates that, for some reason, a filament momentarily stopped spraying and then started again. If all the filaments are contributing roughly the same amount of current, then the magnitude of the current drop indicates that about a dozen filaments must be present.

One might reasonably assume that the DC spraying mode is the result of a delicate and perhaps fortuitous relationship between the source variables and that any external disturbance of the source would upset this relationship and lead to Mode I or II operation. However, this is not generally the case. Figure 25 shows three superimposed time-of-flight traces taken over a period of about two minutes. The fact that the capillary potential can be shorted to ground for a few milliseconds and then allowed to return rapidly to its original level without changing either the current or specific charge distribution of the beam gives an indication of the stability of the spraying mechanism. Furthermore, considering  $V$  as the potential at which the beam changes from Mode II to Mode III, it has often been observed that after Mode III operation has been obtained, the capillary potential can be lowered several hundred volts below  $V$  without the beam returning to Mode II. There is at the present no explanation available for this hysteresis effect.

One can often observe a beam operating in two modes simultaneously, usually in Mode III and Mode II, or in Mode III and Mode I. Occasionally two jets are observed to be spraying in Mode I simultaneously but out of phase with each other (see Figure 17d).

A fourth mode has been observed in electrohydrodynamic spraying wherein an electrical discharge takes place at the capillary tip (Figure 26). Little data is available on this mode simply because most investigators strive to avoid it. A source operating in this mode produces beams containing copious quantities of ions in addition to a broad distribution of low specific charge particles. Capillary erosion becomes severe in this mode, and in some cases the tip have been observed to glow red hot and even melt. One explanation that has been offered for this mode is that secondary electrons heat the capillary tip and increase fluid evaporation, which leads to a local high-pressure region in the vicinity of the capillary tip and subsequent electrical breakdown because of the high fields present. This same behavior is found in sources that are operated at negative potentials, however, indicating that the cause is most likely in the source itself. This mode of operation is detrimental to sources designed primarily for heavy particle generation, but it is interesting enough in itself to warrant more study than it has received.

Figures 27 and 28 show how specific charge and beam current vary as a function of capillary potential for a few solutions. The parameters corresponding to these curves are found in Table I. Plots of specific charge vs.  $V$  for the same solution at different reservoir pressures are presented in Figure 29. Figure 30 illustrates how the specific charge versus capillary voltage curve varies with solute concentration.

As can be seen from these graphs, the behaviour of a given source depends upon both the solute and the capillary from which it is sprayed; for example, curves A and D of Figure 27 are both generated from stainless steel sources with the same solvent and cation, yet the slope of A increases with increasing  $V_0$  while the slope of D decreases. This behaviour is most likely the result of a difference in anions in the two solutions. A similar circumstance exists in A and J of Figure 28. Here identical solutes were used in glycerol, but the capillary materials (stainless steel for A and Platinum for J) apparently caused the curve slopes to increase and decrease, respectively, with increasing voltage.

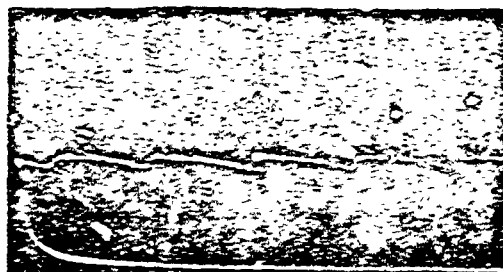


Figure 23. Superimposed T.O.F. Decays, Mode I and Mode III Beam

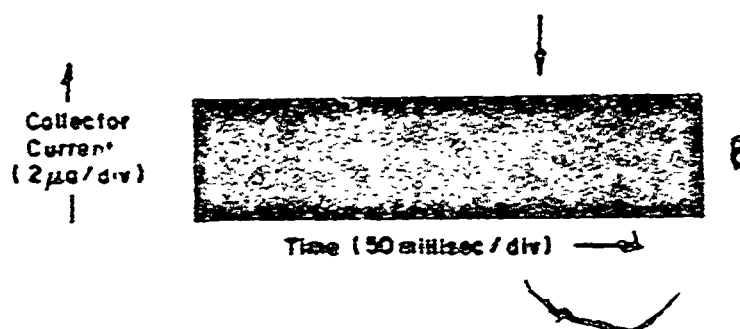


Figure 24. Momentary Current Fluctuation in Mode III

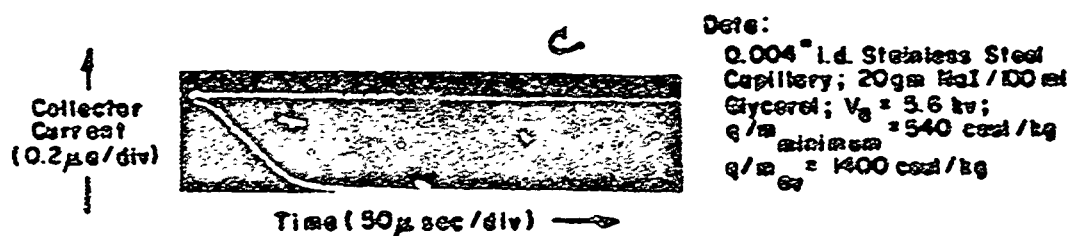


Figure 25. Three Superimposed T.O.F. Traces with Steady-State Currents, Taken Before and After Decays

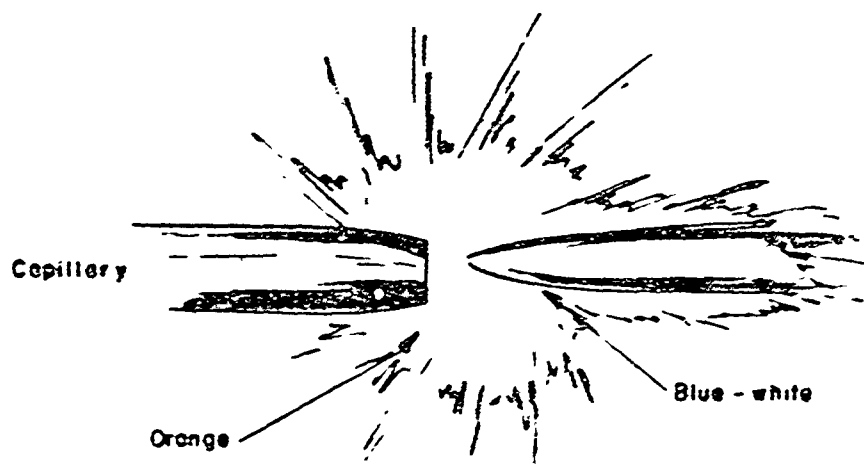


Figure 26. Discharge at Capillary Tip

Table I is a compilation of the results obtained from over two year's study of various fluids. The data presented under the heading "representative performance" indicates the best results that could be achieved consistently with the designated source/solution combination. Data marked with an asterisk is exceptional performance which, for one reason or another, could not be duplicated or was not typical of the source's usual operation. The specific details are described under the column headed "comments."

With the exception of  $H_2SO_4$ /glycerol, solutions which were found to perform well at positive capillary potential would not perform well at negative potentials and vice versa. Figure 31a shows that previously described transition of an NaI/glycerol solution from Mode I to DC as the capillary potential is increased. At negative potentials, however, the pulsed mode degenerated into an unstable combination of Mode II and IV (Figure 31b). Extended examination of NaI/glycerol revealed that this fluid was not capable of producing a DC beam at negative potentials. A possible explanation for this behavior is presented in detail in the following section.

It is interesting to observe the action of various solutions and operating conditions on the capillary. Figure 32a shows the tip of a stainless steel capillary with measurements of 0.32 inch o.d. and 0.0195 inch i.d., and with a 0.012 inch diameter wire inside it; pitting was noted after the capillary was operated at 15-20 kilovolts for several hours. The solution consisted of 3 ml  $H_2SO_4$ /100 ml glycerol. The cause of the pitting is not known.

Cohen has occasionally observed similar pitting on platinum capillaries. The 0.019 inch o.d., 0.004 inch i.d. platinum capillary tip shown in Figure 32b was operated for over 24 hours at both positive and negative potentials between 3 and 13 kv. A solution consisting of 1 gm NaCl in 100 ml tetraethylene glycerol was being sprayed. Figures 32c and 32d are before and after photos of a 0.012 inch o.d. and 0.006 inch i.d. stainless capillary which sprayed a 3 ml  $H_2SO_4$ /100 ml glycerol solution for about 40 hours. The capillary shown in Figures 33a and 33b are 0.019 inch o.d., 0.004 inch i.d. platinum machined to a 0.010 inch

long tip about 0.003 inch in diameter. This capillary is shown as it appeared after accumulating a total operating time of over 400 hours at positive potential with 20 gm NaI/50ml glycerol solutions. Although no deterioration of the tip was observed, several pits such as that shown in Figure 32c were found along the side of the capillary about 2 cm from the tip. This pitting may be due to secondary electrons emitted from the vacuum chamber walls. The tip probably remained undamaged because the extractor plate was operated at about 400 volts below ground to produce an electron potential hill in front of the capillary. Figure 33d shows a stainless steel capillary measuring 0.008 inch o.d. and 0.004 inch i.d. that became plugged with nickel after spraying a 10 gm  $\text{NiCl}_2 \cdot 6\text{H}_2\text{O}$ /50 glycerol solution for four days at a potential of -5 kilovolts.

The beams of charged droplets produced by the electrohydrodynamic spraying process are usually confined within a total angle of  $60^\circ$ . Quite often, the beam axis is found to lie at a small angle relative to the capillary axis; this is probably due to the capillary not being centered in the extractor electrode hole. It is not uncommon to find several distinct beams being produced simultaneously, resulting in a beam of hollow conical cross section. Figure 34 shows how such a beam "polished" an annular portion of a collector, leaving the center undisturbed.

Attempts to measure the specific charge distribution within the beam have not been very successful. Figure 35 shows a horizontal distribution measurement made with a time-of-flight spectrometer and a 20 gm NaI/100 ml glycerol solution being sprayed from a 0.003 inch o.d., 0.004 inch i.d. stainless steel capillary. These measurements were taken at a potential of 6 kv. Figure 36 is a similar distribution measurement made with a 15 gm NaI/100 ml glycerol solution and the quadrupole mass spectrometer. As shown, the general trend is for a beam to become more collimated at higher capillary potentials. Figure 37, made with the same source characteristics as Figure 36, shows how the distribution varies horizontally and vertically.

The specific charge versus collector current curves presented in Figures 38-40 show some of the specific charge distributions that have been obtained. Figure 38 shows a beam consisting predominately of ions. The peaks correspond to those produced by sodium ions surrounded by glycerol molecules. The difference between the experimental values of the peaks and the calculated values is indicated in per cent. Similar ion jets have been observed at negative potentials, as shown in Figure 40. Figure 39 shows the specific charge distribution of a jet containing both heavy particles and ions.

TABLE I  
PARAMETERS FOR CURVES IN FIGURES 27 AND 28

Curve	Solution	Source
A	15gm NaI/100ml Glycerol	.010"o.d. x .004"i.d. stainless steel; $P_R = 2^{\circ}\text{Hg}$
B	" "	.008"o.d. x .004"i.d. stainless steel; $P_R = 1^{\circ}\text{Hg}$
C	1.6gm NaCl/100ml Glycerol	.016"o.d. x .0075"i.d. stainless steel; $P_R = 1.5^{\circ}\text{Hg}$
D	" "	$P_R = 5^{\circ}\text{Hg}$
E	" "	$P_R = 10^{\circ}\text{Hg}$
F	" "	$P_R = 20^{\circ}\text{Hg}$
G	5ml $\text{H}_2\text{SO}_4$ /100ml Glycerol	.016"o.d. x .0075"i.d. stainless steel with .005 dia Pt. wire stuffing; $P_R = 4^{\circ}\text{Hg}$
H	0.78gm NaCl/100ml Tetra-ethyleneglycol	.019"o.d. x .004"i.d. platinum; $P_R = 2^{\circ}\text{Hg}$
I	0.35gm NaOH/50ml Glycerol	.008"o.d. x .004"i.d. stainless steel; $P_R = 0^{\circ}\text{Hg}$
J	20gm NaI/50ml Glycerol	.019"o.d. x .004"i.d. platinum; $P_R = 0^{\circ}\text{Hg}$
K	0.3ml $\text{H}_2\text{SO}_4$ /50ml Glycerol	.008"o.d. x .004"i.d. stainless steel; $P_R = 1^{\circ}\text{Hg}$ , $V_a$ negative
L	1.5gm $\text{MgCl}_2 \cdot 6\text{H}_2\text{O}$ /50ml Glycerol	.008"o.d. x .004"i.d. stainless steel; $P_R = 1.5^{\circ}\text{Hg}$ , $V_a$ negative
M	20gm $\text{ZnCl}_2$ /50ml Glycerol	.008"o.d. x .004"i.d. stainless steel; $P_R = 30^{\circ}\text{Hg}$ , $V_a$ negative

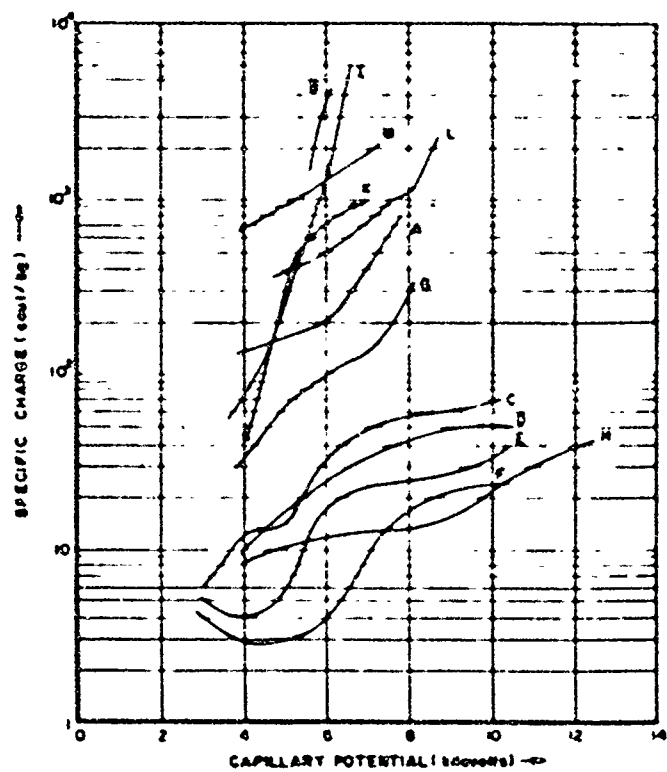


Figure 27. Specific Charge Vs. Capillary Potential

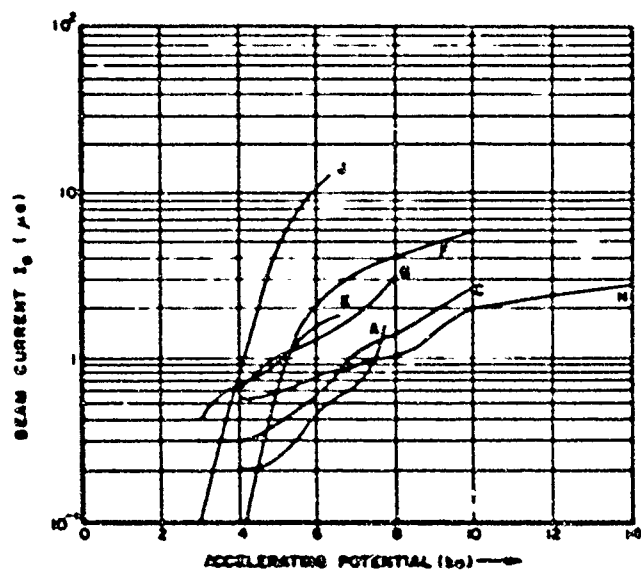


Figure 28. Beam Current Vs. Capillary Potential

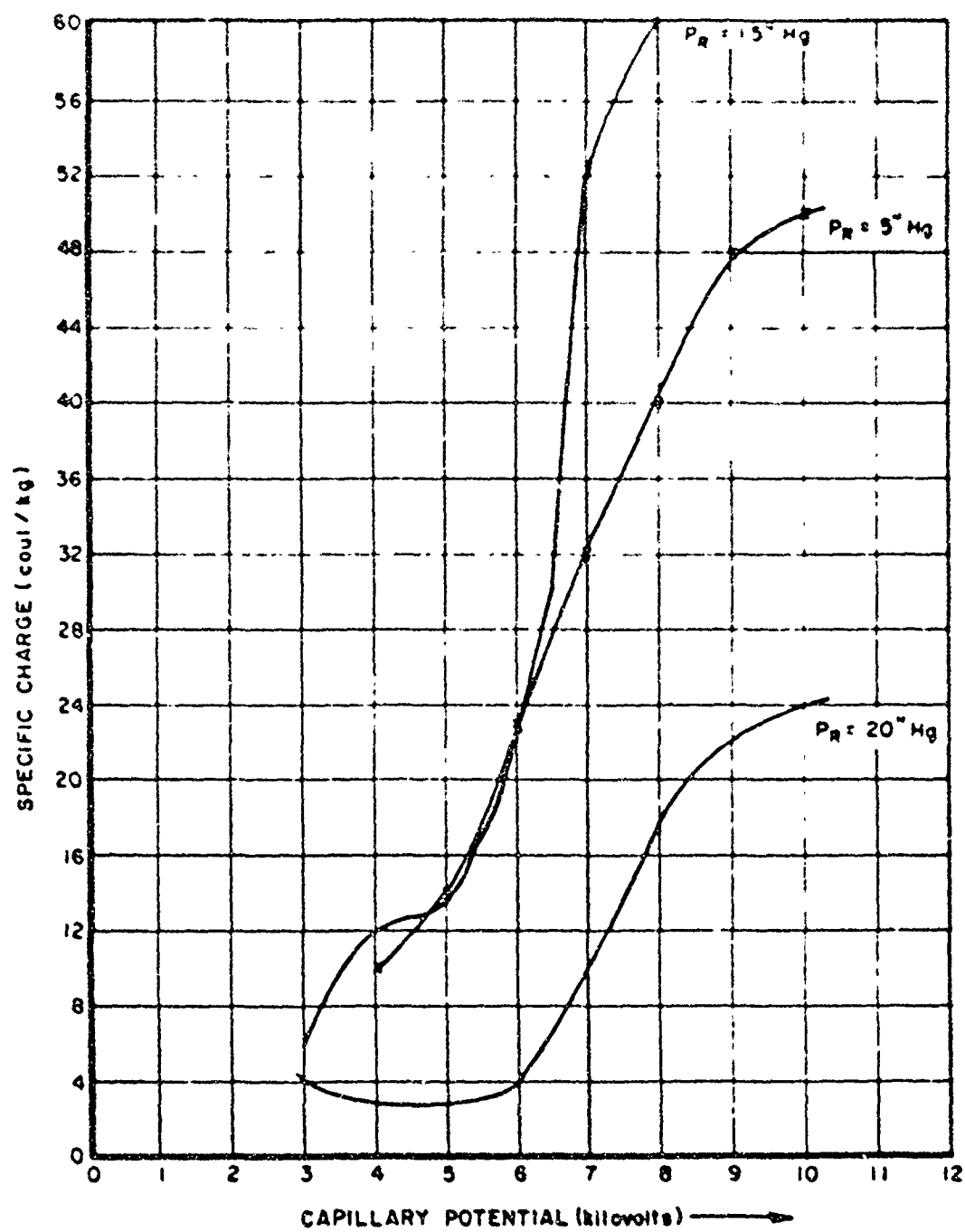


Figure 29.  $q/m$  Vs. Capillary Potential for Different Reservoir Pressures

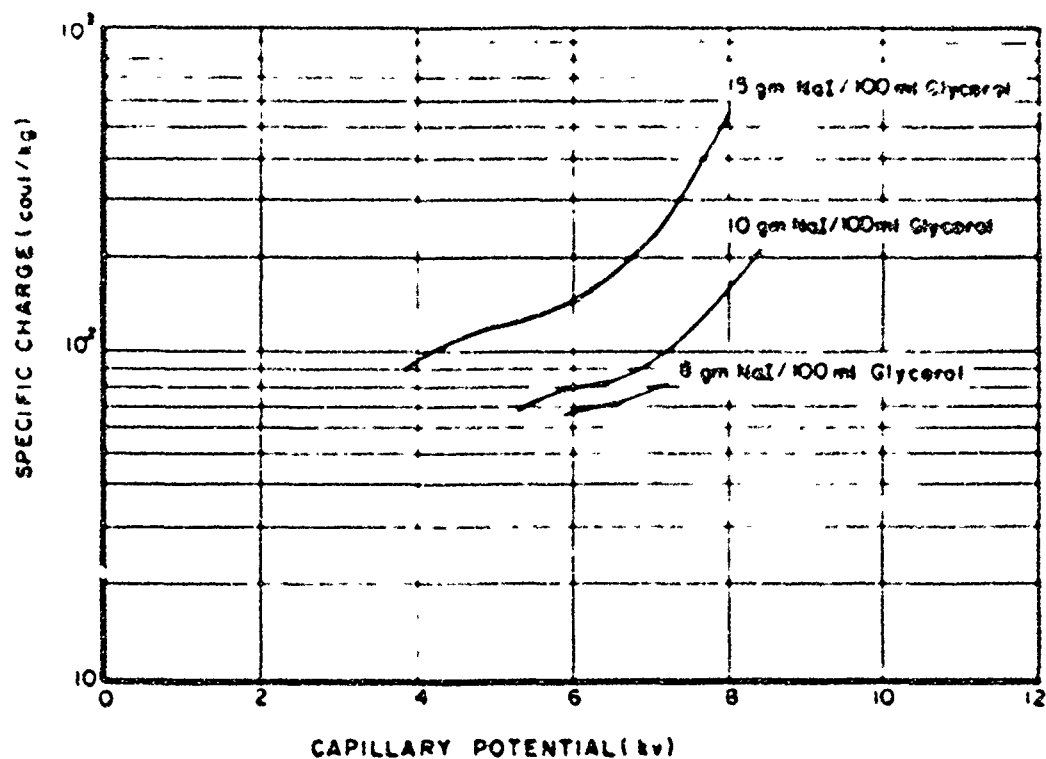


Figure 30.  $q/m$  Vs. Capillary Potential for Various Concentrations of NaI in Glycerol

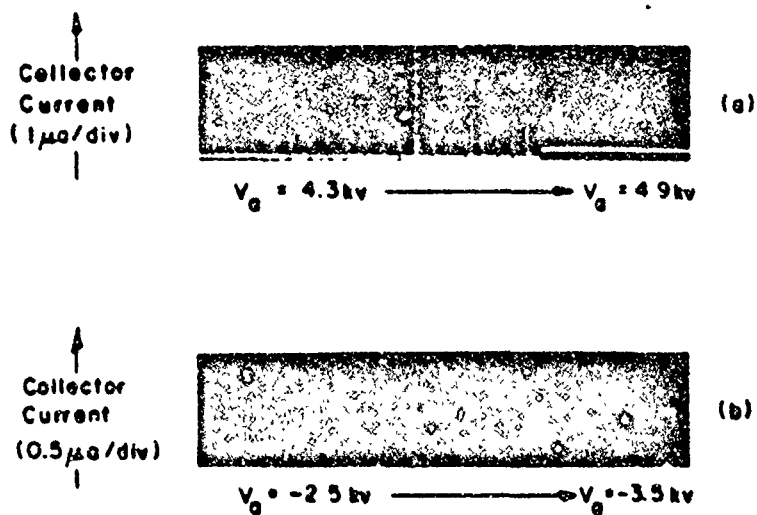


Figure 31. Transition Behavior of NaI/Glycerol Solutions at Positive and Negative Capillary Potentials

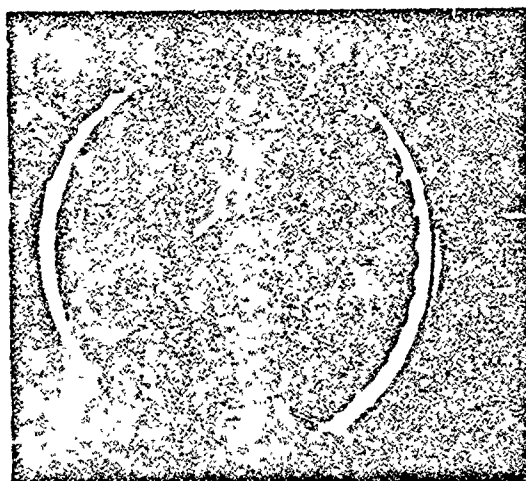


TABLE II  
SOLUTION/SOURCE COMBINATIONS  
EXAMINED IN THE HEAVY PARTICLE REFERENCE PROGRAM

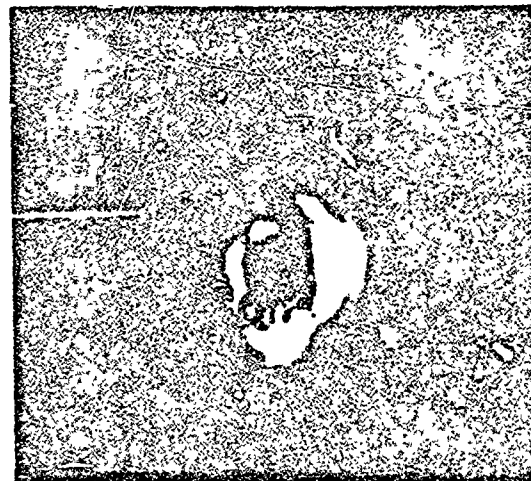
Solution Solids Solvent	Resistivity kil - cm at 30°C	Source Material o.d. x i.d. (mils)	Representative Performance				Comments
			$V_0$ (kV)	$I_0$ ( $\mu$ A)	$I_{scat}/I_0$ (count/kg)	$P_0$ ( $^{\circ}$ Rg)	
30gms NaI/ 100ml Glycerol	1.9 (at 33°C)	Stals. S. 8 x 4	+10 + 8.6 + 6 + 8.2	14.5 5.5 17 36	370 2850 35,000 <sup>a</sup> 55,000 <sup>a</sup>	1 0.5 2 3.5	Blunt, polished capillary Data taken after system ran over night
20gms NaI/ 100ml Glycerol	1.63	Stals. S. 8 x 4	+ 4.6 + 6	0.2 0.8	160 6400	3 1	
1gms NaI/ 100ml Glycerol		Stals. S. 10 x 4	+ 4.4 +10.0	0.1 0.9	25 150	5.75 10	
10gms NaCl/ 100ml Glycerol		Stals. S. 10 x 4	+ 4.4 + 5	1.6 4.5	760 1020	1.3 1.37	Not all NaCl went into solution
7gms NaCl/ 100ml Glycerol		Platinum 24 x 4	+ 4 + 7 + 4 + 7	0.5 0.75 0.75 1.2	12 16 6 9.5	0.5 0.5 5 5	
Polyposphoric Acid		Stals. S. 10 x 4	+ 3.3	10-25	$4 \pm 10^5$	10	Too viscous to control
.02ml Polyposphoric Acid/30ml Octoil		Stals. S. 10 x 4	+ 7.2 +10	0.1	5.5 ~50	16 16	
2ml Polyposphoric Acid/30ml Octoil		Stals. S. 10 x 4	+ 7 + 9.8	0.1 0.3	~1 60	5 1	
.3ml Polyposphoric Acid/30ml Tetraethylam Glycol		Stals. S. 10 x 4	+ 2.4 +10	~0.5 0.4	2 58	4 1	
1.5gms $HgCl_2$ + $6H_2O$ / 50ml Glycerol	14.5	Stals. S. 8 x 4	- 5 - 8.5	0.25 1.95	320 3000	6 6	
0.23ml $HNO_3$ (70%) 50ml Glycerol	9.4 at 28°C	Stals. S. 8 x 4	- 7.65	0.65	4000	0.8	
0.2ml $H_2SO_4$ / 50ml Glycerol	25 at 24°C	Stals. S. 8 x 4	- 7 - 4.6	0.3 0.2	31 26	8 1	No capillary erosion. Blunt tipped capillary.
0.2ml $H_2SO_4$ (96%) 50ml Glycerol	12.5 at 27°C	Stals. S. 8 x 4	- 4.1 - 8.3 - 5.2	0.1 1.8 1	45.2 1156 443	1 0.3 1	Thin rim capillary
2ml $H_2SO_4$ / 100ml Glycerol		Stals. S. 10 x 7.5 stuffed with 5 mil platinum wire	5 8 6	1 3.2 8	75 306 62	4 4 7	
18gms $Cr_2(28H_2)_3$ ( $HNO_3$ ) <sub>2</sub> + $24H_2O$ / 50ml Glycerol	12.6 at 31°C	Stals. S. 8 x 4	- 4 - 6 - 8 - 7.5 - 8.2	0.13 0.8 3.2 2.6 2.1	256 800 935 2150 <sup>a</sup> 2450	11 11 11 11 1.6	Semi-thin rim capillary
4gms $CrCl_3$ + $6H_2O$ / 50ml Glycerol	4.5 at 25°C	Stals. S. 8 x 4	- 4.3 - 2	1.1 ~1	170 >1000	34 5	Thin-rim capillary Intermittent pulsing
25gms $NaCl$ / 50ml Glycerol	50	Stals. S. 8 x 4	- 4 - 7 - 3	0.2 4 0.05	2500 2820 2645	10 30 8	Thin-rim capillary
20gms $CoCl_2$ + $2H_2O$ / 50ml Glycerol	40 at 40°C	Platinum 24 x 4	- 7.25 - 6.6	0.3 0.2	62 30	20 0.2	Tapered tip High peak of ~ 800 count/kg
0.5gms $NaCl$ / 50ml Glycerol	10	Stals. S. 8 x 4	7 6	0.3 0.2	920 700	1 2	

TABLE II (Continued)

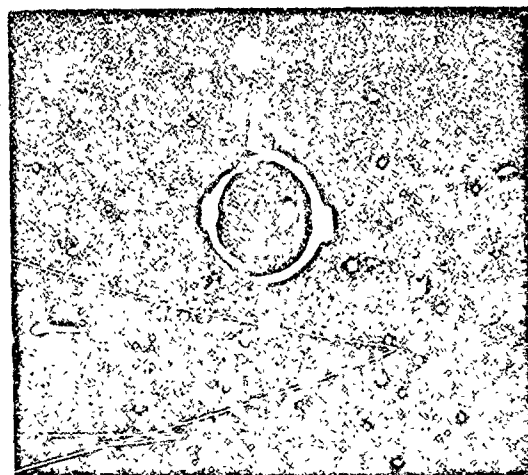
Solution Plate Solvent	Sensitivity hQ - cm at 30°C	Source Material a.d. ± i.d. (mils)	Representative $\alpha$ -values				Comments
			$\alpha_0$ (v)	$\alpha_1$ (v)	$\alpha_2$ (cm/hg)	$\alpha_3$ (%g)	
15gm $\text{CuCl}_2$ / 30ml Glycerol	87	Stale. S. 8 ± 4	- 3.7	0.04	—	8	Considerable spouting to Mode III
$\text{BaCl}_2$ /Glycerol	10.6	Stale. S. 8 ± 4	0 3.1	1.4 2	1000 1700	2 4	Inconsistent plateations
0.35gm $\text{BaCl}_2$ / 30ml Glycerol	3.88 at 22°C	Stale. S. 8 ± 4	0.5 5.0	1.4 2.3	1000 940	0 1.5	Very stable; good distribution
1.2gm Iodine/ 30ml Glycerol		Stale. S. 8 ± 4	-20	~ 1	—	30	
15gm $\text{BaCl}_2$ / 30ml Glycerol	10 at 64°C	Stale. S. 12 ± 6	+10 +16.3	0.7 1	200	3 5.4	
2gm $\text{LiClO}_4 \cdot 2\text{H}_2\text{O}$ / 30ml Glycerol	11.5	Stale. S. 8 ± 6	- 3.46 - 5	0.2 0.28	110 140	2 2	
10ml $\text{BaCl}_2$ /60ml Glycerol	11.5	Stale. S. 8 ± 4	- 5.5 - 5.5 - 7	3 2 3	43 240 1000	30 2 1.4	
10gm $\text{BaCl}_2 \cdot 6\text{H}_2\text{O}$ / 30ml Glycerol	12 at 235°C	Stale. S. 8 ± 4	- 3.3 - 3.4 - 5.4 - 6.2	0.1 0.23 0.4 0.3	260 400 1545 7000	3 3 2 2	Thin-rod capillary
5.55gm $\text{K}_2\text{S}_2\text{O}_8$ / 30ml Glycerol	1.8 at 33°C	Stale. S. 8 ± 4	0.5 8	0.2 1	~ 100 ~ 1000	1.5 7.7	Poor q/v distribution
8gm $\text{AgNO}_3$ / 30ml Glycerol	3.3	Stale. S. 8 ± 4	- 2.2 - 2	0.25 0.15	55 47	5 5	Spouting mode Mode III attainable at low $\alpha_0$ only.
8.9gm $\text{KNO}_3$ / 30ml Glycerol	25 at 23.5°C	Stale. S. 8 ± 4	- 0.5 -10	0.07 1.5-5	23 123	1 0.5	Slime capillary
15gm $\text{BaCl}_2$ / 30ml Glycerol	8	Stale. S. 12 ± 6	0	0.2	—	3	Mode III unattainable
30gm $\text{BaCl}_2$ / 30ml Glycerol	22.5 at 30°C	Stale. S. 8 ± 4	- 9	0.2	89	3	Electrons in heavy capillary badly suited to spray
4.4gm $\text{BaCl}_2$ / 30ml Glycerol	6.4 at 23°C	Stale. S. 8 ± 4	- 4 - 5	0.1 0.3	— —	1 0.5	Spouting $\alpha$ electrons
1.3gm $\text{Ba}(\text{NO}_3)_2 +$ $\text{BaSO}_4$ / 30ml Glycerol	14.5 at 23°C	Stale. S. 8 ± 4	- 4.4 -12 -15	0.1 0.45 ~ 1	30 > 100 —	~ 1 0.5	
Diethylphthalate/ Iodine		Stale. S. 8 ± 4	- 9 -13.5	1 1.4	36 60	0.75 0.75	
15gm Iodine/30ml Diethylphthalate	7.6 at 31°C	Stale. S. 8 ± 4	- 9 -18.25	0.8 > 20	150 ~ 10 <sup>3</sup>	0.8 0.5	
15gm $\text{CuCl}_2 \cdot 2\text{H}_2\text{O}$ / 30ml Tetraethylene Glycol	27 at 29.6°C	Platinum 24 ± 4	-12 - 7.8	1.1 0.25	230 ~ 95	3.4 3	
15gm Iodine/30ml Tetraethylene Glycol	23 at 25°C	Stale. S. 8 ± 4	- 2.1 - 9.5	0.2 1.4	16 300	0.9 1	



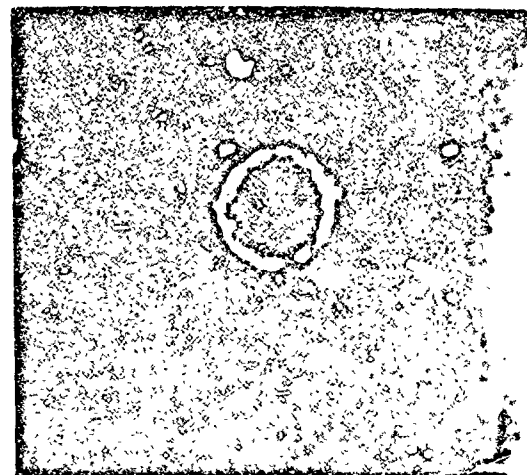
(a)



(b)

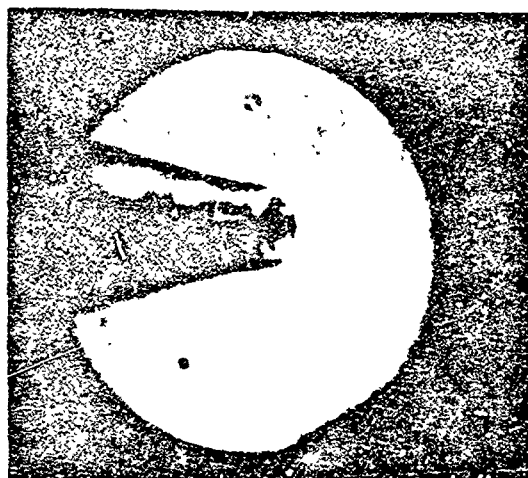


(c)

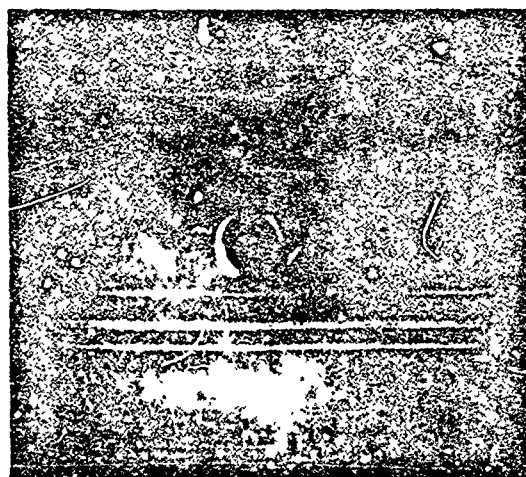


(d)

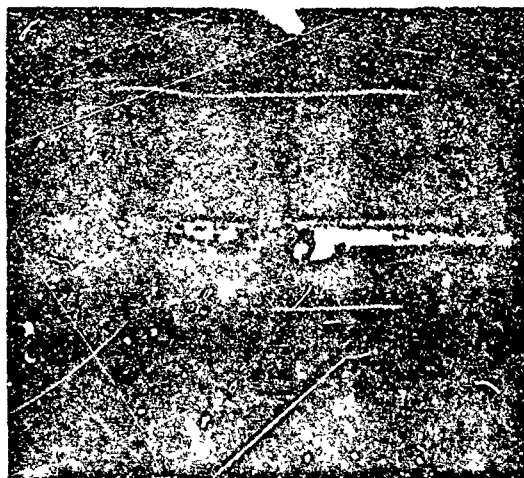
Figure 32. Capillary Tip Deterioration



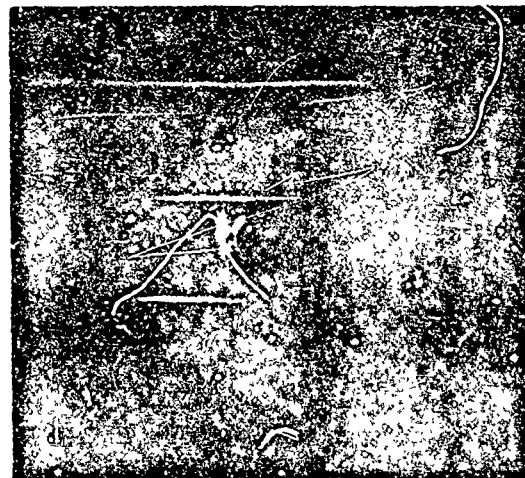
(a)



(b)



(c)



(d)

Figure 33. Capillaries After Extended Operation



Figure 34. Erosion Pattern on T.O.F. Collector After Extended Operation

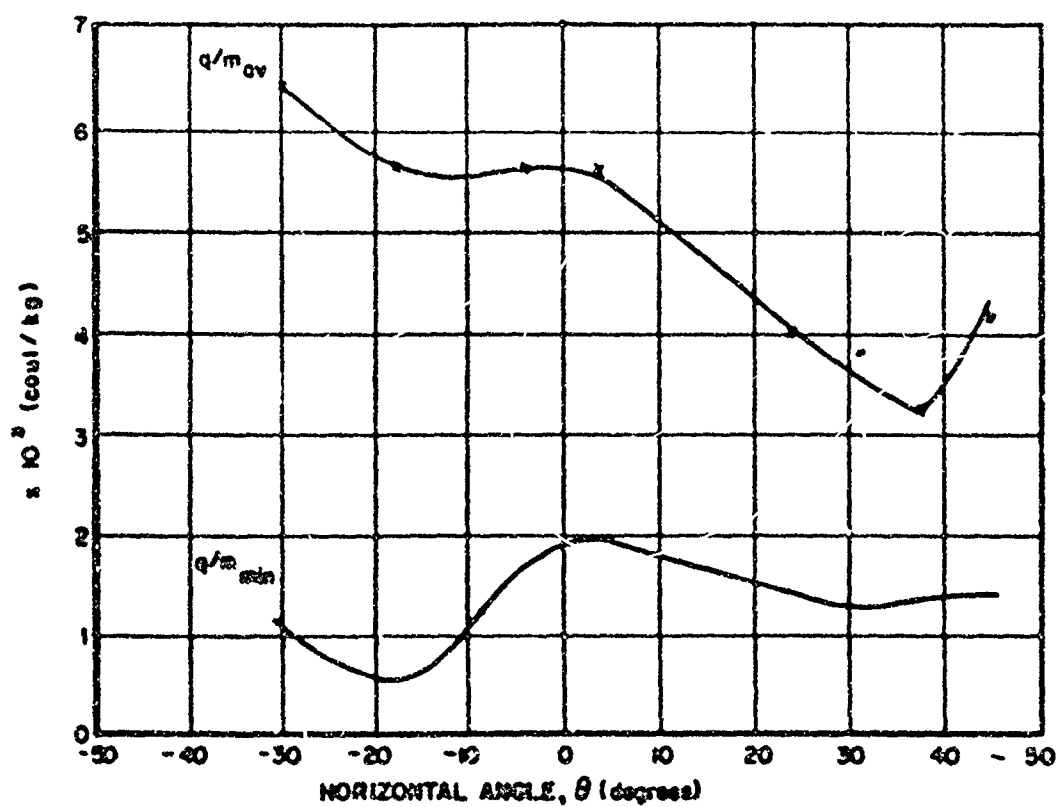


Figure 23.  $q/m$  Variation with Horizontal Angle

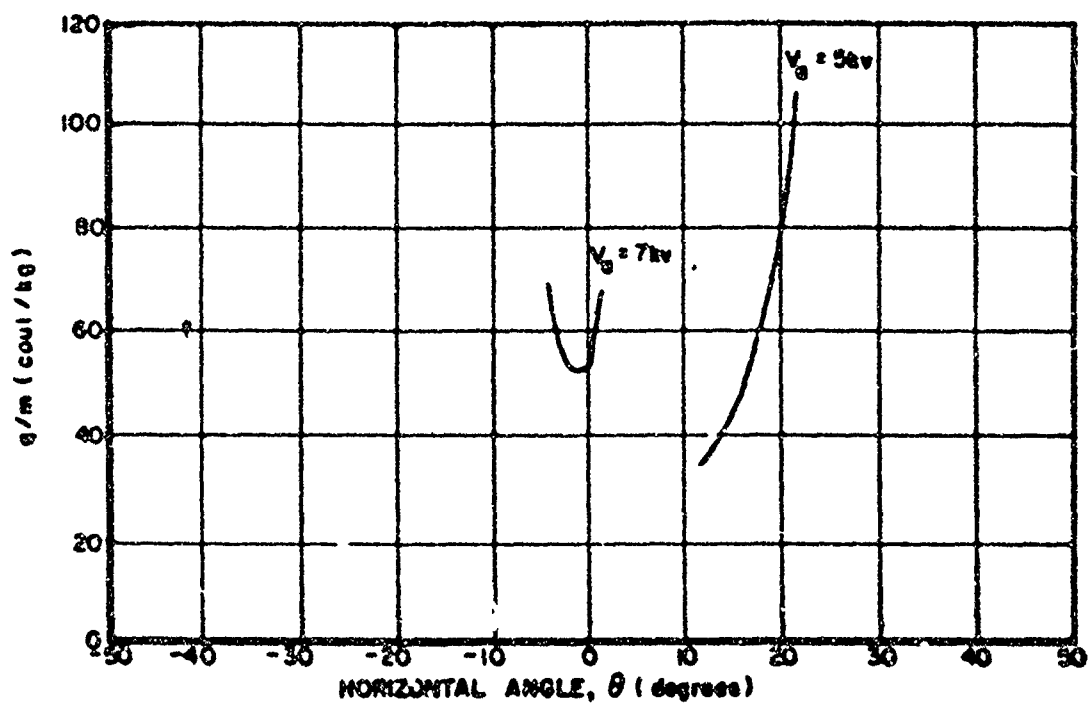
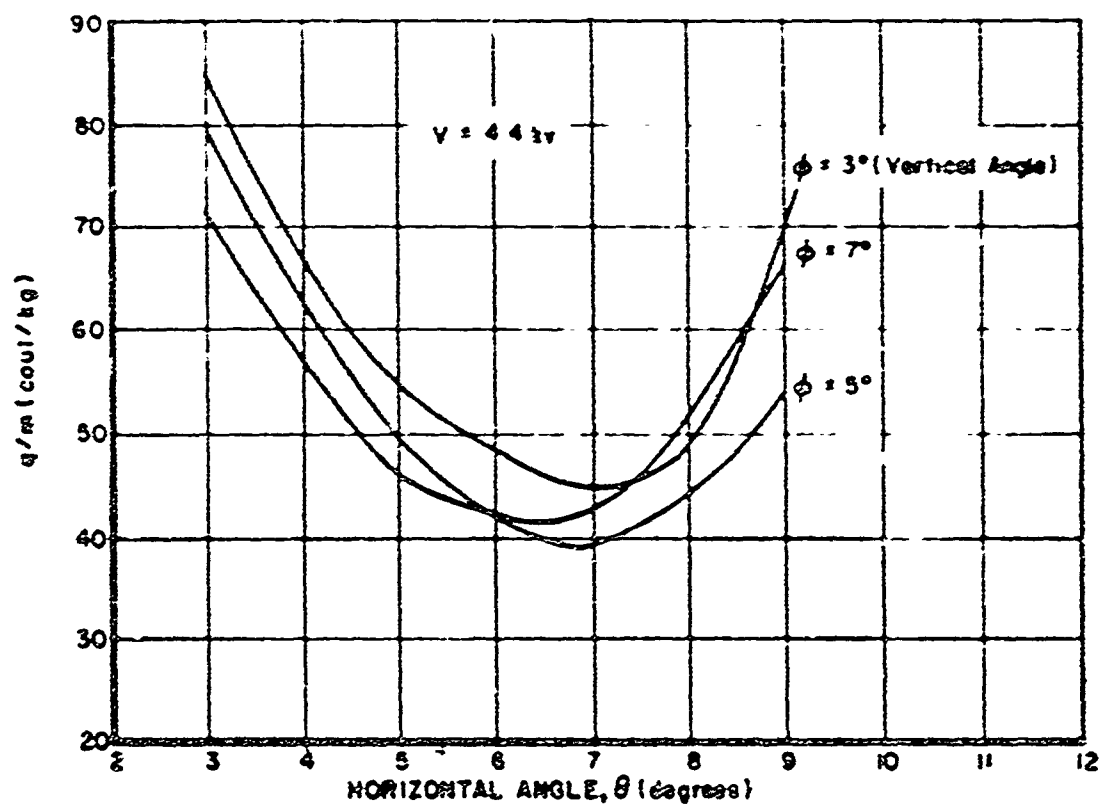


Figure 38.  $q/m$  Angular Variation at Two Voltages

Figure 37. Angular Variation of  $q/m$

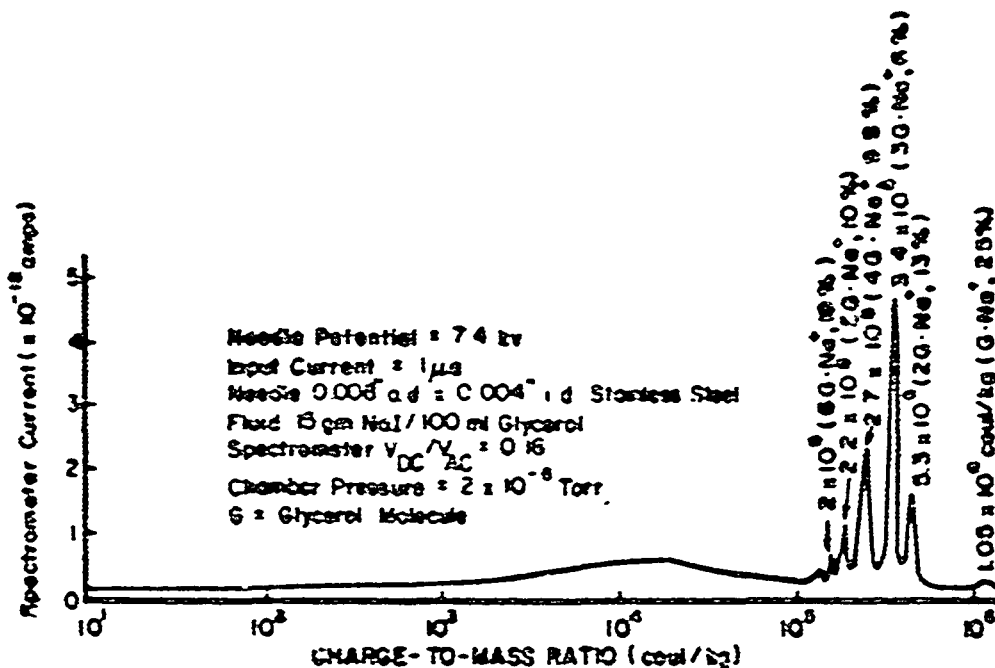


Figure 38. Ion Jet

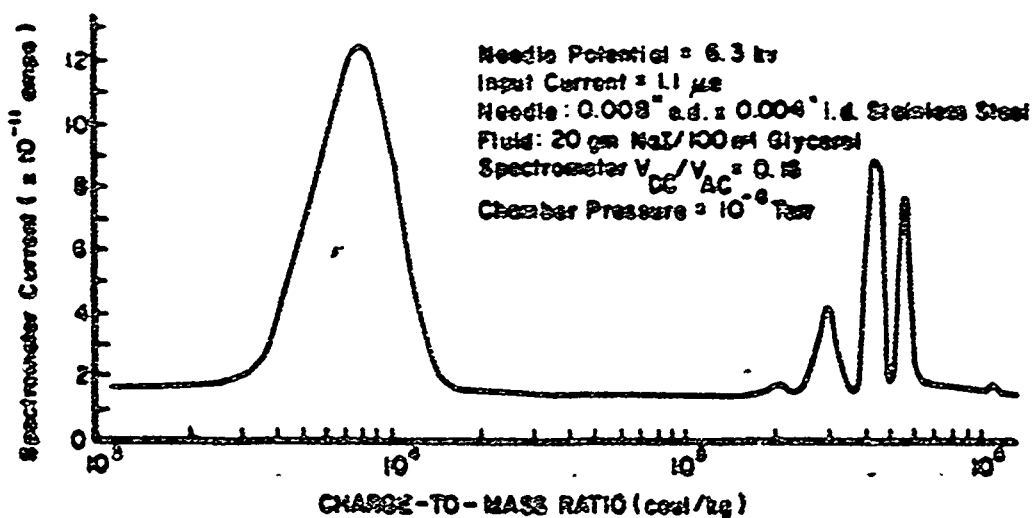


Figure 39. Jet with Heavy Particles and Ions



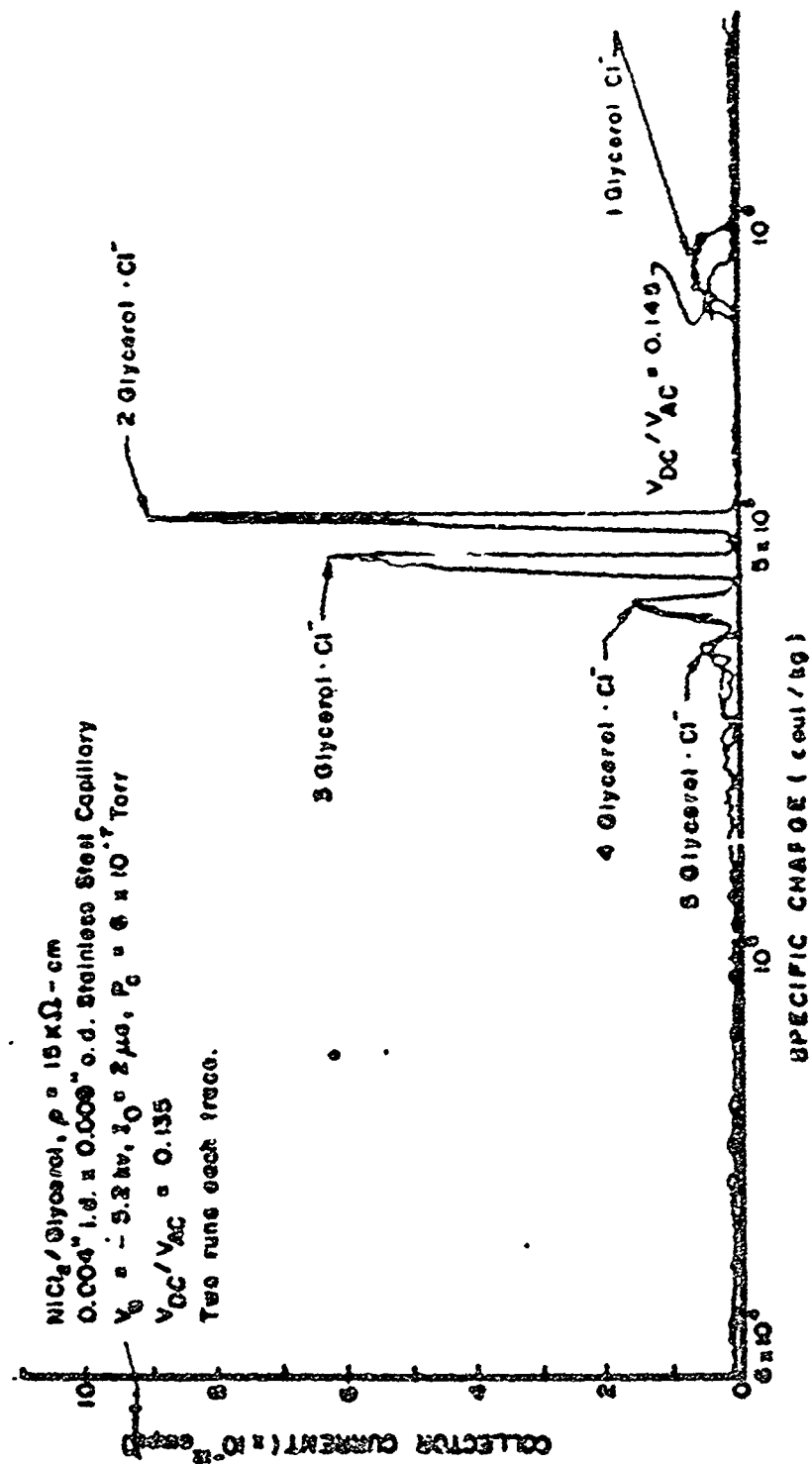


Figure 60. Negative Ion Quadrupole Trace

## SECTION V

## SOME THEORETICAL CONSIDERATIONS

One of the major problems in the study of charged droplet beams is the difficulty in describing the spraying process rigorously by mathematical means. This difficulty arises because the process is microscopic and must be treated on a dynamic rather than a static basis. Furthermore, many of the parameters influencing the spraying, e.g., the solution resistivity, surface tension, vapor pressure, etc., undergo major changes from their normal values when exposed to the conditions existing at the capillary tip during spraying. It is possible, however, to apply some fundamental physical principles to the operation of the source and gain some understanding of the basic constraints under which charged droplets are produced (References 11, 12, 13, 14).

One important consideration is that of the instability forces which act on a surface by virtue of the charge. Such instabilities have been studied recently, both analytically and experimentally, by Hogan (Reference 11), Schneider (Reference 10), and Carson (Reference 9). The two most important instability criteria are the Rayleigh limit and field emission limit.

The Rayleigh limit represents the maximum specific charge that a droplet can possess before the stabilizing surface energy forces are overcome by coulombic repulsion forces, which cause the droplet surface to rupture. Rayleigh originally calculated the limiting specific charge as:

$$C'_R = \frac{6 \sqrt{\epsilon_0 \gamma}}{\rho^{1/2}} \quad (24)$$

where  $C'_R$  is the maximum specific charge that can be possessed by a droplet of radius  $r$ , density  $\rho$ , and surface tension  $\gamma$ . Using energy minimization techniques, Vonnegut and Neubauer (Reference 15) arrived at a limiting specific charge just half that of Rayleigh, i.e.,

$$C'_R = \frac{3 \sqrt{\epsilon_0 \gamma}}{\rho^{1/2}} \quad (25)$$

Pfister (Reference 12) found the latter expression to be in agreement with experiments at low specific charge, although a trend toward Rayleigh's original limit was observed at specific charge levels on the order of  $10^3$  coulombs/kilogram.

A second limit on specific charge arises when the electric field of the droplet becomes sufficiently intense to field emit ions, or electrons if the droplet is negatively charged. The electric field at the surface of a droplet of radius  $r$  and charge  $q$  is  $E = \frac{q}{4\pi\epsilon_0 r^2}$  and the mass of the droplet,  $m = \frac{4}{3}\pi r^3 \rho$ . Dividing the former equation by the latter and rearranging yield the specific charge of the droplet in terms of electric field intensity and droplet radius. Substituting for  $E$  the value  $E_0$  at which ion or electron emission occurs, the ion emission-limited specific charge is found to be:

$$C_{E_0} = \frac{3 \epsilon_0}{\rho r} E_0 \quad (25)$$

Equations 24, 25, and 26, calculated for glycerol, are presented graphically in Figure 41. Rayleigh-type instability predominates at low values of specific charge, and the field emission limit at high values. The field emission limits plotted in Figure 41 have used as  $E_0$  the values  $10^{10}$  volts/meter and  $10^9$  volts/meter, which are representative values for field emission of ions and of electrons, respectively, from metals. The electronic structure of a metal, however, is vastly different from that of an ionically doped fluid such as glycerol. In the case of a metal, the conduction electrons are not bound to a particular atom and, thus, have a Fermi distribution of energies. Since the electrons in an ionic solution are bound to the various ions, the electron energy is comparable to the vibrational energy of the ions. Consequently, the electron emission limit for negative liquid droplets is quite likely on the order of the positive ion emission limit for metals.

The spraying of charged droplets from an electrified capillary is thus seen to be the result of coulombic forces overcoming surface tension forces and rupturing the liquid surface. Obviously, for this to occur, free charge carriers must be present in the liquid. A perfect dielectric, instead of spraying, would tend to flow to the region of highest electric field (a phenomenon known as dielectrophoresis). Experimentally one finds that many dielectric fluids do spray - probably due to field enhancement of their conductivity - but these fluids are characterized by very low currents and specific charges, even at extremely high extraction potentials.

The Rayleigh limit cannot be applied directly to the liquid surface at the tip of a capillary because it is impossible in practice to measure either the charge density or the size of the jets that occur during spraying. At best, the Rayleigh limit provides a feeling for the maximum droplet size that can be expected at a given value of specific charge.

The specific charge of the droplets produced as a charged liquid jet ruptures is a function of the charge density at the jet tip just prior to droplet formation. This charge density, in turn, depends on the electric field in the vicinity of the jet, the charge and mobility of the charge carriers in the liquid, and finally, the rate at which charge is neutralized at the capillary. Thus, for a given capillary potential, the three major factors governing the spraying process are the Rayleigh instability, ionic immobility, and electrode reaction at the capillary. Of these three, the Rayleigh instability is probably the least subject to control; the others depend upon field strength, solvent, solute, and capillary material. Either the ionic mobility or the electrode neutralization reaction may be the rate-determining factor in the spraying process. It is quite likely that, in most cases, a combination of these two factors determines the rate of the spraying and hence the specific charge of the droplet beam. In selecting the doping agents to be used in a particular solvent, one must thus pay close attention to the electrochemical characteristics of the solution. In particular, the doping agent should go into ionic solution, and should be capable of reducing the resistivity of the solvent to the order of a few thousand ohm-centimeters without adversely affecting the viscosity or vapor pressure of the solvent. If a given polarity beam is to be generated, then the ion species of opposite sign in the solvent must be capable of being easily neutralized at the capillary. This compatibility requirement is a result of the electronic nature of the ions and capillary material and can be determined in the following manner.

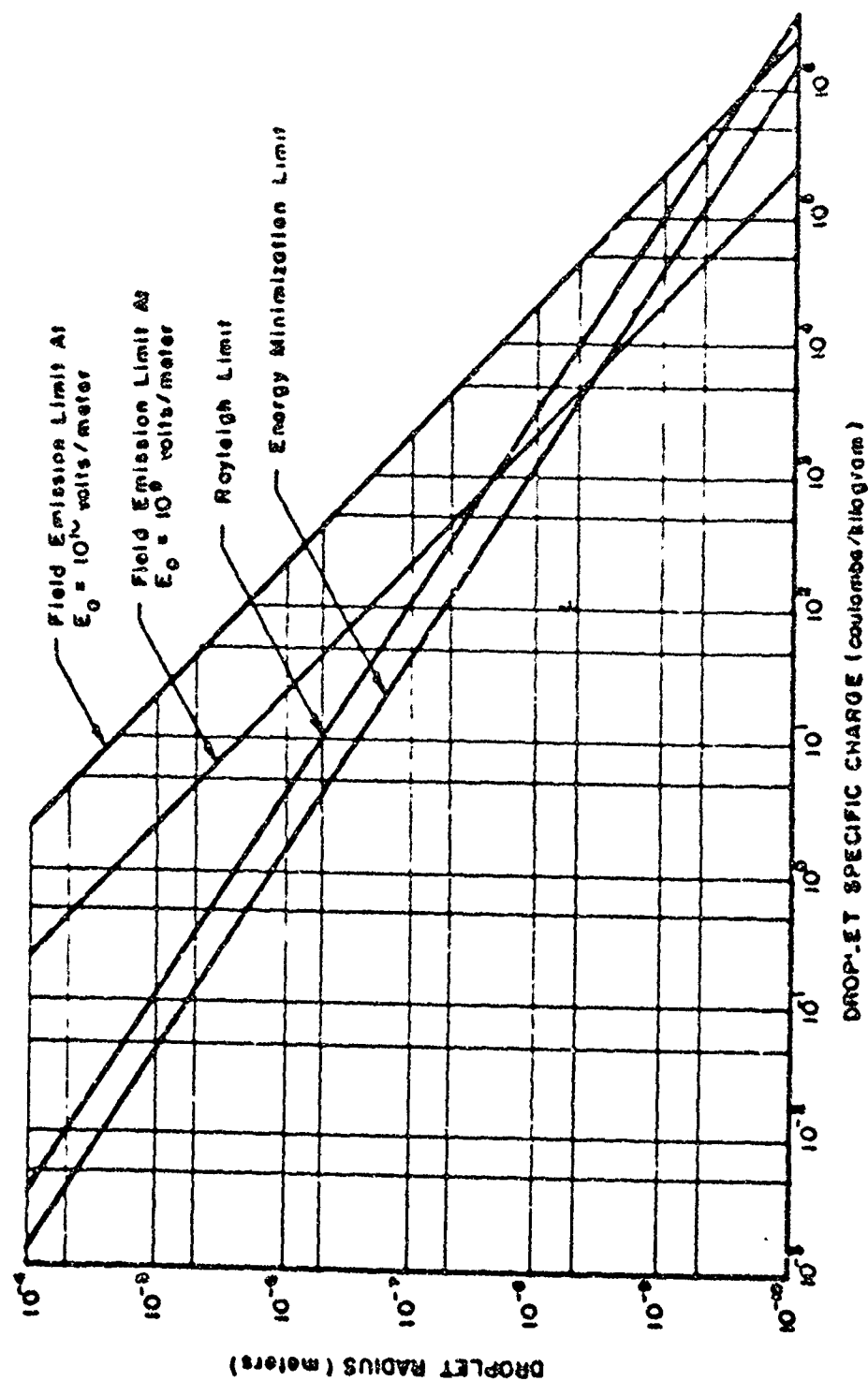


Figure 41. Rayleigh and Field Emission Limits for Glycerol

An ion of charge  $q$  and radius  $a$  in vacuo has associated with it an electric field in which is stored an amount of energy equivalent to the work required to charge the ion. This energy is of magnitude

$$E_{\text{vacuo}} = \frac{1}{4\pi\epsilon_0} \frac{q^2}{2a} \quad (27)$$

In a liquid of uniform dielectric constant,  $k$ , the work required to charge the ion is lower than in vacuo by the factor  $k^{-1}$  so that the energy stored in the ionic field is lower; i.e.

$$E_{\text{liquid}} = \frac{1}{4\pi\epsilon_1} \frac{q^2}{2Ka} = \frac{1}{k} E_{\text{vacuo}} \quad (28)$$

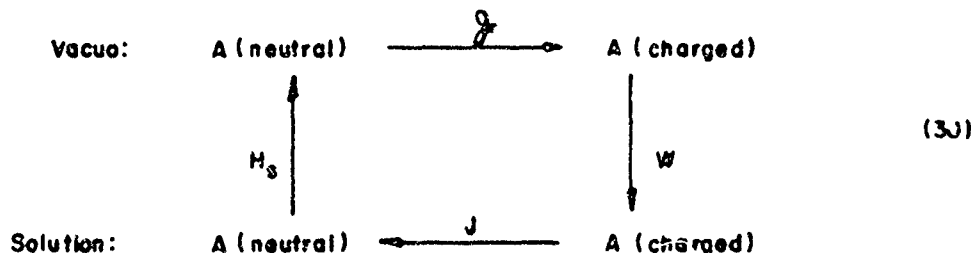
This difference in energy is called the solvation or hydration energy,  $W$ , of the ion in the liquid and is given by the Born equation:

$$W = \frac{1}{4\pi\epsilon_0} \frac{q^2}{2a} \left(1 - \frac{1}{k}\right) \quad (29)$$

The hydration energy of an ion of radius  $2 \times 10^{-10}$  meters is about 3.6 e.v. in liquids such as glycerol and water which have a dielectric constant for which  $(1 - \frac{1}{K}) \approx 1$ .

In order to use Equation 29, one must use the crystal radii of ions and modify these values to account for the variations in the dielectric constant of the liquid in the immediate vicinity of an ion and the effect of solvent molecules on the ion. Latimer (Reference 16) found that the addition of  $0.1\text{\AA}$  to the crystal radii of negative ions and  $0.85\text{\AA}$  to the crystal radii of positive ions in the Born equations produced values of solvation energy in good agreement with experimental values. This method was used to calculate the solvation energies in Table III.

The solvation energy of an ion changes the position of the electronic level of the ion in solution from the value in vacuo. This effect is demonstrated by carrying ion A through a Born-Haber cycle:



In the case of a positive ion  $A^+$ , the depth  $J_+$  of the lowest vacant electron level in solution is equal to the work required to remove an electron from the neutral atom in solution. This work is equivalent to that required to remove the neutral atom from the solution; i.e., the heat of solution,  $H_s$ , of the atom plus the work required to ionize the atom (the atom's

TABLE III

## IONIC PARAMETERS IN GLYCEROL

Ion	Ionization Energy In Vacuo, $Q^*$ (electron volts)	Solvation Energy $W$ (electron volts)	Ionization Energy In Solution $J$ (electron volts)	Approximate Interfacial Ionization Energy $C = J + \frac{1}{2} (Q^* - J)$ (electron volts)	Ionic Mobility $\mu$ @ 18°C
Ag <sup>+</sup>	7.54	3.54	4.20	5.87	54
Ba <sup>+</sup>	5.14	2.96	2.23	3.71	
Ba <sup>2+</sup>	9.95	12.9	0.01	4.98	55
Ca <sup>+</sup>	6.09	3.48	2.61	6.09	
Ca <sup>2+</sup>	11.82	15.3	0	5.91	51.6
Cd <sup>+</sup>	8.96	3.54	5.42	7.19	
Cd <sup>2+</sup>	16.84	15.5	4.68	10.66	45.9
Co <sup>+</sup>	7.81	---	---	---	---
Co <sup>2+</sup>	17.3	17.95	---	---	---
Cr <sup>+</sup>	6.74	~3	~4	~5.37	
Cr <sup>2+</sup>	16.6	~14	~6	~11.3	
Cu <sup>+</sup>	7.68	3.89	3.79	5.73	
Cu <sup>2+</sup>	20.34	17.95	6.28	13.31	45.5
Fe <sup>+</sup>	7.83	~3.5	~4	~5.91	
Fe <sup>2+</sup>	16.16	~17.74	~2	~9	45.3
Fe <sup>3+</sup>	~30	~42.6	~5.14	~17.57	
H <sup>+</sup>	13.53	11.1	4.67	9.1	313
Hg <sup>+</sup>	10.39	3.32	7.07	8.73	
Hg <sup>2+</sup>	18.65	14.43	7.52	13.08	
K <sup>+</sup>	4.32	3.23	1.09	2.70	64.5
Li <sup>+</sup>	5.36	4.61	0.75	3.06	33.1
Mg <sup>+</sup>	7.61	4.22	3.39	5.00	
Mg <sup>2+</sup>	14.96	18.7	0.48	7.72	45.5
Na <sup>+</sup>	5.12	3.87	1.05	3.09	43.3
Ni <sup>+</sup>	7.61	~3.37	~4.24	~5.93	
Ni <sup>2+</sup>	18.2	~17.2	~4.37	~11.29	
Sb <sup>+</sup>	8.0	11.1	4.77	4.70	
Sb <sup>2+</sup>	~18	~17	~5	~11	
Sb <sup>3+</sup>	24.7	~39.4	~2.3	~15.5	
Sr <sup>+</sup>	5.67	3.25	2.42	4.05	
Sr <sup>2+</sup>	10.96	14.3	-0.07	~5	54.0
Zn <sup>+</sup>	9.36	4.07	5.29	7.33	
Zn <sup>2+</sup>	17.89	16.8	5.16	11.52	46.7
I <sup>-</sup>	-4.1†	5.83	-8.06	-6.08	46.6
Cl <sup>-</sup>	-3.78†	3.69	-6.23	-5.0	65.3
Br <sup>-</sup>	-3.52†	3.44	-5.98	-4.75	67.3
I <sup>-</sup>	-3.12†	3.12	-5.47	-4.29	66.1
S <sup>-</sup>	-2.5†	3.08			
O <sup>-</sup>	-2.34†	2.46	-2.26	-2.22	
OH <sup>-</sup>	-2†				174
NO <sub>3</sub> <sup>-</sup>					61.6
SO <sub>4</sub> <sup>-</sup>					67.9
IO <sub>3</sub> <sup>-</sup>					33.9
MnO <sub>4</sub> <sup>-</sup>					53.4

\* Handbook of Physics and Chemistry, 39th Edition; Chem. Rubber Publishing Co.

\*\* Principles and Applications of Electrochemistry, 3rd Edition, Creighton and Koehler; John Wiley &amp; Sons, Inc.

† Zahlenwerte und Funktionen aus Physik, Chemie, Astronomie, Geophysik und Technik; Landolt-Börnstein, Springer Verlag, Berlin, Germany (1950)

ionization potential,  $J_+$ , minus the solvation energy,  $W_+$ , lost when the ion is returned to the solution. Thus,

$$J = J_+ - W_+ \quad (31)$$

assuming  $H_g$  to be negligibly small. The result of the ion's solvation energy is to raise the position of the vacant electron level in solution relative to its position in vacuum.

In the case of a negative ion,  $B^-$ , the depth,  $J_-$ , of the highest occupied electron level will be equal to the work required to remove the electron in this level infinitely far from the neutral atom. This work requires removing the ion from solution at an energy investment equal to the solvation energy,  $W_-$ , of the ion and then removing the supernumerary electron, the last operation requiring an amount of work equal to the electron affinity of the neutral atom. Returning the neutral atom to the solution results in a negligible energy gain in the form of heat of solution. The total energy expended in the above process is

$$J_- = J_- + W_- \quad (32)$$

Therefore, the occupied electron level is lowered in solution. This shifting of electron levels is presented graphically in Figure 42.

In the case of doubly charged ions, Equations 31 and 32 become

$$J_{++} = J_{++} - (W_{++} - W_+) \quad (31a)$$

and

$$J_{--} = J_{--} + (W_{--} - W_-) \quad (32a)$$

where  $J_{++}$  and  $J_{--}$  are the respective electronic levels in solution of doubly charged positive and negative ions.  $W_+$  and  $W_{++}$  are the solvation energies of the singly and doubly charged positive ion while  $W_-$  and  $W_{--}$  are the solvation energies of the negative ion.

We must also account for the fact that some ions form diatomic molecules upon neutralization. In this case, a further modification of Equations 31 and 32 is necessary:

$$J_+ = J_+ - W_+ + \frac{1}{2} D \quad (31b)$$

$$J_- = J_- + W_- - \frac{1}{2} D \quad (32b)$$

Here  $D$  denotes the dissociation energy of the neutral diatomic molecule.

As mentioned previously, the importance of the above factors appears in the neutralization reaction occurring at the capillary. At positive capillary potentials, the electrochemical reaction occurring at the capillary tip is one in which negative ions are neutralized while positive ions escape in droplets. The neutralization is accomplished as an electron passes from the anion to the capillary. Following Gurney (Reference 17) and Butler (References 18, 19), we view the average rate of the neutralization to be dependent upon the relative magnitudes of the capillary work function,  $\phi$ , and the depth of the electron level at the metal

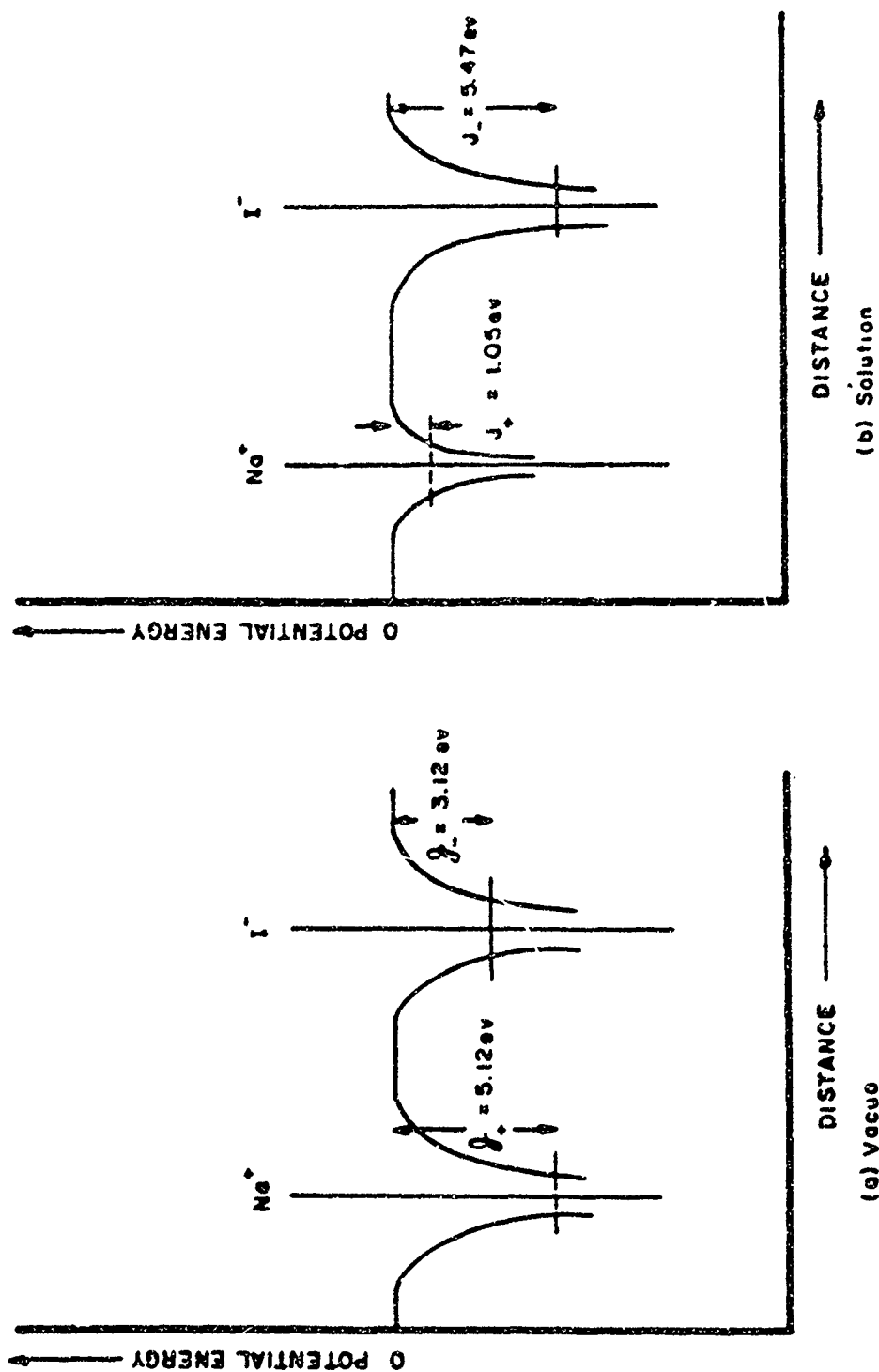


Figure 42. 1-Electron Levels of Sodium and Iodine Ions



solution interface. Thus, since neutralization requires the electron to pass from the anion to the capillary, the optimum energy relationship for this reaction should be

$$\phi_c > J_- + R \quad (33)$$

where R is included to reflect the waning influence of the solvent molecules on the ion's electron level as the ion approaches the capillary/solution interface. Since the electron level will have a depth between its value of  $\phi_-$  in vacuo and  $J_-$  in the interior of the solution, an arbitrary level

$$G_- = J_- + \frac{1}{2} (\phi_- - J_-) \quad (34)$$

has been defined for purposes of selection and tabulated for glycerol solutions of various ions in Table III. Equation 33 thus becomes

$$\phi_c > G_- \quad (35)$$

Therefore, the requirement for an anion to be used in a solution for the generation of positive charged droplet beams is that the anion's interfacial electron energy level is less than the capillary work function.

At negative capillary potentials, the neutralization process consists of an electron being transferred from the capillary to the cation. The resulting condition for cation/capillary compatibility at negative capillary potentials is

$$\phi_c < G_+ \quad (36)$$

The fact that Equation 36 is not satisfied for the  $\text{Na}^+$  ion explains the extremely poor performance of solutions of sodium salts at negative potentials. It should be emphasized that these relationships have been deduced assuming very elementary models of ionic solutions, and that they do not therefore apply to more complicated situations where complexes or ligands are formed.

The above logic led to the selection (Reference 14) of about a half dozen doping agents which performed quite satisfactorily. It was found, however, that although materials selected on the basis of the criteria of Equations 35 and 36 were always capable of Mode III operation, they did not always lead to high specific charges or efficient specific charge distributions. While this could be due to many factors, it was found that if the ion being neutralized had a higher mobility than the ion ejected from the capillary, then much better specific charge distributions resulted (e.g.,  $\text{NaOH}$ /glycerol produced better distributions than  $\text{NaI}$ /glycerol at positive potentials and  $\text{H}_2\text{SO}_4$ /glycerol yielded better performance at negative capillary potentials than at positive.) Under these conditions, the average specific charge also increased, indicating the possible importance of the neutralization reaction on this parameter. Some values of ionic mobilities for aqueous solutions are tabulated in Table III. These values do not vary significantly from solvent to solvent for all ions with the possible exception of the  $\text{H}^+$  ion.

The above considerations have treated the charging process as inductive. Gignoux (Reference 20) has advanced the theory that droplet charging results from a corona type discharge present at the capillary tip during spraying. Several factors mitigate against this

view, however. First is the repeated observation that source performance always improves with lowered ambient pressure. It is when the local pressure in the vicinity of the capillary increases to about  $10^{-5}$  Torr that one begins to observe diffuse glow at the capillary tip, poor specific charge distributions, and deteriorating performance in general. Secondly, no visible discharge or glow has ever been observed at the capillary, even with a telescope and a completely darkened room, when the source has been performing at its best. Finally, the corona charging view is not consistent with the observed dependency of specific charge peaks and distributions on the electron levels of the solvated ions.

Equations 35 and 36 establish the ionic and metallic characteristics necessary for the production of a stable charged particle beam, but give no indication of the current or specific charges obtainable from a charged particle source possessing these characteristics. Pfeiffer (Reference 12) examined some of the major parameters influencing the specific charge of electrohydrodynamically sprayed droplets and obtained an expression relating specific charge to the surface tension  $\gamma$ , permittivity  $\epsilon$ , density  $D$ , and resistivity  $\rho$  of the working fluid:

$$C \approx \left[ \left( \frac{k_2 \pi}{6} \right)^3 (q \gamma)^2 \frac{\epsilon^3}{D^4} \right]^{1/7} \left( \frac{E}{\rho M} \right)^{3/7} \quad (37)$$

where

$E$  is the electric field at the capillary tip,

$M$  is the mass flow rate of the fluid through the capillary, and

$k_2$  is an area proportionality constant with a value between 1 and 4. Pfeiffer concluded that the fluid resistivity and surface tension at field strengths below  $250 \times 10^5$  volts/meter would be affected significantly by variations in the electric field  $E$  and would make the droplet specific charge approximately proportional to  $E^2$ . In the intermediate field strength region of  $250 \times 10^5$  to  $700 \times 10^5$  volts/meter, the field effects on the resistivity are expected to approach a constant value and cause the specific charge to become roughly proportional to  $E^{1/2}$ . At field strengths above  $700 \times 10^5$  volts/meter, electron emission was expected to become significant in the conduction process and the droplet specific charge to increase in some exponential fashion with increasing electric field strength. These conclusions have been found to agree with experimental data (References 13, 14).

The primary motivation for the work described in this report has been the promise of a very efficient and versatile electric propulsion thruster, the details of which are described in the following chapter. Specific charge levels and currents suitable for such applications can now be produced, but much work remains to be done. Some of the areas yet to be explored are spraying of liquid metals, operation of high-current high-specific-charge sources, and study of positive and negative beam interactions, to name but a few. As was pointed out above, understanding both the hydrodynamics and the electrochemical aspects of the process has barely begun. A study of these problems will lead to not only a better understanding of the electrohydrodynamic process in particular, but to increased knowledge of electrode processes and electrokinetic phenomena in general.

## SECTION VI

## APPLICATION OF COLLOIDS TO PROPULSION

The benefits of applying electric propulsion to space missions have been amply illustrated by many authors and summarized by Stuhlinger (Reference 21). Electric propulsion systems are power-limited, which leads to an optimum specific impulse for a particular mission. This optimum  $I_{sp}$  is a function of mission time and power-supply specific power. Resistor-jets, arcjets, MPD arcjets, and ion engines cover the specific impulse range of approximately 700-2000 and 4000-20,000 seconds. The range of 2000-4000 seconds, however, has not been satisfactorily covered by any device.

Covering this range has been the objective of new propulsion schemes, including the colloid thruster. Also, colloid thrusters are presently attractive for meeting the requirements for low power and low thrust (100-200  $\mu$  lbs) engines suitable for altitude control and station keeping for earth satellites. Two parameters of interest from the propulsion standpoint, the beam current and charge-to-mass ratio of the droplet, depend upon the capillary potential, flow rate of propellant, and the solution being sprayed. Positive particles having charge-to-mass ratios of 100-30,000 coulombs/kg can be obtained in the laboratory. Negative colloids can be produced having charge-to-mass ratios in the range of 300-4000 coulombs/kg. Ten microamperes per capillary needle and a thrust of 1-3  $\mu$  lb per needle is presently possible.

Originally, a colloid thruster was viewed as a variation of the conventional ion engine (see Figure 43). Laboratory results, however, indicate that use of the extractor electrode alone will be sufficient to accomplish missions of moderate specific impulse. The advantage of the colloid engine over an ion engine is its high ionization efficiency, which is especially critical at low power levels. Dr. R. E. Hunter of AFAPL proposed a colloid thruster which simultaneously expels positive and negative droplets. This concept eliminates the need for neutralization by electron injection, which is an inefficient method of neutralization. Arranging capillaries in a matrix so that each is surrounded by four capillaries of opposite polarity establishes a virtual accelerating electrode in front of the array, as shown in Figure 44. Another scheme would be to use a common extractor plane with the capillary needles positive and negative with respect to the extractor, as shown in Figure 45.

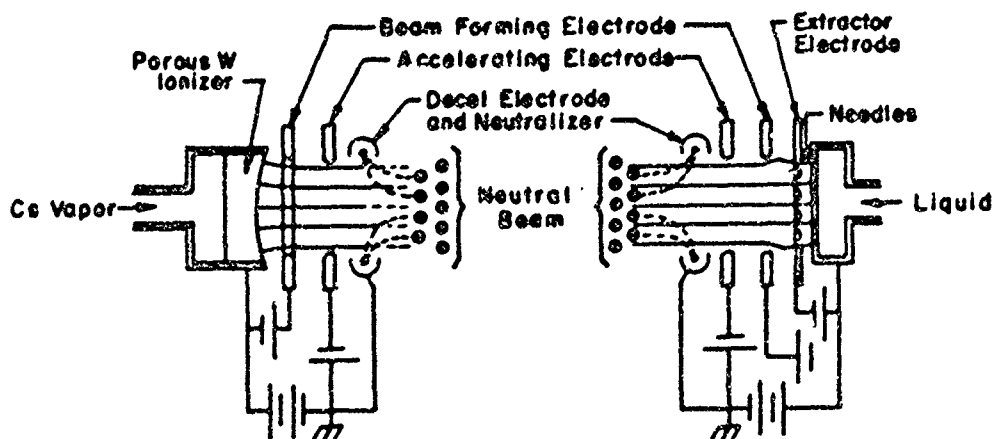


Figure 43. Schematic Diagrams of Ion and Colloid Thrusters

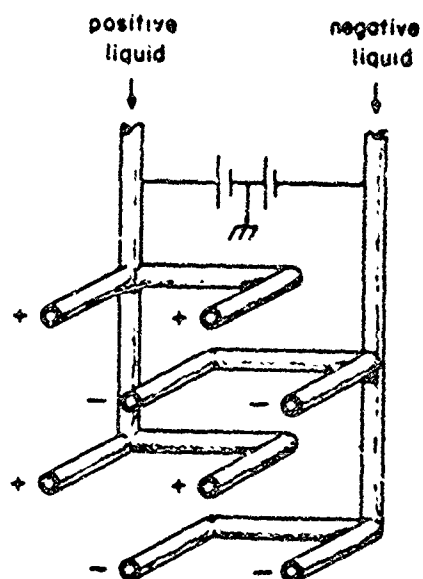


Figure 44. Schematic to Electrodeless Colloid Thrustor

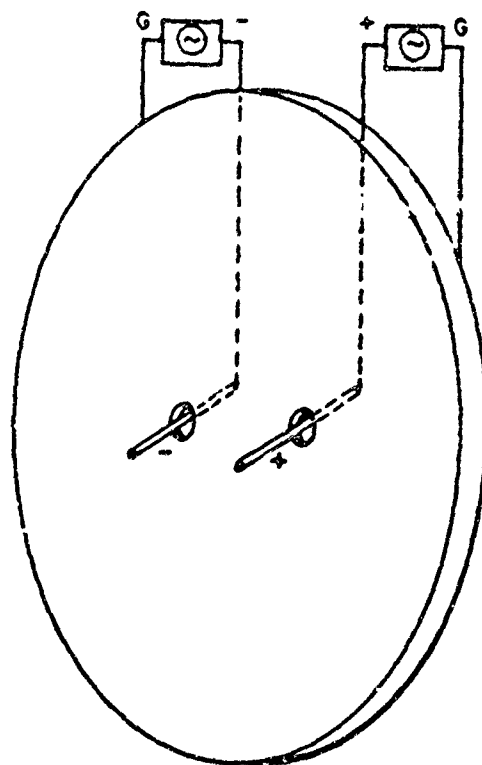


Figure 45. Schematic of Electrodeless Thrustor with Extractor as Common Ground

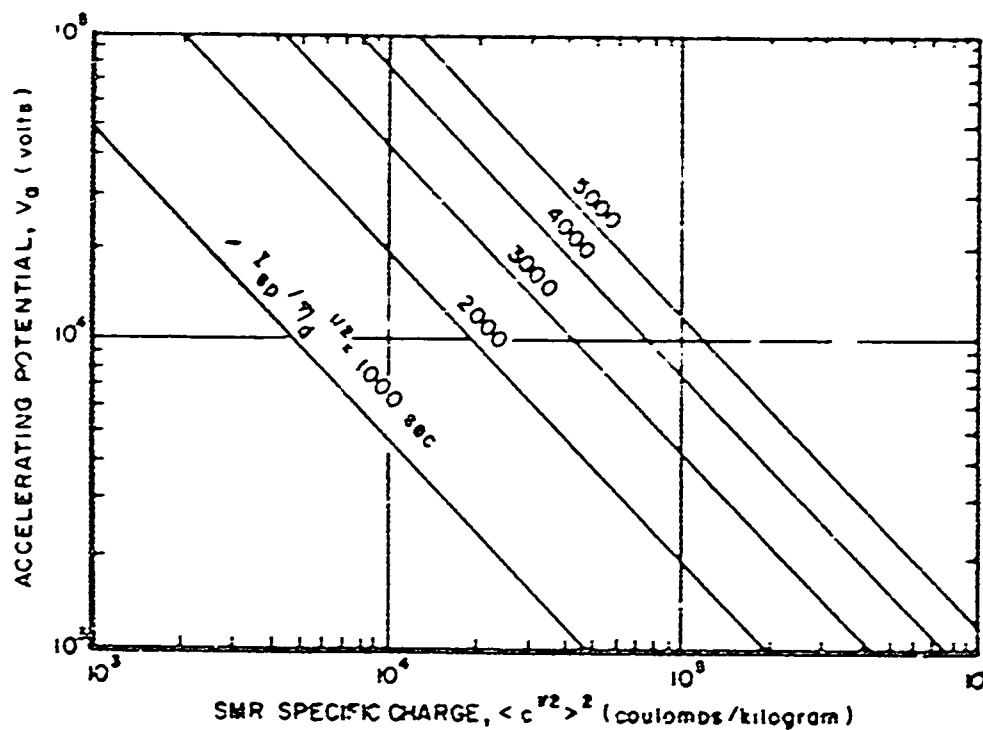


Figure 46a. Accelerating Potential Vs. SMR Specific Charge

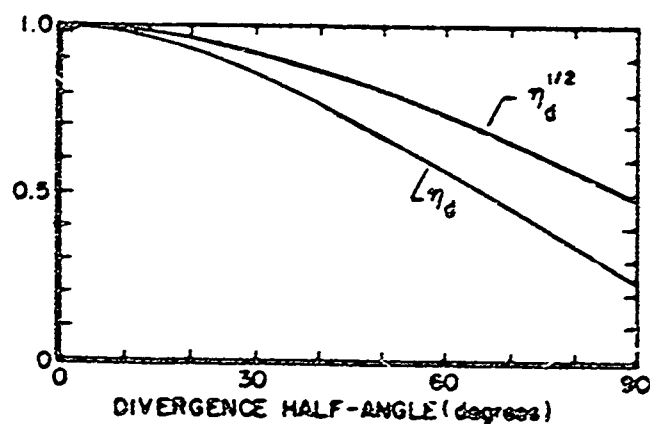


Figure 46b. Divergence Efficiency Variation with Spray Half-Angle

The following discussion and analysis will attempt to give a rough indication of the range of application for a colloid thruster based upon today's technology and assuming the necessary life times are possible.

$$F = \frac{1 + \cos \alpha}{2 \langle c \rangle} \dot{Q}_0 (2U)^{1/2} \langle c \rangle^{1/2} \quad (38)$$

$$\frac{1 + \cos \alpha}{2} = \eta_d^{1/2} \quad (\text{See Figure 46b}) \quad (39)$$

$$I_{sp} = \frac{(2U)^{1/2}}{\dot{Q}_0} \langle c \rangle^{1/2} \eta_d^{1/2} \quad (\text{See Figure 46a}) \quad (40)$$

$$M_{ps} = M_E + M_p + M_{po} \quad (41)$$

where

$M_{ps}$  = propulsion system mass

$M_E$  = engine mass

$M_p$  = propellant mass

$M_{po}$  = power supply mass

$c$  = (q/m) charge to mass ratio

$\langle \rangle$  = average

$\alpha$  = specific power (kw/kg)

$$\alpha = \frac{P}{M_{po}} \quad (42)$$

$$M_{po} = \frac{P}{\alpha} = \frac{1}{2\alpha} \frac{\dot{m} V_e^2}{\eta} = \frac{FT V_e}{2\alpha \eta T} \quad (43)$$

$\eta$  = efficiency  $V_e$  = exhaust velocity

$\eta_M$  = mass utilization  $T$  = mission time

$$M_p = \frac{FT}{\dot{Q}_0 I_{sp} \eta_M} = \frac{FT}{V_e \eta_M} \quad (44)$$

$$\left( \frac{M_{ps} - M_E}{FT} \right) = \frac{1}{\eta_M V_e} + \frac{V_e}{2\alpha \eta T} \quad (45)$$

$$\partial \left( \frac{M_{ps} - M_E}{FT} \right) / \partial V_e = - \frac{1}{\eta_M V_e^2} + \frac{1}{2\eta T \alpha} = 0 \quad (46)$$

$$\therefore V_{e \text{ opt}} = \sqrt{\frac{\eta}{\eta_M} (2 a T)} \quad (47)$$

and

$$\left( \frac{M_{ps} - M_E}{F T} \right)_{\text{opt}} = \sqrt{\frac{2}{\eta \eta_M a T}} \quad (48)$$

By Equations 47 and 40:

$$< c^{1/2} >_{\text{opt}} = \frac{\eta}{\eta_M} \frac{a T}{U} \frac{1}{\eta_d} \quad (49)$$

By Equations 49 and 48

$$\left( \frac{M_{ps} - M_E}{F T} \right)_{\text{opt}} = \frac{1}{< c^{1/2} >_{\text{opt}}} \sqrt{\frac{2}{\eta_M^2 \eta_d U}} \quad (50)$$

$$P_B = \frac{1}{2} \dot{m} V_e^2 = \frac{1}{2} F V_e \quad (51)$$

$$P_B = \eta P \quad (52)$$

$$\eta \frac{P}{F} = \frac{V_e}{2} = < c^{1/2} > \sqrt{\frac{U}{2}} \quad (53)$$

where

$P_B$  = beam power

Equations 40, 45, 48, 49, and 53 were used to plot the graphs shown as Figures 47 through 53. Shaded areas indicate the possible range of application for a colloid thruster. The two values of specific power are for solar cells and the SNAP 10-A nuclear power plant. These values are representative of the present state of the art in space power plants or sources.

Figure 47 shows that missions from about 1/3 to 1 year fall in the specific impulse gap for minimum weight when the specific power for solar cells is used in the calculations. The SNAP 10-A power supply has a specific power much less than that of solar cells; hence the optimum specific impulses for 1/3 to 1 year for this source are below the  $I_{sp}$  gap. Any improvements in nuclear power generators in the next few years should give values somewhere between the two extremes illustrated.

The solid shaded area in Figures 47 and 48 is the possible capability of a colloid thruster without post acceleration, based on present laboratory data. The lined area represents the capability assuming post acceleration up to 100,000 volts is possible. This also assumes that the lifetime required is obtainable; to date, the longest continuous run of a colloid source is 269 hours.

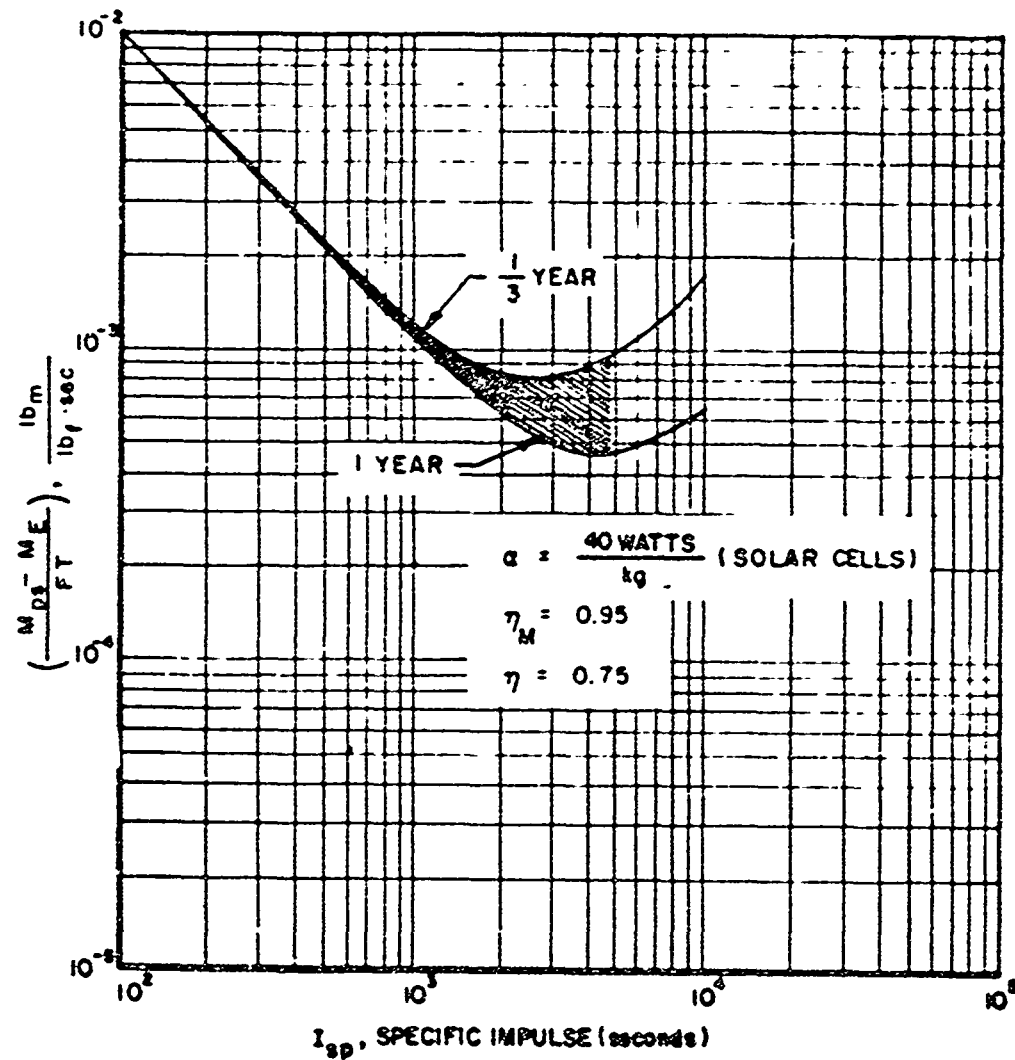


Figure 47. Ratio of Propulsion System Mass to Total Impulse Vs.  $I_{sp}$  for Solar Cells



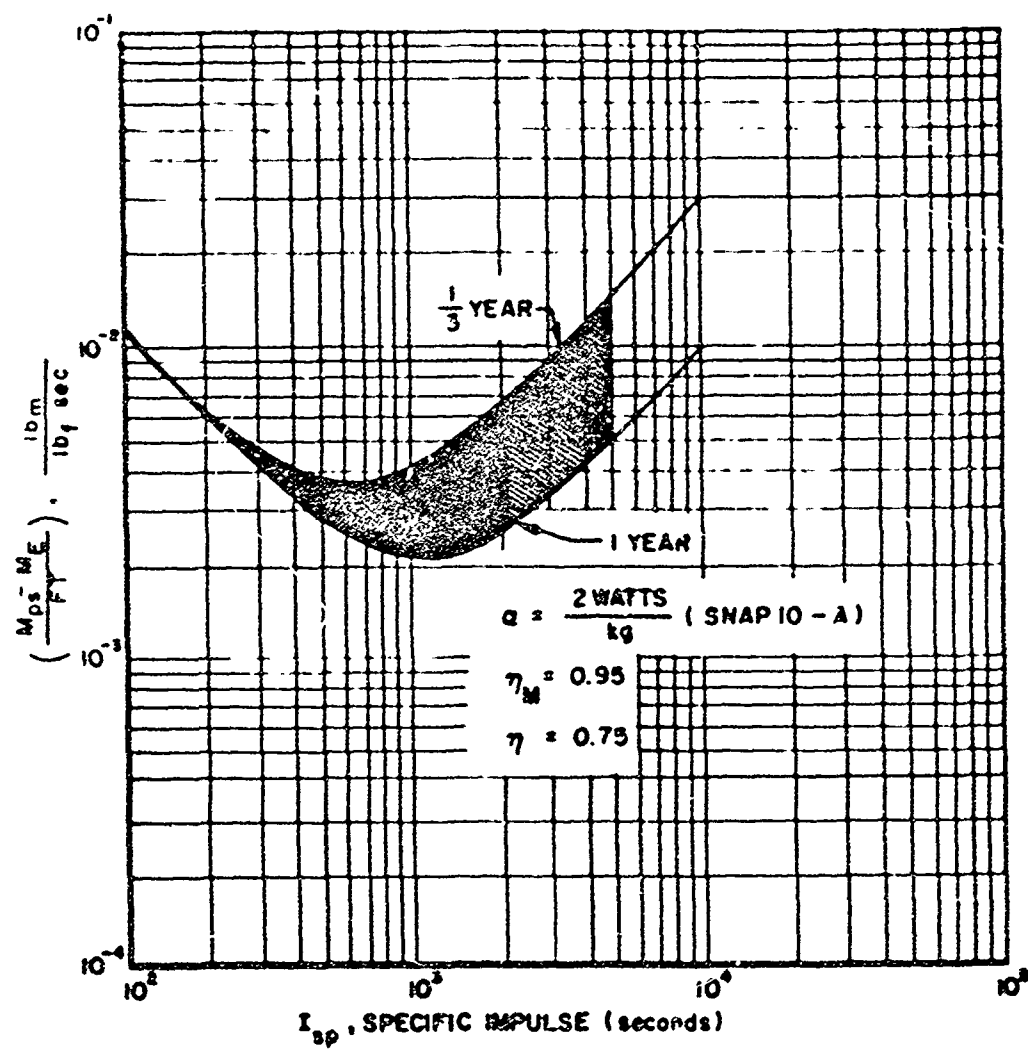


Figure 48. Ratio of Propulsion System Mass to Total Impulse Vs.  $I_{sp}$  for Nuclear Power Supply

The areas enclosed by the dotted and dashed lines in Figures 49 and 50 are based upon the charge-to-mass ratios which are easily obtained in the laboratory. The dotted line is for no post acceleration; the dashed line assumes post-acceleration voltages up to 100,000 volts. Charge-to-mass ratios up to about 30,000 have been obtained, but not with regularity. Continued research may result in charge-to-mass ratios up to 100,000 coulombs/kg, which will greatly reduce the required accelerating voltages for specific impulses in the 2000-5000 second regime.

Based upon the charge-to-mass ratios presently obtainable, the colloid thruster is approaching the optimum specific impulse characteristic of solar cells for missions on the order of a year. It is capable of producing the optimum specific impulse for any present or near-future nuclear power sources based on 1-5 year mission times.

There are satellite missions which require on the order of 10-200  $\mu$  lb of thrust. For a colloid thruster the power level required is so small that the weight of the power supply is negligible compared to that of the fixed engine, power conditioning, and propellant. This is due to its high efficiency,  $\approx 75\%$ . The contact ion engine pays a high penalty at these thrust levels for ionizer power which reduces its efficiency to  $\approx 5\%$ . For such missions, the colloid thruster could be operated at only moderate  $I_{sp}$  to keep the propellant weight at a reasonable value; the power needed can be obtained from the primary power source of the satellite. For example, to provide 10  $\mu$  lb of thrust for one year, a colloid engine operating at 600 seconds  $I_{sp}$  and 75% efficiency would require only 0.07 watt and 0.5 lb of propellant. Single needle colloid sources operated in the laboratory have produced about 3  $\mu$ lb thrust at an  $I_{sp}$  of about 500 seconds. Therefore, if the necessary lifetimes can be realized, the colloid thruster is ideal for this type of mission.

For high power missions (100 watts and up) the problem will be the number of capillary needles required. At 10  $\mu$  amps per needle, a mission requiring 500-watt, 1000-second specific impulse would require about 8000 capillary needles for a  $q/m$  of 10,000 and an accelerating voltage of 4000 volts. This would present quite a fabrication problem. The current output per needle must be pushed upward for high power missions.

In summary, the colloid thruster is at the stage of development where it could be used for low power, low thrust missions of several months duration at moderate specific impulses. For moderate to high power levels and specific impulses the ground work has been laid for further development and future application. The two parameters which must be increased by continued test and research are the charge-to-mass ratio and current output per needle; improvement in these two areas will permit smaller engine sizes and lower accelerating voltages, which will be critical for high power missions. Figures 51, 52, and 53 are included for the convenience of making quick calculations of various parameters associated with a colloid thruster. Figure 51 permits a rapid determination of  $P/F$ ,  $q/m$ ,  $U$ , and  $I_{sp}$ .

Figure 53 was made by assuming  $\eta_d = 1$  and  $\frac{1}{\langle c \rangle} \langle c^2 \rangle = \frac{1}{c^2}$

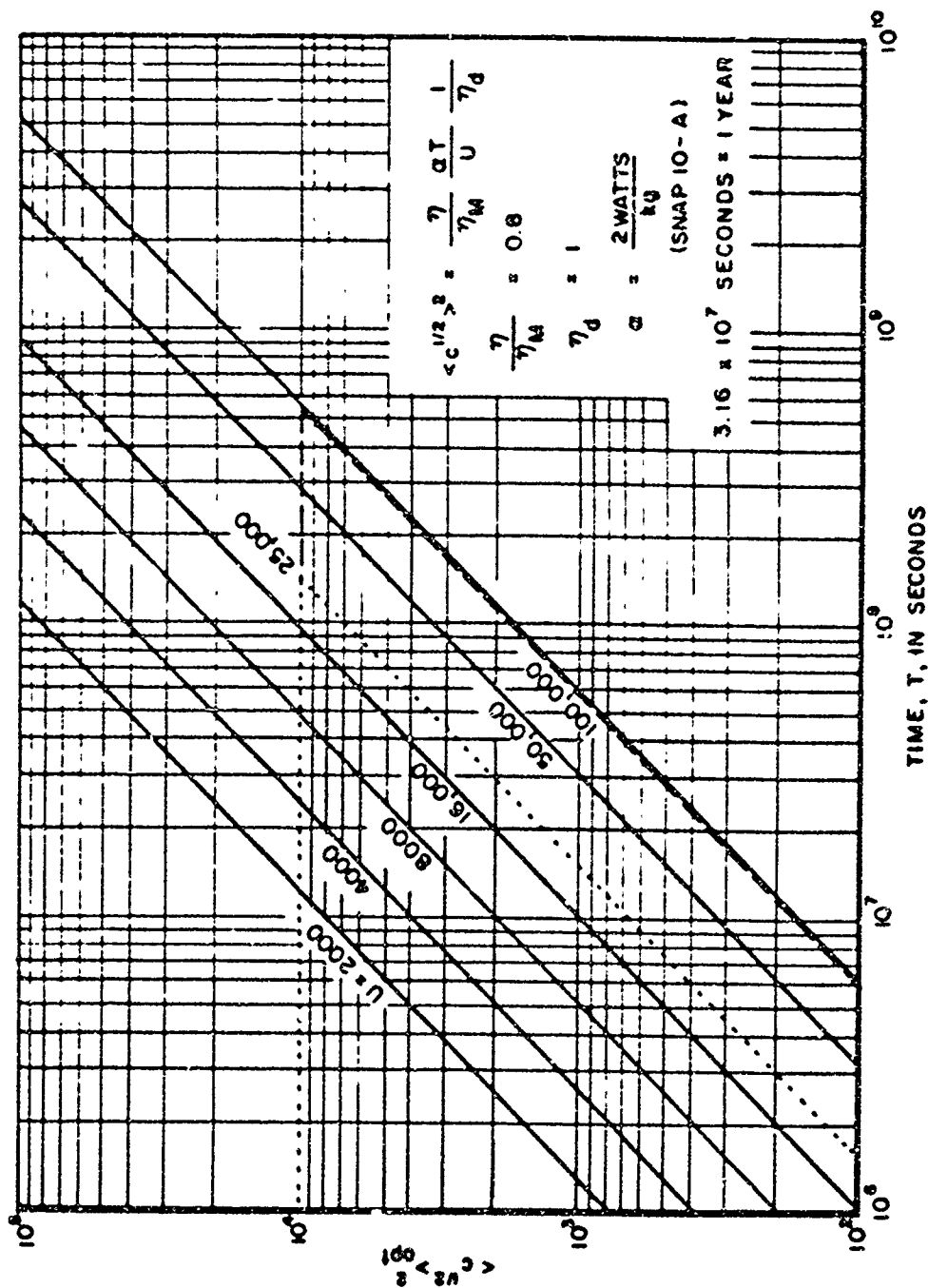
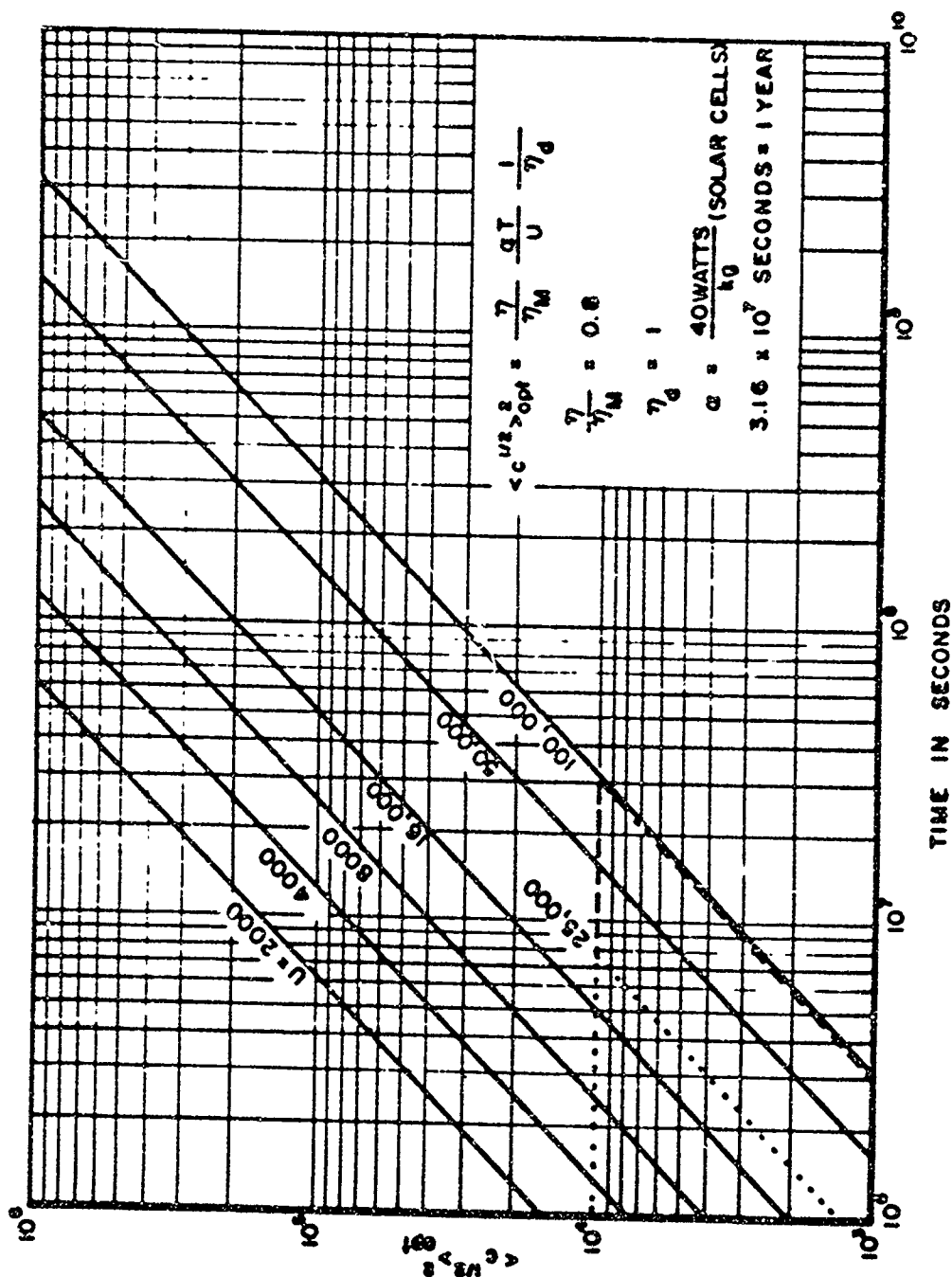


Figure 49. Optimum SMR Specific Charge Vs. Mission Time for Various Accelerating Voltages, Nuclear Power Supply



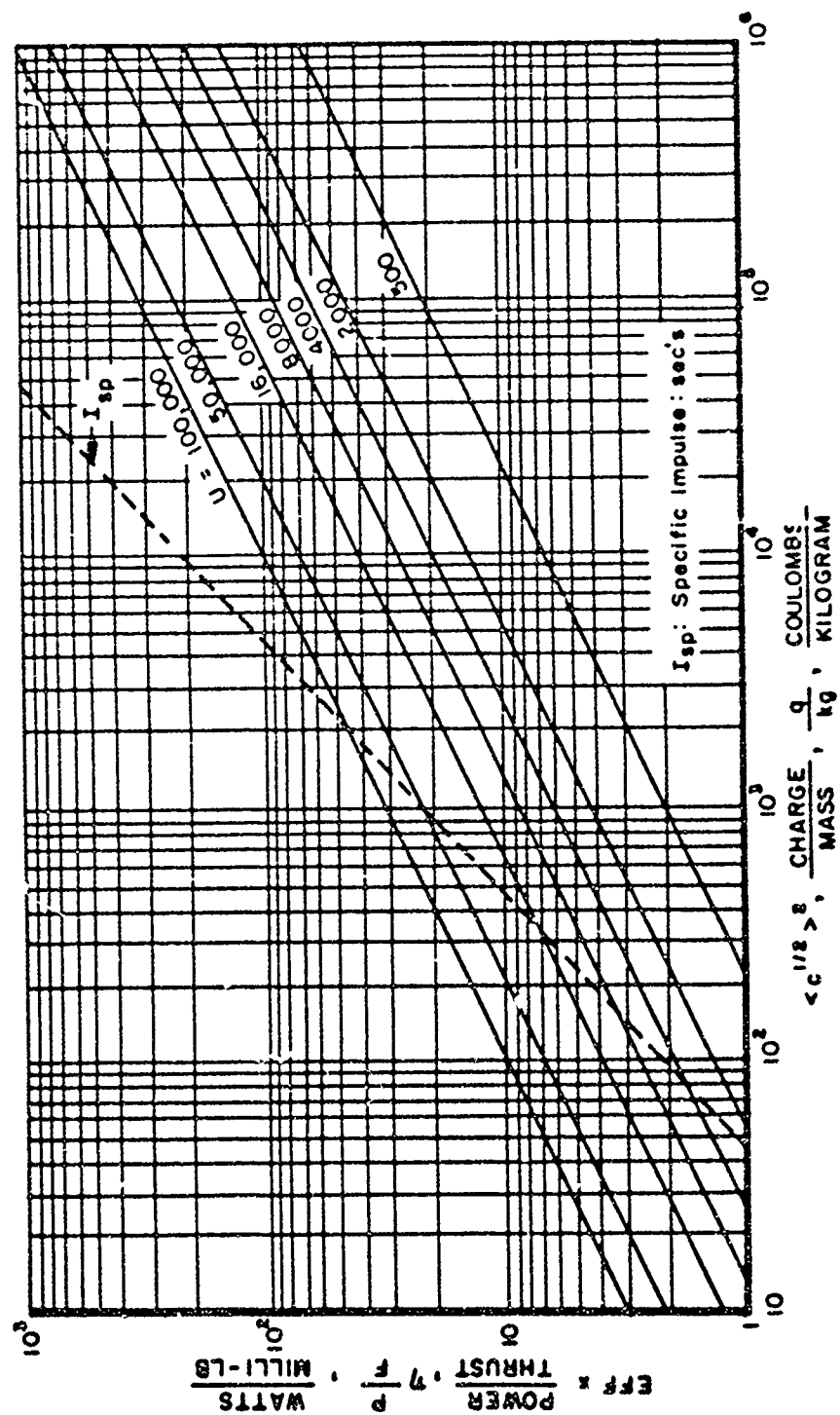


Figure 51. Efficiency X Power-to-Thrust Ratio Vs.  $I_{sp}$  and SMR Specific Charge for Various Accelerating Voltages

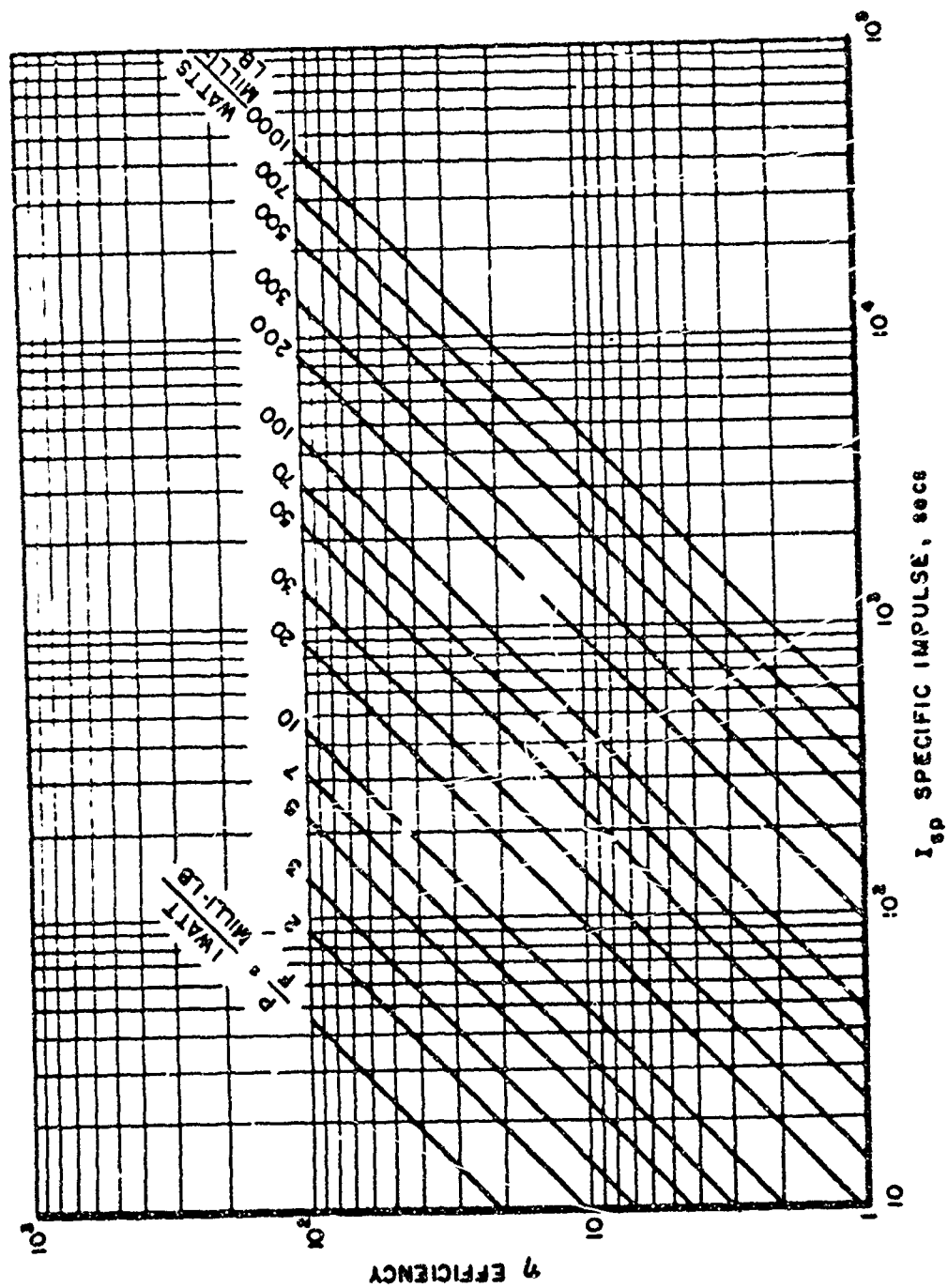


Figure 52. Efficiency Vs. Specific Impulse for Various Power-to-Thrust Ratios

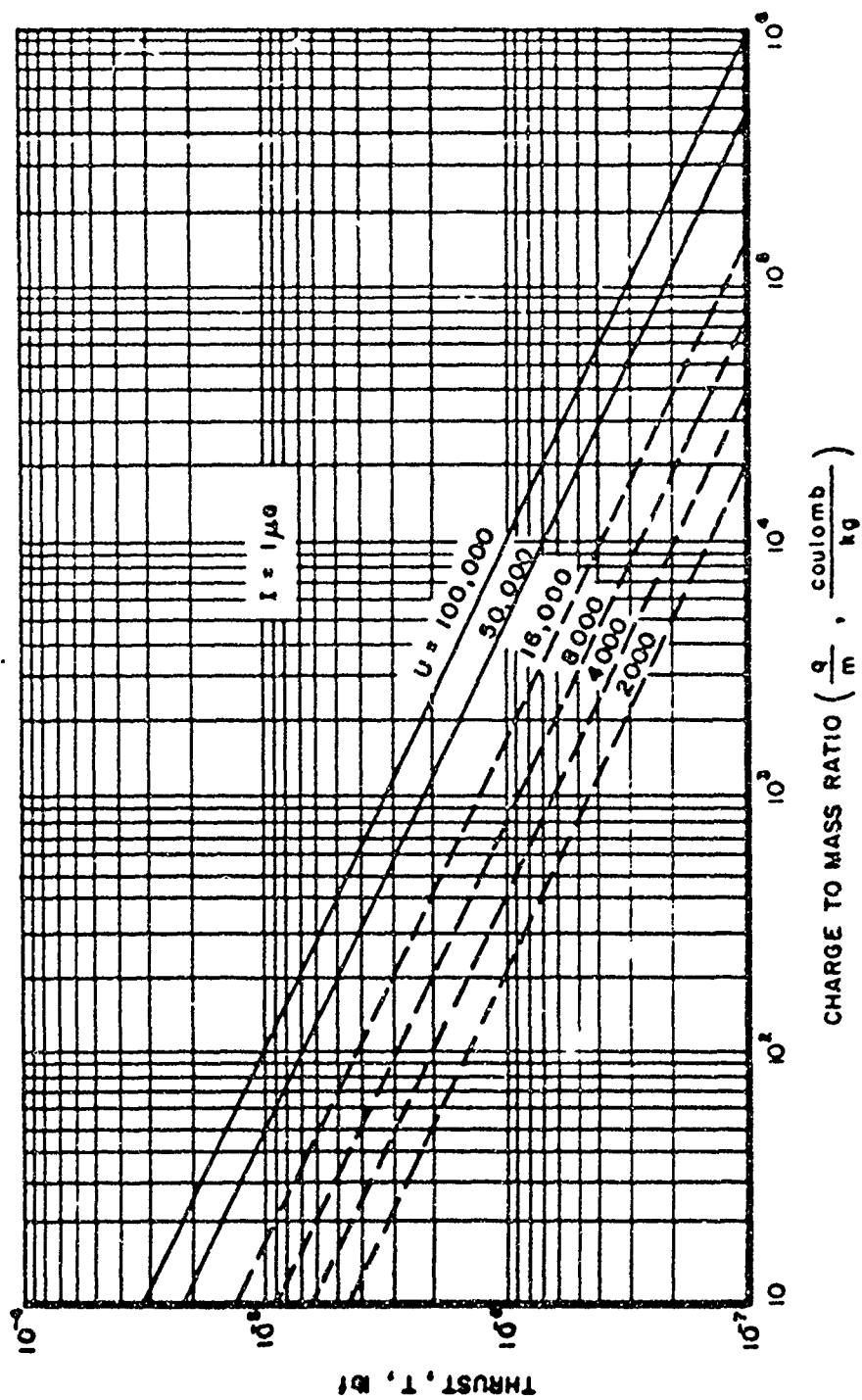


Figure 53. Thrust Vs. Specific Charge for Various Accelerating Voltages and a Current of 1 Microamp

## REFERENCES

1. Paul, W. and Raether, M.; "Das Electrische Massenfilter," Zeitschrift fuer Physik, B. D. 140, S. 262-273 (1955).
2. Cohen, E.; Research on Charged Colloid Generation, APL TDR 64-75, June 1964.
3. Hunter, R. E. and Wineland, S. H.; "Charged Colloid Generation Research," Space Electronics Symposium, Vol. 6, AAS Science and Technology Series, Eric Burgeon, Ed. (1965).
4. Hunter, R. E.; Exploring the Feasibility of the Electroless Colloid Thruster, (Appendix); Ph.D Dissertation, the Ohio State University, 1965.
5. Cohen, E.; Research on the Electrostatic Generation and Acceleration of Submicron-Size Particles, ARL-63-88, OAR (1963).
6. Hunter, R. E. and Wineland, S. H.; "Exploration of the Feasibility of an Electroless Colloid Thruster Concept," Sixth International Symposium on Space Science and Technology, Tokyo, Japan (1965).
7. Gignoux, D., et al.; Further Development of a Charged Liquid Colloid Source for Electrostatic Propulsion, NASA CR 54642 (1965).
8. Cohen, E., Somol, C. J., and Gordon, D. A.; A 100 Kv, 10-Watt Heavy Particle Thruster, AIAA Paper No. 65-377 (1965).
9. Carson, R. S.; Electrical Spraying of Macroscopic Liquid Particles Under Pulsed Conditions, Report No. CPRL-1-64, Engineering Experiment Station, University of Illinois (1964).
10. Hogan, J. J., Carson, R. S., and Schneider, J. M.; Factors Influencing Electrically Sprayed Liquids, Pg 3, AIAA Paper 64-12 (1964).
11. Hogan, J. J.; Parameters Influencing the Charge-to-Mass Ratio of Electrically Sprayed Liquid Particles, Report No. CPRL-2-63, Engineering Experiment Station, University of Illinois (1963).
12. Pfeifer, R. J.; Parametric Studies of Electrohydrodynamic Spraying, Report No. CPRL-4-65, Engineering Experiment Station, University of Illinois (1965).
13. Hendricks, C. D., and Pfeifer, R. J.; Parametric Studies of Electrohydrodynamic Spraying, AIAA Paper No. 66-252. (1966).
14. Wineland, S. H., and Hunter, R. E.; Negatively Charged Colloid Generation Research, AIAA Paper No. 66-251 (1966).
15. Vonnegut, B., and Neubauer, R. L.; J. Colloid Sci V.7, p. 616 (1952).
16. Latimer, W. M., et. al.; "The Free Energy of Hydration of Gaseous Ions, and The Absolute Potential of the Normal Calomel Electrode," Journal of Chemical Physics, Vol. 7, pp 108-111, February, 1939.



(REFERENCES (Continued))

17. Gurney, R. W.; Ions in Solution, Cambridge, 1936.
18. Butler, J. A. V.; Electrocapillarity, Chemical Publishing Company, 1940.
19. Butler, J. A. V.; Electrokinetic Phenomena at Interfaces, Methuen and Co., (1951).
20. Gignoux, D.; Development of Techniques for Producing Charged Colloidal Particles, Contract NAS3-7924, April 1966.
21. Stuhlinger, E.; Ion Propulsion for Space Flight, McGraw Hill Book Company, 1964.

UNCLASSIFIED

Security Classification

DOCUMENT CONTROL DATA - R&D		
(Security classification of title, body of abstract and indexing annotation must be entered when the overall report is classified)		
1. ORIGINATING ACTIVITY (Corporate author) Air Force Aero Propulsion Laboratory Wright-Patterson Air Force Base, Ohio		12. REPORT SECURITY CLASSIFICATION UNCLASSIFIED
		13. GROUP
3. REPORT TITLE THE ELECTROHYDRODYNAMIC GENERATION OF CHARGED DROPLET BEAMS		
4. DESCRIPTIVE NOTES (Type of report and inclusive dates)		
5. AUTHOR(S) (Last name, first name, initial) Wineland, S. H., Burson, W. C., Hunter, R. E.		
6. REPORT DATE August 1966	7a. TOTAL NO. OF PAGES 78	7b. NO. OF REFS 21
8a. CONTRACT OR GRANT NO.	8b. ORIGINATOR'S REPORT NUMBER(S) AFAPL-TR-66-72	
9. PROJECT NO. 3141 c. Task No. 314104	9b. OTHER REPORT NO(S) (Any other numbers that may be assigned this report)	
10. AVAILABILITY/LIMITATION NOTICES This document is subject to special export controls and each transmittal to foreign governments or foreign nationals may be made only with prior approval of the Air Force Aero Propulsion Laboratory, W-PAFB, Ohio.		
11. SUPPLEMENTARY NOTES		12. SPONSORING MILITARY ACTIVITY Air Force Aero Propulsion Laboratory W-PAFB, Ohio
13. ABSTRACT <p>Thrustors capable of high exhaust velocity (specific impulse) and efficiency are desirable for space propulsion. The acceleration of charged droplets (colloids) by an electric field can provide a thruster that meets these requirements. This effort was concentrated on producing positive and negative colloids by the electrohydrodynamic spraying of ionically doped glycerol solutions from metal capillary needles.</p> <p>To date, the results of this program indicate that both positive and negative colloids can be produced with charge-to-mass ratios of sufficient magnitude to be utilized by an electrostatic space thruster. Charge-to-mass ratios have been obtained in the ranges of approximately 100-30,000 coulombs/kilogram for positive colloids and 100-4000 coulombs/kilogram for negative colloids. Current levels of 10 microamps per needle are easily obtained.</p>		

DD Form 1473  
JAN 66

UNCLASSIFIED

Security Classification

UNCLASSIFIED  
Security Classification

KEY WORDS	LIMIT A		LIMIT B		LIMIT C	
	NO. 1	NO. 2	NO. 1	NO. 2	NO. 1	NO. 2
Colloids						
Electric Propulsion						
Electrohydrodynamic Spraying						
Charged Particle Generation						

INSTRUCTIONS

1. **ORIGINATING ACTIVITY:** Enter the name and address of the contractor, subcontractor, grantee, Department of Defense activity or other organization (corporate author) issuing the report.
- 2a. **REPORT SECURITY CLASSIFICATION:** Enter the overall security classification of the report. Indicate whether "Restricted Data" is included. Marking is to be in accordance with appropriate security regulations.
- 2b. **GROUP:** Automatic downgrading is specified in DoD Directive 5200.10 and Armed Forces Industrial Manual. Enter the group number. Also, when applicable, show that optional markings have been used for Group 3 and Group 4 as authorized.
3. **REPORT TITLE:** Enter the complete report title in all capital letters. Titles in all cases should be unclassified. If a meaningful title cannot be selected without classification, show title classification in all capitals in parentheses immediately following the title.
4. **DESCRIPTIVE NOTES:** If appropriate, enter the type of report, e.g., interim, progress, summary, annual, or final. Give the inclusive dates when a specific reporting period is covered.
5. **AUTHOR(S):** Enter the name(s) of author(s) as shown on or in the report. Enter last name, first name, middle initial. If military, show rank and branch of service. The name of the principal author is an absolute minimum requirement.
6. **REPORT DATE:** Enter the date of the report as day, month, year, or month, year. If more than one date appears on the report, use date of publication.
- 7a. **TOTAL NUMBER OF PAGES:** The total page count should follow normal pagination procedures, i.e., enter the number of pages containing information.
- 7b. **NUMBER OF REFERENCES:** Enter the total number of references cited in the report.
8. **CONTRACT OR GRANT NUMBER:** If appropriate, enter the applicable number of the contract or grant under which the report was written.
- 9a. **PROJECT NUMBER:** Enter the appropriate military department identification, such as project number, subject number, system number, task number, etc.
- 9b. **ORIGINATOR'S REPORT NUMBER(S):** Enter the official report number by which the document will be identified and controlled by the originating activity. This number must be unique to this report.
- 9c. **OTHER REPORT NUMBER(S):** If the report has been assigned any other report number (either by the originator or by the sponsor), also enter this number(s).
10. **AVAILABILITY/LIMITATION NOTICE:** Enter any limitations on further dissemination of the report, other than those

imposed by security classification, using standard statements such as:

- (1) "Qualified requesters may obtain copies of this report from DDC."
- (2) "Foreign dissemination and dissemination of this report by DDC is not authorized."
- (3) "U. S. Government agencies may obtain copies of this report directly from DDC. Other qualified DDC users shall request through \_\_\_\_\_."
- (4) "U. S. military agencies may obtain copies of this report directly from DDC. Other qualified users shall request through \_\_\_\_\_."
- (5) "All distribution of this report is controlled. Qualified DDC users shall request through \_\_\_\_\_."

If the report has been furnished to the Office of Technical Services, Department of Commerce, for sale to the public, indicate this fact and enter the price, if known.

11. **SUPPLEMENTARY NOTES:** Use for additional explanatory notes.

12. **SPONSORING MILITARY ACTIVITY:** Enter the name of the departmental project office or laboratory sponsoring (paying for) the research and development. Include address.

13. **ABSTRACT:** Enter an abstract giving a brief and factual summary of the document indicative of the report, even though it may also appear elsewhere in the body of the technical report. If additional space is required, a continuation sheet shall be attached.

It is highly desirable that the abstract of classified reports be unclassified. Each paragraph of the abstract shall end with an indication of the military security classification of the information in the paragraph, represented as (TS), (S), (C), or (U).

There is no limitation on the length of the abstract. However, the suggested length is from 150 to 225 words.

14. **KEY WORDS:** Key words are technically meaningful terms or short phrases that characterize a report and may be used as index entries for cataloging the report. Key words must be selected so that no security classification is required. Identifiers, such as equipment model designation, trade name, military project code name, geographic location, may be used as key words but will be followed by an indication of technical context. The assignment of links, rules, and weights is optional.

UNCLASSIFIED  
Security Classification